2002

Repair of Wood Piles with Fiber Reinforced Composites

Antonis Petrou Michael

REPAIR OF WOOD PILES WITH FIBER REINFORCED COMPOSITES

By

Antohis Petrou Michael

B.S. in Civil Engineering, Tennessee Technological University, 1999

A THESIS

Submitted in Partial Fulfillment of the

Requirements for the Degree of

Master of Science

(in Civil Engineering)

The Graduate School

The University of Maine

December, 2002

Advisory Committee:

Roberto Lopez-Anido, Assistant Professor of Civil Engineering, Advisor

Thomas C. Sandford, Associate Professor of Civil Engineering

Barry Goodell, Professor of Wood Science and Technology

REPAIR OF WOOD PILES WITH FIBER REINFORCED COMPOSITES

By Antonis P. Michael

Thesis Advisor: Dr. Roberto Lopez-Anido

An Abstract of the Thesis Presented
In Partial Fulfillment of the Requirements for the
Degree of Master of Science
(in Civil Engineering)
December, 2002

Piles made of treated wood have been traditionally used for the construction of piers and other waterfront structures. The main concern related to wood piles is deterioration due to marine borers, which limits the lifespan and requires frequent repair and replacement. Furthermore, since the use of preservative treatments for wood piles has been reduced due to environmental concerns, there is a current need for efficient methods for wood pile protection.

Marine borer activity in Maine coastal waters was assessed through a survey directed to harbor masters correlated with historic data. In order to illustrate the type and extent of wood pile deterioration, two case studies in Maine harbors are presented.

A special prefabricated Fiber Reinforced Polymer (FRP) composite shield or jacket was developed to repair wood piles in the field. FRP composite shells or sleeves are bonded with an underwater curing adhesive to form a shield. The main concern for durability of the adhesive bond is the resistance to freeze-thaw cycles. To assess adhesive bond durability, single lap shear tests were performed after exposure to freeze-thaw cycles.

Two types of load-transfer mechanisms between the wood pile and the FRP composite shield were developed and tested: (1) cement-based structural grout; and (2) steel shear connectors with an expanding polyurethane chemical grout. Push-out tests by compression loading were performed to characterize the interfaces and discriminate the effect of the design parameters. The outcome of the push-out tests was the evaluation of the shear force-slip non-linear response and the progressive failure mechanism.

The structural response of full-size pre-damaged wood piles repaired with the FRP composite shield system was characterized. A three-point bending test procedure was used to simulate the response of a pile subjected to lateral loads. The load-deformation response, deflected shape profile, relative longitudinal displacements (slip), strain distribution, ultimate bending moment capacity and mode of failure were evaluated. Wood piles were pre-damaged by reducing approximately 60% of the cross-section over a portion of the pile. It was found that a pre-damaged wood pile repaired using the FRP composite shield with cement-based grout exceeded the bending capacity of a reference wood pile. The repair system using the FRP composite shield with steel shear connectors and polyurethane grout did not fully restore the bending capacity of a reference wood pile; however it can be used for marine borer protection when wood damage is not critical.

A beam structural model to predict stiffness and strength properties of wood piles restored with FRP composite shells was developed. The model accounts for different pile dimensional properties and various amounts of pre-damage. The structural model was successfully correlated with experimental data from three-point bending tests of wood piles.

ACKNOWLEDGEMENT

The research work presented in this thesis was funded by the National Oceanographic and Atmospheric Administration, US Department of Commerce, through the Sea Grant College Program at the University of Maine. The project title was "Repair of Wood Piles with Fiber Reinforced Composites".

TABLE OF CONTENTS

LIST OF TABLES

LIST OF FIGURES

Chapter 1

Executive Summary

1.1 Introduction

Piles made of treated wood have been traditionally used for the construction of piers and other waterfront structures. The main concern related to wood piles is deterioration due to marine borers, which limits the lifespan and requires frequent repair and replacement. Furthermore, since the use of preservative treatments for wood piles has been reduced due to environmental concerns, there is a current need for efficient methods for wood pile protection.

The objective of this thesis is to develop an efficient method for protection and structural restoration of deteriorated wood piles in situ. The method utilizes fiber-reinforced polymer (FRP) composite shells or sleeves that encapsulate the deteriorated wood pile section.

The present thesis is organized in eight chapters. An executive summary of the thesis is presented in this chapter. The main conclusions are summarized in the last chapter.

1.2 Assessment of Wood Pile Deterioration due to Marine Organisms

In Chapter 2 a description of the major groups of marine organisms causing significant wood pile damage is presented. These organisms are divided into two groups:

(a) fungi, and (b) marine borers. The basic physical and biological characteristics of these organisms are presented, as well as the type of damage that they cause in marine wood piles. The objective of Chapter 2 is to characterize deterioration of wood piles due to marine organisms, and to assess damage in the wood pile zones of a typical waterfront installation. Marine borer activity in Maine coastal waters was assessed through a survey directed to harbor masters correlated with historic data. In order to illustrate the type and extent of wood pile deterioration, two case studies in Maine harbors are discussed.

1.3 Repair of Wood Piles with Prefabricated FRP Composite Shells

An effective method for combined environmental protection and structural restoration of wood piles in waterfront facilities is not available. The objective of Chapter 3 was to survey the available methods for wood pile protection and structural restoration with the intent of developing an effective method. In addition to reviewing the available repair methods, a field inspection of a harbor in Maine was conducted to assess existing technologies. A wood pile repair method that utilizes bonded FRP composite shells and a grouting material is proposed. Fiber, resin, adhesive, coatings and grouting materials were systematically analyzed to deliver the required system performance. Two fabrication methods for the FRP composite shells are discussed based on the experience gained in the fabrication of laboratory prototypes. Furthermore, a step-by-step procedure amenable for field installation is proposed. Finally, a preliminary cost analysis was conducted to assess the feasibility of the proposed system.

1.4 Freeze-Thaw Resistance of FRP Composites Adhesive Bonds with Underwater Curing Epoxy

The method developed for the protection and structural restoration of wood piles requires the field placement of FRP composite pre-manufactured shells around the piling. The FRP composite shells need to be attached with an underwater curing adhesive that produces a satisfactory structural bond. The adhesively bonded shells develop "composite action" when supporting loads. The main concern for durability of the adhesive bond is the resistance to freeze-thaw cycles. To assess adhesive bond durability, single lap shear tests were performed after exposure to freeze-thaw cycles. These experiments presented in Chapter 4 served to characterize the loss of adhesive bond strength between FRP composite coupons representative of the shell material. It was found that the adhesive strength of the underwater curing epoxy tested in this work is severely reduced after exposure to freezing and thawing cycles.

1.5 Experimental Characterization of FRP Composite-Wood Pile Interface by Push-Out Tests

Structural restoration of spliced or damaged wood piles with FRP composite shells requires that shear forces be transferred between the wood core and the encasing composite shells. When a repaired wood pile is loaded, shear stress will develop between the wood pile and the FRP composite shell through the grouting material. Alternatively, shear force transfer is developed through shear connectors. The main objective of Chapter 5 was to characterize the interfaces in wood piles repaired with FRP composites shells and grout materials. Two interfaces were characterized: (a) wood pile/grout

material and (b) grout material/innermost FRP composite shell. A set of design parameters that control the response of both interfaces were identified: (a) Extent of cross-section reduction of wood pile due to deterioration (necking); (b) Type of grout material (cement-based or polyurethane); (c) Use of shear connectors, and (d) Addition of a frictional coating on the innermost shell. Push-out tests by compression loading were performed to characterize the interfaces and discriminate the effect of the design parameters. The outcome of the push-out tests was the evaluation of the shear force-slip non-linear response and the progressive failure mechanism. A set of repair systems that represent different combinations of the design parameters were fabricated and the interfaces evaluated. It was found that the combination of cement-based grout and polymer concrete overlay on the innermost shell provided the most efficient shear force-slip response. Furthermore, normalized representations of shear stress transfer at the wood/grout/FRP composite interfaces and through shear connectors were developed to aid in the design process.

1.6 Experimental Characterization of FRP Composite-Wood Pile Structural Response by Bending Tests

A special prefabricated Fiber Reinforced Polymer (FRP) composite shield or jacket was developed to repair wood piles in the field. Two types of load-transfer mechanisms between the wood pile and the FRP composite shield were developed and tested: (1) cement-based structural grout; and (2) steel shear connectors with an expanding polyurethane chemical grout. The objective of Chapter 6 was to characterize the structural response of full-size pre-damaged wood piles repaired with the FRP

composite shield system. A three-point bending test procedure was used to simulate the response of a pile subjected to lateral loads. The load-deformation response, deflected shape profile, relative longitudinal displacements (slip), strain distribution, ultimate bending moment capacity and mode of failure were evaluated. Wood piles were pre-damaged by reducing approximately 60% of the cross-section over a portion of the pile. It was found that a pre-damaged wood pile repaired using the FRP composite shield with cement-based grout exceeded the bending capacity of a reference wood pile. The repair system using the FRP composite shield with steel shear connectors and polyurethane grout did not fully restore the bending capacity of a reference wood pile; however it can be used for marine borer protection when wood damage is not critical.

1.7 Beam Model of Damaged Wood Pile Repaired with FRP Composite Shells

A beam design model was developed to predict stiffness and strength properties of wood piles restored with a Fiber Reinforced Polymer (FRP) composite shield or jacket. Two types of load-transfer mechanisms between the wood pile and the FRP composite shield were studied: (1) cement-based structural grout; and (2) steel shear connectors with an expanding polyurethane chemical grout. The design model accounts for wood pile damage by reducing the cross-section over a portion of the pile length. Laminate analysis was applied to estimate FRP composite elastic and strength properties. The model allows computation of shear forces at the interfaces between three different materials (wood pile, grout, and FRP composite shield) present in a repaired wood pile. The beam model was correlated with experimental results from three-point bending tests of pre-damaged wood

piles repaired with FRP composite shields. The model was applied to predict the maximum bending loads, modes of failure and mid-span deflections of pre-damaged and repaired wood piles. It was found that the proposed model equations have reasonable accuracy and they can be used as a design tool to determine the FRP composite reinforcement needed to restore the structural capacity of a damaged wood pile. The proposed beam model can be applied to various boundary conditions representative of actual piles in waterfront structures (e.g., fixed-free supports).

Chapter 2

Assessment of Wood Pile Deterioration due to Marine Organisms

2.1 Abstract

In this chapter a description of the major groups of marine organisms causing significant wood pile damage is presented. These organisms are divided into two groups: (a) fungi, and (b) marine borers. The basic physical and biological characteristics of these organisms are presented, as well as the type of damage that they cause in marine wood piles. The objective of this chapter is to characterize deterioration of wood piles due to marine organisms, and to assess damage in the wood pile zones of a typical waterfront installation. Marine borer activity in Maine coastal waters is assessed through a survey directed to harbor masters correlated with historic data. In order to illustrate the type and extent of wood pile deterioration, two case studies in Maine harbors are discussed.

2.2 Introduction

The problem of deterioration of wood piles due to marine organisms dates back to the early use of wood in piers and other waterfront facilities. Even though wood pile deterioration has been prevented to some extent with the use of preservative treatments, it still remains a concern. Some of the chemicals used for wood preservation have been linked to human health hazards and, therefore, their use has been restricted. For these reasons, waterfront owners are looking for alternative solutions for wood pile protection.

There are two major groups of organisms that deteriorate wood in waterfront structures. The most destructive group is marine borers; however fungi can cause significant damage over time as well. The different groups of marine organisms attack the wood in different zones of a pile. For example fungi are typically found above the waterline, while marine borers primarily attack wood in the tidal zone.

Wood-boring organisms found in salt-water that cause damage to wood piles can be classified as: (1) molluskan borers (shipworms and pholads); and (2) crustacean borers (Gribble) (Goodell 2000). Both shipworm and Gribble attack the wood piles for shelter and, in the case of Gribble, excavated wood is digested through the aid of microbial symbionts (Goodell 2000).

Studies conducted in Maine over a period of 23 years (1936 – 1959) using wood test boards revealed problems associated with shipworms during certain years and at specific geographic locations (Wallour 1959). Gribble, and specifically *Limnoria* spp. were present in Maine waters every year during the period studied and caused significant damage.

The objective of this chapter is to characterize deterioration of wood piles due to wood deterioration organisms, and to assess damage in the micro-environment zones of a typical waterfront installation. An early study on marine borer activity in Maine waters is reviewed. The results of a recent survey on wood pile deterioration in Maine harbors are discussed. Two case studies in Maine harbors that illustrate typical Gribble and shipworm damage are presented.

2.3 Review of Wood Pile Deteriorating Organisms

2.3.1 Fungi

Wood decay fungi, which contain no chlorophyll, are found growing either as parasites on living plants or as saprophytes on the dead remains of plants (U.S. Army 1978). Fungi reproduce by means of microscopic spores, which can be single or multi-cellular. Some of the symptoms of fungal decay are the following: (1) Change of color; advanced decay of wood by fungi is almost always accompanied by a change in color of the attacked wood (Cartwright and Findlay 1958; Kelly 1999), (2) Softening; the area where fungal decay has initiated appears to be soft in texture as the decay advances (Cartwright and Findlay 1958; Kelly 1999), (3) Change in density; as the wood is decayed more and more it loses mass. Wood in advance stages of fungal decay will be extremely light when the wood is dry. (4) Change in odor; wood attacked by fungi will usually have a mushroom like smell but the presence of this smell does not necessarily mean that decay is present.

Regular wood decay fungi cannot survive in salt water. However, it was found that some fungi species could grow on the above water portion of wood piles submerged in salt water. Although the damage caused by fungi on wood piles is relatively small compared to the damage caused by marine borers, such as Gribble and shipworms, it is of concern because fungal damage could prompt attack by Gribble (Cartwright and Findlay 1958). In addition, the portion of the wood pile that is in the atmospheric zone is not affected by salt water, but by fresh water coming from rain. This creates favorable conditions for the growth of conventional fungi (brown or white rot) that can cause considerable damage (U.S. Army 1978).

2.3.2 Molluskan Borers: Shipworms

One of the families of shipworms is the family of Teredinidae, which includes *Teredo* spp. and *Bankia* spp. This type of marine borer has a modified shell smaller than that of clams (Abood et al. 1995; Goodell 2000). *Teredo* is a wormlike borer with a slimy gray body (Chellis 1961; U.S. Army 1990). Modified small shells near the head form a pair of abrasive plates that are used to burrow, producing wood particles that are ingested. External evidence of attack is hard to find because small siphons are the only portions extending to the wood surface. Initially *Teredo* larvae begin excavation with a 0.5 to 3 mm diameter hole. The borer can extend its tunnel along the grain (Goodell 2000). The size of this type of marine borer varies ranging from 150 mm to 1.8 meters length and diameters up to 25 mm (Chellis 1961). The length of the tunnels depends on the extent of the attack. When the attack is extensive the tunnels become crowded and their length is limited. Tunnels are lined with a white shell-like material that can be found mixed with shavings if the wood is bored with a drill during inspection (Highley 1999). Cellulosic portions of the wood are digested with the help of bacterial symbionts. Borer activity will turn the wood into a honeycomb-like matrix, which will lead to a severe reduction in strength even though the outer shell looks sound (Goodell 2000). A picture of *Teredo navalis* is shown in Figure 2.1(a). A sketch of a *Teredo* borer is shown in Figure 2.1(b). *Bankia* spp. is very similar to *Teredo*, but is usually larger (Chellis 1961). A *Bankia* borer is shown in Figure 2.2.

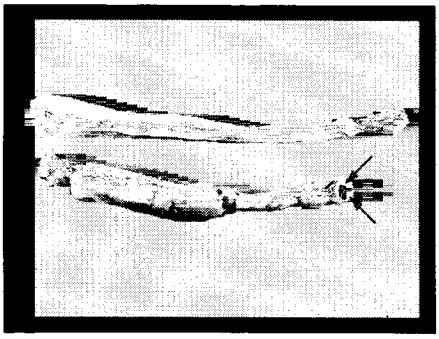

(a)

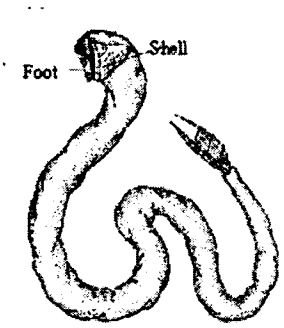

(b)

Figure 2.1 - (a) *Teredo navalis* from (Gillis and Haro 2001); (b) *Teredo navalis* Sketch from (Klekowski and Klekowski 1997)

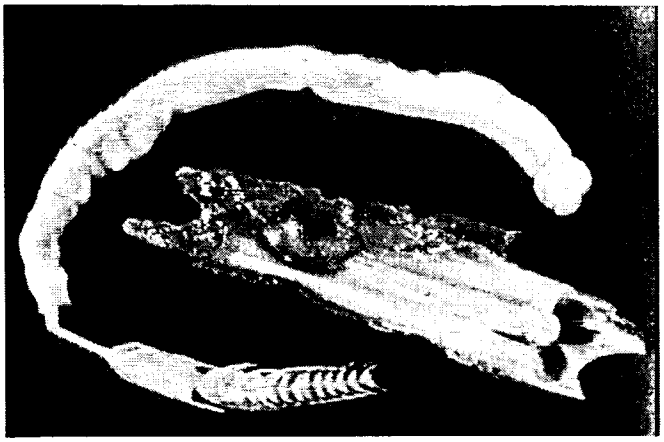

Figure 2.2 - *Bankia* spp. from (Wilson 2001)

Typical shipworm damaged wood pile sections extracted from Belfast Harbor, Maine are shown in Figure 2.3.

Figure 2.3 – Typical Shipworm Damage, Belfast, Maine

2.3.3 Molluskan Borers: Pholads

Borers, such as *Martesia* spp. and *Xylophaga* spp., belong to the pholad family. They are similar to shipworms. The adult body of pholads, unlike shipworms, remains surrounded by shells as it grows in its burrow (Highley 1999). Pholad shells do not fit tightly but they have ridges which function as rasps for burrowing. Pholads also have up to four external plates in addition to the two primary plates covering their soft body parts. When pholads die, remnants of the primary plates remain in the burrow. Although pholads are particularly aggressive in tropical waters, deepwater species can operate in cold waters causing extensive damage to wood. The length of pholad tunnels is relatively small (up to 60-70 mm) and their diameters are up to 25 mm. The tunnel opening could be smaller than the diameter of the borer (Chellis 1961; Goodell 2000). Since, pholads are usually found in waters deeper than 33 m, they are not a main concern for wood piles.

2.3.4 Crustacean Borers: Gribble

Limnoria lignorum, is one species of *Limnoria. Limnoria* spp. are also known by the common names Gribble and sea louse. Gribble resemble the wood louse and have a length between 3 and 6 mm. Their width ranges from one-third to one-half of their length. They are often slipper-shaped with horny boring mandibles, two sets of antennae and seven sets of legs as can be seen in Figure 2.4(a). Their legs are equipped with sharp hooked claws. Gribble can roll themselves into a ball, swim, crawl, and jump (Chellis 1961). Gribble can swim throughout their lives and they can leave the attacked wood to tunnel at another location. They commonly attack in coastal regions making shallow burrows in the surface of the wood (Johnson 2002) as shown in Figure 2.4(b). When large numbers of Gribble attack, only a thin layer of wood is left between the burrows. The action of the waves and tidal currents wash away these thin layers exposing new surfaces for the Gribble to attack. This causes extensive thinning of the wood section In wood piling, the damage caused by Gribble is typically greater in the tidal zone (Chellis 1961).

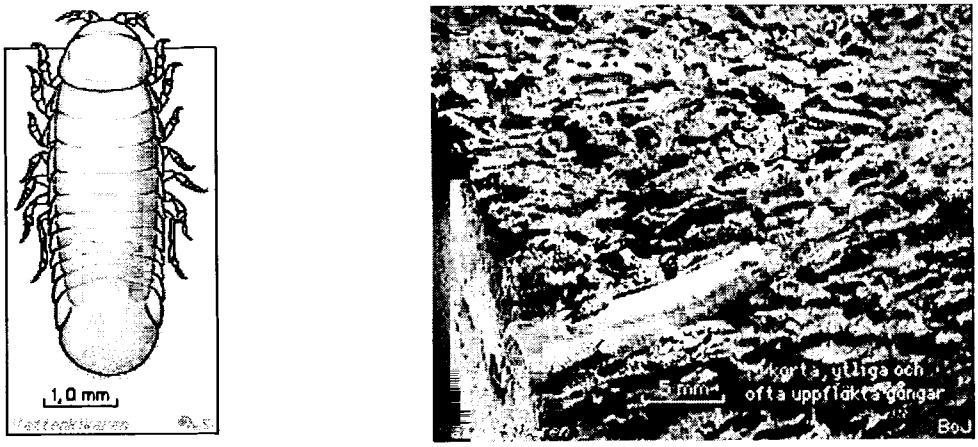

Figure 2.4 - (a) *Limnoria lignorum* from (Aquascope 2000);(b) *Limnoria* Damaged Wood from (Aquascope 2000)

2.4 Geographical Distribution of Marine Borers in U.S. Coastal Waters

The distribution of marine borers along coastal waters in the United States is depicted in Figure 2.5. The absence of certain species from a region in the map shown in Figure 2.5 does not mean that this type of marine borer cannot be found there, but simply that it does not cause significant deterioration problems (AWPA 1999b). Solid lines indicate areas in which the designated marine borers are a hazard to wood without appropriate preservative treatment. Dashed lines designate areas where periodic attacks occur. It is worth noticing that changes in environmental conditions in a given area may affect marine borer activity significantly (AWPA 1999b). Therefore, the map shown in Figure 2.5 should be used as a general guide and should be supplemented with local information.

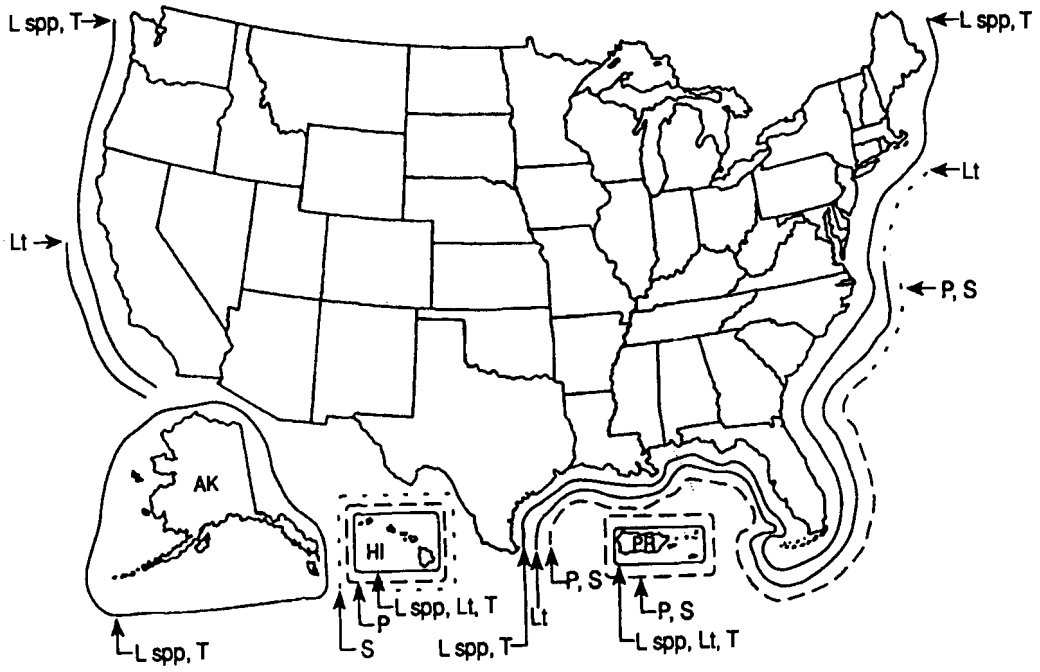

Figure 2.5 - Distribution of Marine Borer Hazards in U.S. Coastal Waters (AWPA 1999a)

Notation for Figure 2.5:

L spp – *Limnoria* species other than L. *tripunctana*, including *lingorum, quadlipunctana, pfefferi*

Lt – *Limnoria tripunctana*

T – Teredinids or shipworms, mainly species of the genera *Teredo* and *Bankia*

P – Pholads, mainly species of the genera *Martesia* and *Xylophaga*

S – Sphaeroma, pdmadly, terebrans, mainly in brackish water

2.5 Damage Zones in Wood Piles

Wood piles that support piers or other marine structures are driven into the mud and extend above to the deck or structure they support. The vertical variation of exposure conditions of the wood pile allows the creation of different micro-environment zones, as shown in Figure 2.6 (US Army Corps of Engineers et al. 2001).

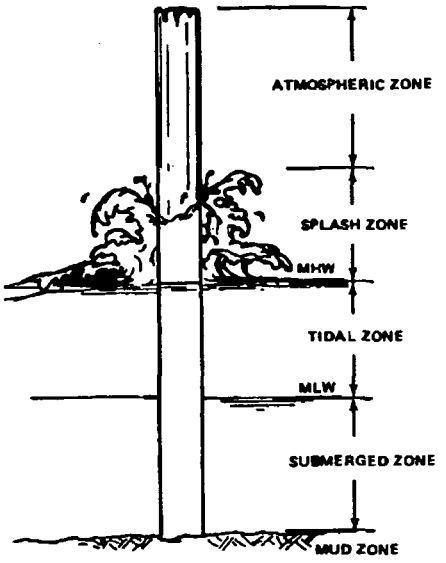

Figure 2.6 – Exposure Zones of Marine Wood Piles (US Army Corps of Engineers et al. 2001)

This exposure variation affects the type and the extent of damage produced by marine organisms. A typical damage profile in the different zones of a wood pile is illustrated in Figure 2.7(a). Similar to the case of corroded steel piles in marine structures (Coburn 2000), inspection of marine wood piles indicate the presence of five different zones: Atmospheric, splash, tidal, continuously submerged, and soil. Wood pile damage due to marine organisms in each zone is assessed.

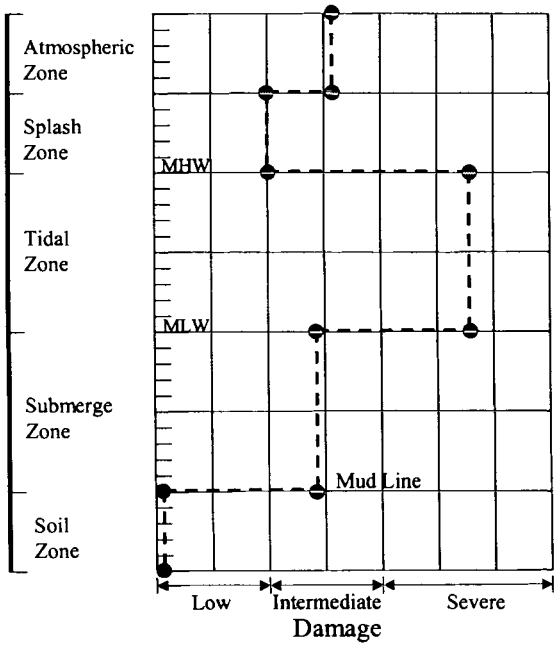

(a)

(b)

Figure 2.7 - (a) Typical Damage Profile of a Wood Pile; (b) Wood Pile at Mudline in Portland Harbor, Maine.

2.5.1 Atmospheric Zone

The atmospheric zone is the top portion of the wood pile, which is above the splash zone. This zone is accessible for maintenance and repair. In this zone, the presence of fresh water from the rain and oxygen creates a favorable environment for the growth

of fungi. Fungal spores could be inside the wood in an inert state for years. When the conditions in this zone are favorable, fungi will grow and start decaying the wood. Fungi will start decaying the wood from the inside and work their way to the outer surface. Wood piles are often vulnerable to fungal attack in their center portion because preservative treatment does not penetrate all the way into the wood section. Marine borers such as Gribble and shipworms will not attack the wood in the atmospheric zone, since they cannot survive in this environment.

2.5.2 Splash Zone

The mean high water level at the bottom and the atmospheric zone at the top delimit the splash zone. The wood pile surface is exposed to continuous water spray. This zone is accessible for maintenance and repair at low tide with some limitations. Although this zone is subjected to continued salt-water spray, it is possible for fungi to survive and damage the wood because there is adequate oxygen and the salinity is not very high. Fungal activity will probably be lower in this zone since the conditions are not the most favorable.

2.5.3 Tidal Zone

The tidal zone is delimited by the mean low water level and the mean high water level. This zone is exposed to cycles of water immersion. This zone is accessible for maintenance and repair at low tide with difficulty. The tidal zone is typically the most heavily attacked zone of a wood pile. In this zone, marine borers such as shipworms and Gribble attack the wood and cause significant damage. The conditions in this zone seem

to be the most favorable for the marine borers to flourish. The presence of salt water and oxygen is a necessity for the survival of marine borers. If the mud line is above mean low water level then the attack is most severe at the mud line. In the case of Gribble, a significant reduction in the cross section at the mud line can be observed.

2.5.4 Continuously Submerged Zone

The continuously submerged zone extends between the mudline and the mean low water level. This zone is permanently under water. If the mudline is above the mean low water level, then this zone does not exist. This zone is only accessible for maintenance and repair with cofferdams or specialized underwater techniques. Marine borers such as shipworms and Gribble can attack the wood since salt water and oxygen are available at this zone. However, the attack and the extent of damage may not be as severe as the damage in the tidal zone.

2.5.5 Soil Zone

The soil zone is the zone below the mudline. In general, this zone does not require maintenance. In this zone there is no oxygen available, which prevents the survival of marine borers. For this reason, wood piles below the mud line are generally in good condition. In Figure 2.7(b) it can be observed that above the mud line some reduction in cross sectional area occurred, but below the mudline there is no visible reduction.

2.6 Marine Borers in Maine Waters

Between 1936 and 1959 W.F. Clapp Laboratories, Inc. of Duxbury, Massachusetts monitored the marine borer activity at different locations around the United States and the world by conducting wood test board studies. An assessment of *Teredo* and *Limnoria* activity on Maine harbors was reported (Wallour 1959). The report revealed the presence of *Teredo* at specific geographical locations along the coast of Maine. In order to identify the extent of the damage caused by either *Teredo* or *Limnoria,* keys were developed for each case. The key for *Teredo* activity is shown in Figure 2.8 and the key for *Limnoria* activity is shown in Figure 2.9.

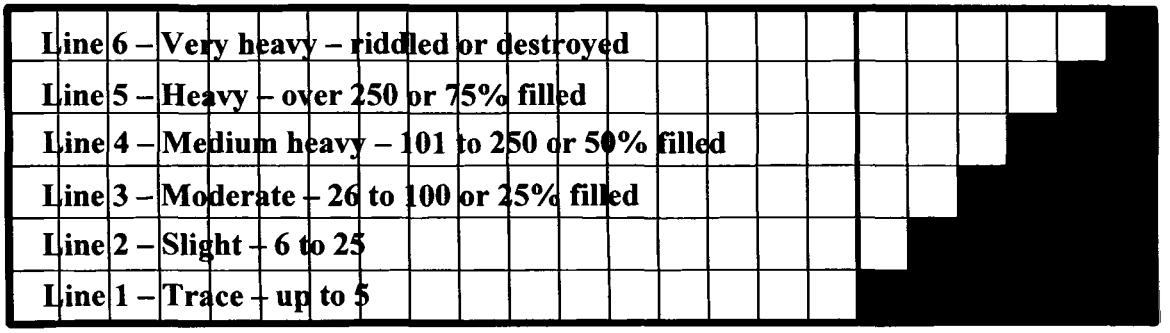

Int. - Interrupted
Disc. - Discontinued
N. R. - Not received
- Operated but showed no attack

Figure 2.8 - Key to Determine Extent of Attack to Wood Test Boards by *Teredo* (Wallour 1959)

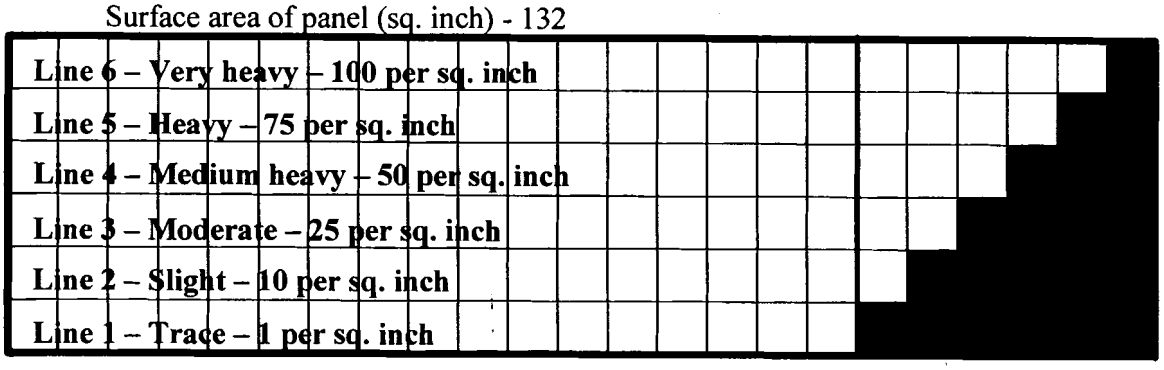

Figure 2.9 - Key to Determine Extent of Attack to Wood Test Boards by *Limnoria* (Wallour 1959)

Although, in general the presence of *Teredo* was not accompanied by severe wood board destruction, certain years showed devastating damage to the wood test boards. Medium heavy and heavy damage was reported in places such as Searsport, Rockland, Thomaston, Scarborough and Portland. Typical wood test board results for *Teredo* attack in Searsport, Maine are shown in Figure 2.10 (Wallour 1959).

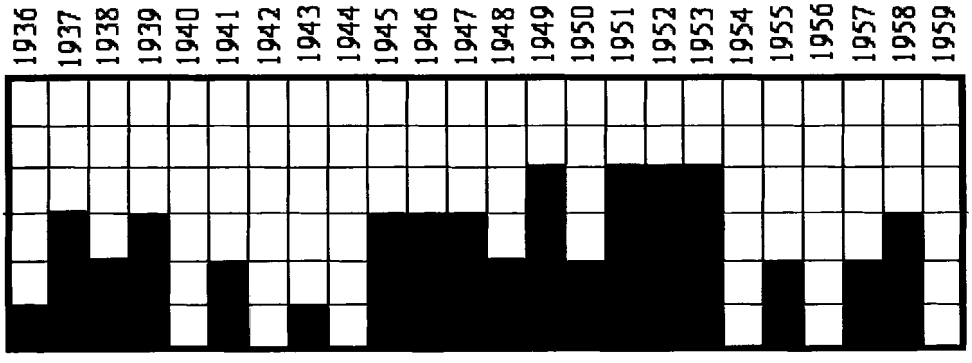

Figure 2.10 – Typical Wood Test Board Results for *Teredo*, Searsport, Maine (Wallour 1959)

On the other hand, *Limnoria* was found to be widespread in Maine waters with significant activity in places such as Southwest Harbor, Rockland, Searsport, Wiscasset and Portland. Portland was especially affected by *Limnoria* damage with the amount of attack ranging from heavy to very heavy in most cases. Typical results of *Limnoria* attack to wood test boards in Portland, Maine are shown in Figure 2.11 (Wallour 1959).

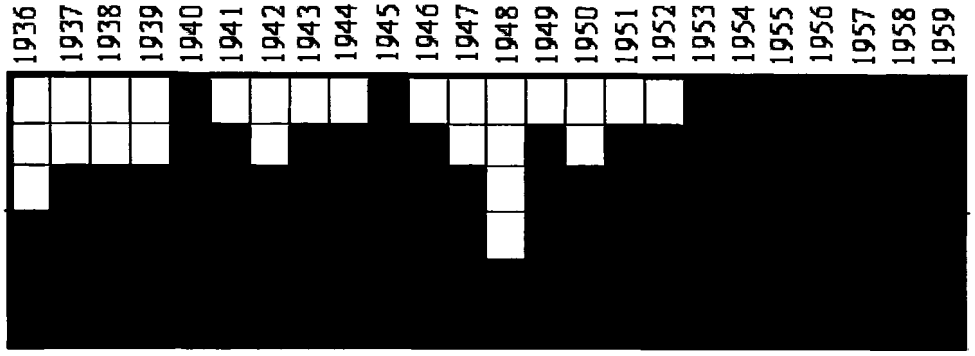

Figure 2.11 – Typical Wood Test Board Results for *Limnoria*, Portland, Maine (Wallour 1959)

A survey conducted by the University of Maine between November and December of 2000 on shipworm damage in wood piles is summarized in Table 2.1. Responses from 13 harbor masters along the coast of Maine are correlated with the response from Boston harbor. The questions addressed in Table 2.1are: (1) traditional extent of marine borer damage; (2) recent changes in the amount of marine borer attack; and (3) type of marine borer organism. The survey results revealed problems with shipworm damage in wood piles at the same geographic locations in Maine coastal waters reported 41 years earlier (Wallour 1959).

Table 2.1 - Survey Responses on Traditional and Recent Marine Borer Attacks in Maine

City or town harbor (from South to North)	Traditional extent of marine borers damage	Change in relative amount of attack in recent years	Type of marine borer
Boston, MA (out-of-state correlation)	Moderate	No	*Limnoria tripunctana*
York, ME	Non-existing	No	Unknown
Wells Harbor, ME	Non-existing	No	Unknown
Kennebunk, ME	Unknown	No	Gribble
Portland, ME	Moderate	No	*Teredo*
Falmouth, ME	Non-existent	No	Unknown
Georgetown, ME	Non-existing	No	Unknown
Wiscasset, ME	Moderate	No	Gribble
Saint George, ME	Moderate	No	*Teredo* and Gribble
Rockland, ME	Non-existing	No	Unknown
Belfast, ME	Non-existing	Yes	*Teredo*
Searsport, ME	Moderate	Yes	Unknown
Castine, ME	Non-existing	No	Unknown
Mount Desert, ME	Non-existing to moderate	No	Unknown

2.7 First Case Study: Wood Pile Deterioration in Portland Harbor, Maine

The condition of structural wood piles in Portland Harbor piers was visually inspected in May 2000. The objective of the inspection was to determine the type and extent of damage in structural wood piles. Wood pile damage in two piers was inspected during low-tide, Portland Pier (7) and Custom House Wharf (6), as shown in Figure 2.12.

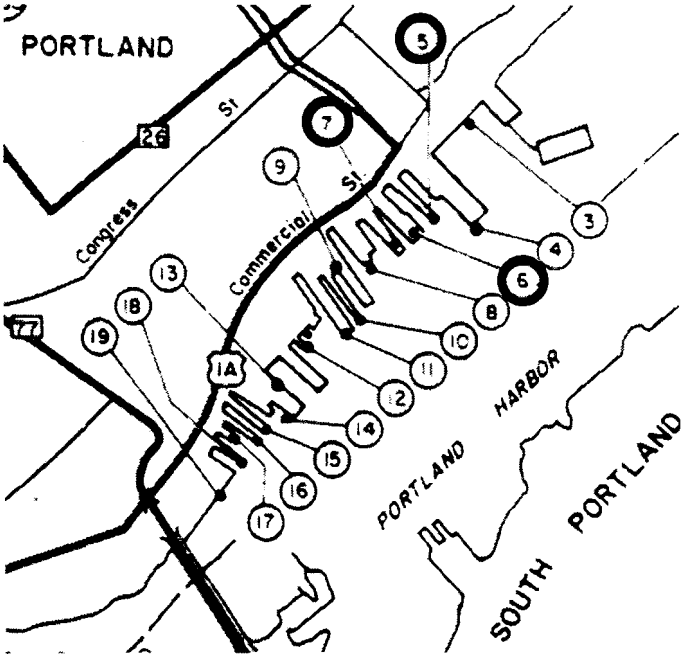

Figure 2.12 - Piers Inspected in Portland Harbor, adapted from (Maine DOT 1986)

The Portland Pier has a timber retaining wall with solid fill, wood piles and a wood deck supporting a parking lot (Maine DOT 1986). The Custom House Wharf has an earth-filled pier structure with wooden-timber and a steel crib bulkhead, wood piles and an asphalt paved wood deck. There are several marine type businesses operating on the pier (Maine DOT 1986).

Damage was observed at the Portland pier in several wood piles, as shown in Figure 2.13. In some cases, a loss of cross section (necking) up to 70 percent was observed. It was

noticed that several damaged old piles were left in place, and new wood piles were driven nearby. In other cases the damaged old piles were cut off, and a new pile portion was spliced on top.

(a) (b)

Figure 2.13 - (a) Damage by Gribble, Portland, Maine; (b) Damage by Fungi, Portland, Maine

The observations made at the Custom House Wharf were similar to the ones made at Portland Pier. Several piles had reduced cross-sections in the tidal zone between low and high tide. Other piles had extensive damage at the butt, as well. A wood pile was measured at two locations: the diameter at the butt was 254 mm and the diameter at the mud line level (1.83 m below the butt) was only 165 mm. This loss of cross section represents about 50 percent reduction in the cross sectional area. To assess the condition of a wood pile below the mud line, a hole of approximately 130 mm in depth was

excavated in the surrounding soil. Visual inspection indicated that the wood pile had no reduction in cross-section or any apparent damage below the mud line. This observation confirms previous findings on the condition of extracted wood piles from the Portland Harbor. In general, the wood pile damaged observed in Portland harbor was attributed to *Limnoria*. This finding is in agreement with an earlier report (Wallour 1959).

2.8 Second Case Study: Wood Pile Deterioration in Belfast Harbor Municipal Pier, Maine.

Structural wood piles that had been damaged by marine borers were inspected in September 2000 by a team of scientists and engineers from the University of Maine. The wood piles at Belfast harbor were untreated and had been in service for approximately one to one and one-half years.

Wood fender piles with diameters up to 380 mm that were extracted from the harbor revealed severed damage from shipworms. Typical shipworm damage to wood piles extracted from the harbor is shown in Figure 2.14.

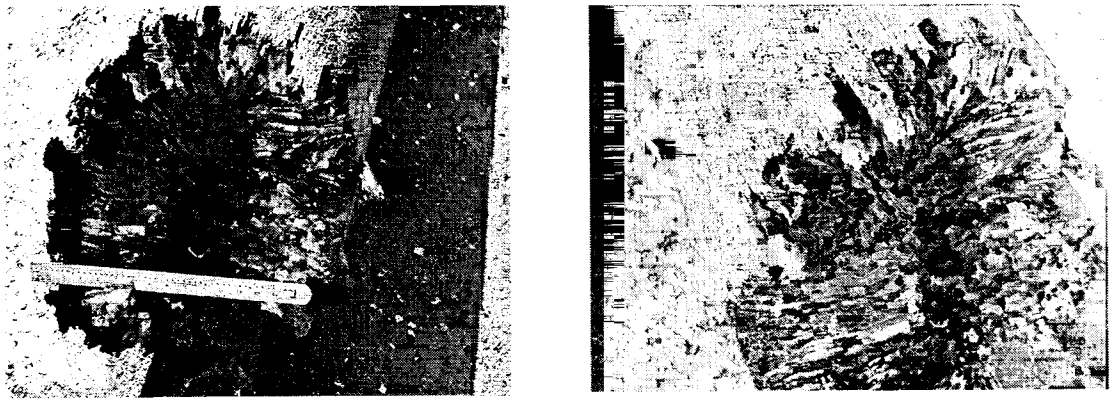

Figure 2.14 - Wood Piles with Shipworm Damage Extracted from Belfast Harbor, Maine

Although the outside appearance of the wood pile did not show any signs of deterioration, the inside was severely deteriorated. The density of the channels made by the borers indicated a very large infestation of shipworms that did not have adequate space and time to grow to their full potential nor to orient along the grain of the wood.

The short time span and the extent of the damage illustrate the importance of protecting wood piles or providing the means to repair such structures. It is worth noting that the city of Belfast replaced the deteriorated wood piles with piles made of a tropical wood, called Greenheart, which was imported from Venezuela. The exploitation of naturally-durable tropical woods for piling can contribute to global environmental concerns.

2.9 Conclusions

Based on the survey of information presented in this chapter, the following conclusions are drawn:

1. There is a serious problem with marine pile deterioration specifically in the state of Maine, and generally along the coastal waters of the United States. This problem is not new as the results from wood board tests conducted as far back as in the 1940's show. Both shipworms and Gribble were found to cause significant wood pile damage in Maine waters.
2. The presence of shipworms at specific geographic locations in Maine coastal waters and their aggressiveness contradicts the general preconception that shipworms are not active in cold waters.

3. Field observations indicate that marine borer organisms need to be characterized to understand the potential and nature of wood pile attack. Furthermore, classification of damage zones in wood piles serves not only to assess damage but also to develop a protection strategy.

Chapter 3

Repair of Wood Piles with Prefabricated FRP Composite Shells

3.1 Abstract

An effective method for combined environmental protection and structural restoration of wood piles in waterfront facilities is not available. The objective of this chapter is to survey the available methods for wood pile protection and structural restoration with the intent of developing an effective method. In addition to reviewing the available repair methods, a field inspection of a harbor in Maine was conducted to assess existing technologies. A wood pile repair method that utilizes bonded FRP composite shells and a grouting material is proposed. Fiber, resin, adhesive, coatings and grouting materials were systematically analyzed to deliver the required system performance. Two fabrication methods for the FRP composite shells are discussed based on the experience gained in the fabrication of laboratory prototypes. Furthermore, a step-by-step procedure amenable for field installation is proposed. Finally, a preliminary cost analysis is conducted to assess the feasibility of the proposed system.

3.2 Introduction

3.2.1 Scope and Objective

An effective method for both protection and structural restoration of wood piles in waterfront facilities is not available in the literature. The objective of this chapter is to

survey the available methods for wood pile protection and structural restoration with the intent of developing an effective combined method. To attain this objective, not only the literature was reviewed but also a field inspection of a harbor was conducted. A wood pile repair method that utilizes FRP composite shells and a grouting material is proposed. Materials were systematically analyzed to deliver the required system performance. Two fabrication methods for the FRP composite shells are discussed based on the experience gained fabricating laboratory prototypes. Furthermore, based on the findings of this study, a step-by-step procedure amenable for field installation is proposed. Finally, a preliminary cost analysis is conducted to assess the feasibility of the proposed system.

3.2.2 Background

Marine borers cause extensive damage to wood piling used to support piers, marinas or other waterfront structures and in many cases replacement of these pilings has been the only alternative. The use of preservative treatments prolongs the life of wood piles for many years and has previously been used extensively to protect piling in wooden waterfront structures. However, environmental concerns regarding the preservatives used for this purpose lead to restrictions in their use. For this reason some states, such as Maine, banned the use of creosote, one of the most common and most effective preservatives used for protection of wood piles from marine borers,. This, in turn, aggravated the problem of wood pile deterioration. Another preservative chemical used in wood piles, chromated copper arsenate (CCA), contains heavy metals and questions about its hazard to human health have been raised. The federal government has recently placed restrictions regarding the use of CCA preservative in residential applications. A

study on CCA leaching of treated wood piles in seawater and in fresh water estimated long-term release of chemical elements (Lebow et al. 1999).

The service life of deteriorated marine wood piles can be prolonged in some instances by repairing the pile. Repair methods include encasing of the damaged wood pile with some type of jacket or sheeting (e.g., plastic, steel or concrete), or removing the damaged portion and replacing it with a new piece that is spliced with the old wood pile. For example, a method for repairing damaged creosote treated wood piles using a wire-mesh reinforced shotcrete jacket was proposed (Chellis 1961). A method for ground repair of wood poles involving screwing a metal sleeve around the base of the pole and filling the space between the sleeve and the pole with aggregates and resin was presented (Douglas 1986; Shepard 1987).

The Unified Facilities Criteria (UFC) handbook for operation and maintenance of waterfront facilities presents various repair methods for damaged wood piles (US Army Corps of Engineers et al. 2001). The first method discusses protection of wood piles by wrapping them with polyvinyl chloride or polyethylene wraps. Method two discusses partial posting of a damaged wood pile by joining a new pile butt with bolted pretreated timber fish plates. The third method discusses repair of wood piles by concrete encasement. Two types of forms can be used: (a) Flexible form (Sea form fabric form) and (b) Split fiberboard forms. These forms have no structural significance but they are used to keep the concrete contained until it hardens. The fourth method discusses repair or retrofit of timber piles with an underwater curing epoxy and fiber reinforced wraps. The fabrics are saturated with the epoxy and then applied to the wood pile. The fifth repair strategy discusses replacement of the damaged wood pile with a new wood pile.

The sixth repair strategy discusses replacement of the damaged wood pile with a new concrete pile.

3.2.3 Available Methods for Protection of Wood Piles

One strategy for protection of wood piles from marine borer attack is encasing new piles with a plastic wrap or jacket (Baileys 1995; U.S. Navy 1987). Most of the methods available are only suitable for protection and provide no structural restoration capabilities. Therefore, they can only be used to protect new pilings, or pilings with minimal damage and adequate structural properties. Master Builders, Inc., of Cleveland, Ohio, developed a process (A-P-E, Advanced Pile Encapsulation) for protection of piles, risers, jackets and other marine structures. This method employs a molded fiberglass outer jacket that is used as a form for containing the grout. The grout used in this process, an aggregate epoxy mix, is pumped through injection ports from the bottom up (Doyle Publishing 1996; Master Builders 2001). This method uses an epoxy grout that is usually expensive and a non structural fiberglass jacket that is expensive and offers no structural restoration. Tapecoat Company, of Evanston, IL, developed a modular encapsulation system that provides protection to marine structures. The product trade name is TC Enviroshield and the series T is used for wood piles. This system consists of a flexible outer jacket that wraps the pile and restrains the flow of water. This system is reported to lower the dissolved oxygen content of the water inside the wrap, which prevents marine borers from attacking the wood pile (Doyle Publishing 1996; Tapecoat 2001). This product can only be used to protect structurally sound wood piles but not to restore structural capacity. Denso North America, of Houston, TX, also developed a line of

products used for protection of wood piles. These include the Denso's SeaShield Series 100 that encapsulates the pile and seals out oxygen and water providing protection from marine borers for timber piles. Denso also developed jackets, trade names SeaShield Fab-Form and Poly-Form, which are used as forms for concrete or epoxy encasement to structurally restore wood piles (Denso North America 2000; Doyle Publishing 1996). These jackets and encasements have no structural significance and cannot be used to repair deteriorated wood piles. Rockwater Manufacturing Corp. developed a marine pile system for marine borer protection of wood piles. This system is very similar to the other systems available in the sense that it is reported to reduce the oxygen levels of the water inside the wrap. The company also provides fiberglass pile jackets, that when used with underwater grouts, can provide structural support (Doyle Publishing 1996; Rockwater 1999). The wraps and fiber glass pile jackets are non structural and they can not be used for wood pile restoration. Osmose Marine, based in Griffin, GA, developed a protection system for marine piles using a polyvinyl chloride (PVC) wrap, trade name Pile-Gard, which creates an airtight seal. This product, which reportedly limits the oxygen supply to marine borers, was invented in the 1950's and therefore has a long history of protecting piles (Doyle Publishing 1996; Liddell 1967; Osmose 2001). This method can only be used to protect undamaged wood piles or wood piles that have adequate structural capacity, since the method does not provide structural restoration.

3.2.4 Available Methods for Structural Restoration of Wood Piles

Hardcore Composites of New Castle, DE, developed a method, tradename Hardshell System, which is reported to protect as well as repair and restore timber piles.

This system uses E-glass / vinyl ester composite shells fabricated by the vacuum assisted resin transfer molding (VARTM) process. The shells are manufactured in two halves and they are joined using bonded "H" connectors. The "H" connector is a female-male type of connector in which one of the half shells has the female end and the other acts as the male. Adhesive is applied to the female portion of the seam and straps are used to hold the two pieces together until the adhesive cures and the grout is pumped (Hardcore Composites 1999; Hardcore Composites 2000). The fact that the bond area of the "H" connector is relatively small raises doubts about the ability of the system to provide structural continuity in the circumferential direction. The second company that has a system that rehabilitates wood piles is Fyfe Co. L.L.C., also known as "The Fibrwrap™ Company", based in San Diego, CA. This repair method uses a fabric reinforcement that is wrapped around the pile and then impregnated underwater with an epoxy resin providing a barrier against marine borers (Fyfe 1998). Since the fabric reinforcement impregnation is performed underwater, after the epoxy cures, the portion that is repaired is sealed from the surrounding environment. Impregnation of the fabric reinforcement underwater is difficult to execute and monitor. Even if the fibers are impregnated before they are introduced into the water, the resin may not cure properly.

3.3 Assessment of Existing Wood Pile Repair Methods in Portland Harbor, Maine

The condition of structural wood piles, repaired using various methods in Portland Harbor piers, was visually inspected in May 2000. The objective of the inspection was to assess methods currently used to repair damaged wood piles. Wood pile repair methods

in three piers: Portland Pier (7), Custom House Wharf (6) and Maine Wharf (5), were inspected during low-tide, as depicted in Figure 3.1.

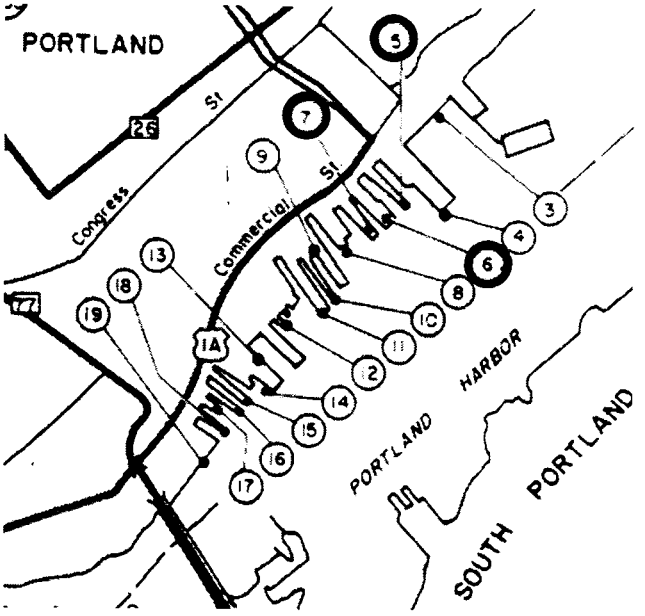

Figure 3.1 - Piers Inspected in Portland Harbor, adapted from (Maine DOT 1986)

The Portland Pier has a timber retaining wall with solid fill, wood piles and a wood deck supporting a parking lot (Maine DOT 1986). The Custom House Wharf has an earth-filled pier structure with wooden-timber and a steel crib bulkhead, wood piles and an asphalt paved wood deck. There are several marine-type businesses operating on the pier (Maine DOT 1986). The Maine Wharf pier has wood piles with a concrete deck (Maine DOT 1986).

3.3.1 Inspection of Portland Pier

The wood pile repair method used in this pier consisted of a corrugated (profile wall) high-density polyethylene (HDPE) pipe encasing (See Figure 3.2(a)). The corrugated HDPE pipe was split in two halves, which were placed around the wood pile and held

together with circumferential metal straps. The metals straps were spaced approximately 910 mm to 1220 mm. The space in-between the wood pile and the corrugated HDPE pipe was grouted with un-reinforced concrete. Typical dimensions of the corrugated HDPE pipe used were 686 mm for the external diameter and 584 mm for the internal diameter. The thickness of the corrugated profile wall was 51 mm. Several problems of this repair method were observed in individual piles: 1) The steel straps were cut and the corrugated HDPE pipe halves were opened as shown in Figure 3.2(b); 2) Wood damage was observed at pile sections above the repaired area; 3) The concrete fill was deteriorated and disintegrated with relative little effort; and 4) At the opened joint of the corrugated HDPE pipe the concrete was spalling and exposing the interior wood pile.

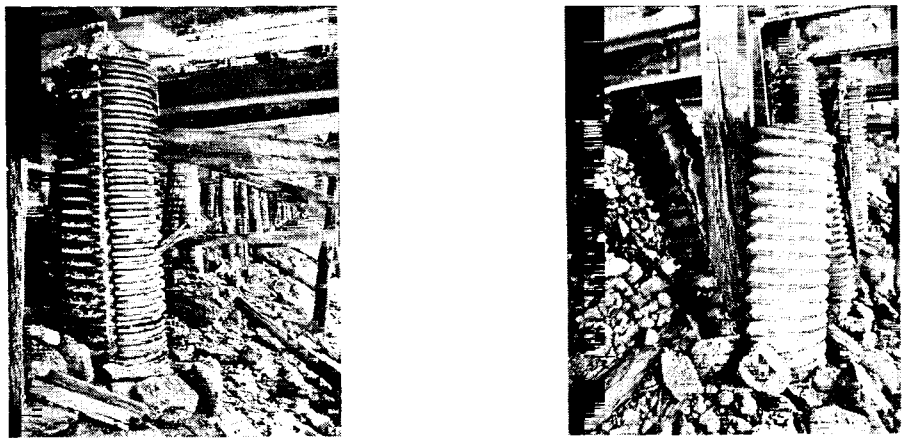

(a) (b)

Figure 3.2 - Repair Method using Corrugated HDPE Pipe Encasing: (a) Repaired Wood Pile; and (b) Failure of HDPE Pipe Encasing

3.3.2 Inspection of Custom House Wharf

Attempts to repair damaged wood piles were made on this pier, as well. The same repair method used at Portland Pier was used in this pier. However, some of the corrugated HDPE pipes were placed as a continuous section and not as two halves. This implies that the old pile was probably cut off and a new portion was connected to the old pile, encased with the corrugated HDPE pipe and grouted with concrete. The use of a continuous corrugated HDPE pipe eliminated the problem of concrete spalling observed at the joints. The wood piles at this structure were of smaller size and therefore a smaller size corrugated HDPE pipe was used (exterior diameter of 533 mm, interior diameter of 457 mm and corrugated wall thickness of 38 mm). According to one of the workers in the business operation in the pier, the wood pile repairs were performed two years earlier.

Another type of wood pile repair method observed was splicing. In this method the top portion of the old damaged pile was removed and a new wood pile portion was spliced using steel bolts, as shown in Figure 3.3.

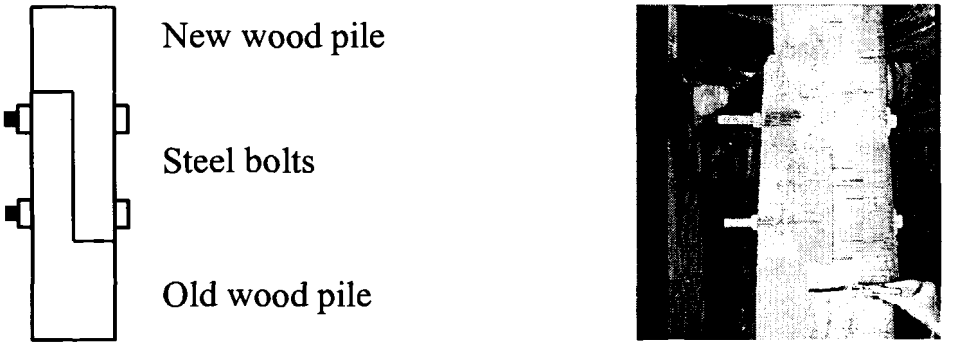

Figure 3.3 - Splicing of Wood Piles with Steel Bolts

For a wood pile with an approximate diameter of 254 mm, the steel bolts were spaced 203 mm apart. A problem that was observed in the splices was a gap between the

horizontal surfaces of the two wood pile portions, which does not allow for proper vertical load transfer by bearing. The splice also allows water to contact the untreated center of the wood pile.

3.3.3 Inspection of Maine Wharf

At the Maine wharf, repair methods were also applied to several damaged wood piles. Several piles were repaired using splicing, as shown in Figure 3.3. Corrugated HDPE pipes were also used at this facility. The pipes were placed around the pile in two halves and metal straps were used to hold them together. At the vertical joints metal plates were used to close the gap and contain the concrete. The concrete was in good condition. A combination of corrugated HDPE pipes and the splicing method with steel bolts was observed. Part of the splice length was buried in concrete and part was exposed as shown in Figure 3.4.

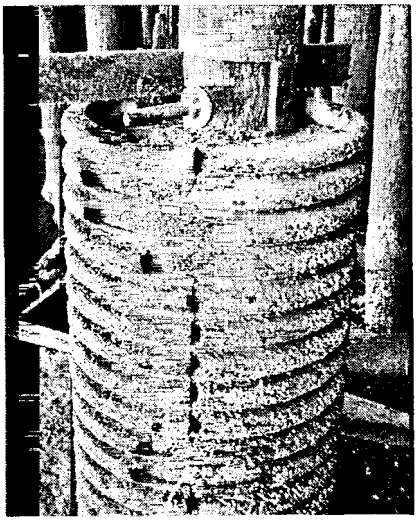

Figure 3.4 - Repair Method using of HDPE Pipe Encasing and Splicing with Steel Bolts.

3.4 Proposed Repair Method using FRP Composite Shells

The available protection or restoration methods have limited applicability in most cases. Plastic wraps can protect against marine borers but cannot be used to restore structural capacity. Steel jackets can corrode especially in the marine environment and concrete encasement can develop problems with spalling. Fiber reinforced composite jackets that are installed in halves with an "H" connector have limited bonded area and premature failure of the bond is possible. Impregnation of the fibers underwater can be difficult and proper curing of the resin may not be achieved.

The proposed wood pile repair method utilizes a fiber-reinforced polymer (FRP) composite encasement, or shield, that encapsulates and splices the deteriorated portion of the pile. The encasement was developed based on experience with appropriate technologies in the structural FRP composites (Kshirsagar et al. 2000; Lopez-Anido 2000a; Lopez-Anido 2000b; Lopez-Anido and Xu 2002) field combined with the needs for wood pile reinforcement and protection observed in the field observations, survey, and literature review The shield is made of bonded thin and flexible FRP composite cylindrical shells that deliver the required strength to repair damaged wood piles. The cylindrical shells had a slit or opening along their length, which enabled them to be opened and placed around the deteriorated wood pile. Since it was advantageous to encase the pile with a series of overlapping shells, the minimum number of FRP composite shells required is two; however additional shells can be added depending on the structural restoration needs. The slit of each cylindrical shell is staggered to avoid lines of weakness through the entire shield (See Figure 3.5).

In the proposed method, the space between the FRP composite shield and the wood pile is filled with a grouting material. The grouting material does not provide a structural bond with the wood pile but rather provides interlocking (friction) between the wood pile and the FRP composite shells. Since the grout is not expected to completely seal the wood core, seawater saturates the pile creating a layer of stagnant water, potentially with limited oxygen supply.

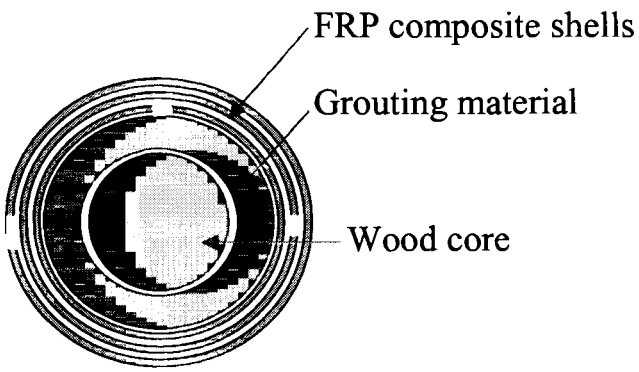

Figure 3.5 – Cross-Section of Wood Pile Repaired with FRP Composite Shells

Assuming a lack of oxygen, marine borers already inside the wood pile would be expected to die and new borers would be prevented from attacking the wood pile. A schematic of the proposed repair system is depicted in Figure 3.6.

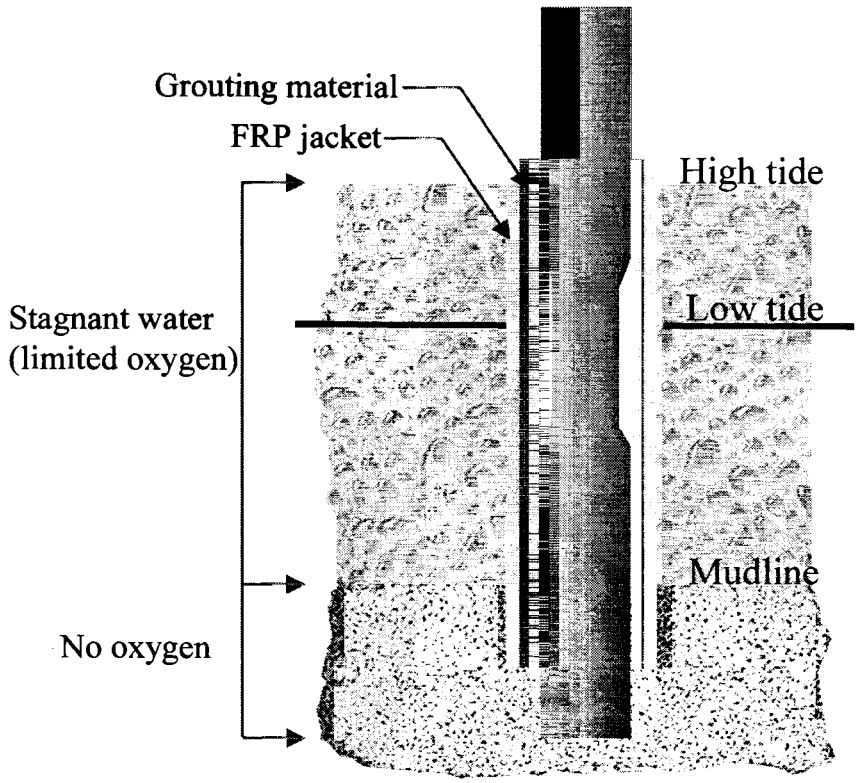

Figure 3.6 – Schematic of Wood Pile Repair with FRP Composite Shells

FRP composite shells need to be driven 0.3 to 0.6 meters below the mud line to avoid secondary attack by marine borers (Baileys 1995; Chellis 1961). Extending the FRP composite shells 0.6 m above the high water level could prevent secondary attack by marine borers in the splash zone (Baileys 1995; Chellis 1961). The proposed structural restoration method utilizes the un-damaged zone of the existing wood pile by encasing and splicing the damage portion plus the required development length (i.e., partial length reinforcement).

3.5 Material Selection - Prototype Development

3.5.1 FRP Composite Shell

A unidirectional woven E-glass fabric with a weight of 880 g/m^2, trade name VEW 260, was selected as the primary continuous reinforcement. The fabric reinforcement is delivered in rolls with a width of 1.22 m and an approximate weight of 105 kg. This type of fabric reinforcement was selected because of adaptable directional properties (e.g., continuous fiber reinforcement in selected orientations), ease of fabrication (e.g., cutting and placement) and cost competitiveness. This particular fabric, depending on the fiber architecture that was developed, provides most of the strength in each direction that is placed. The amount of reinforcement in each direction depends on the loading and therefore the stresses imposed on the part. Chopped Strand Mat (CSM) weighing 305 g/m^2, trade name MAT 113, was used as secondary non-continuous and randomly oriented reinforcement.

The proposed fiber architecture for the FRP composite shell consisted of three layers of unidirectional continuous fabric reinforcement in the longitudinal or axial direction (0°), one layer of unidirectional continuous fabric reinforcement in the hoop or circumferential direction (90°), and two outer CSM layers (See Figure 3.7).

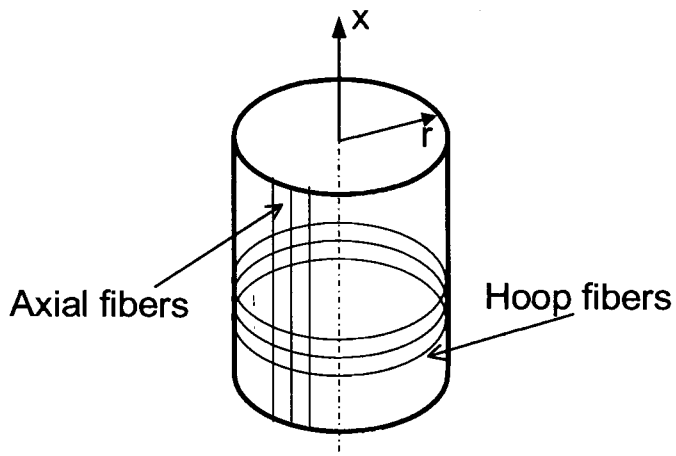

Figure 3.7 - Fiber Reinforcement of FRP Composite Shell

The fiber architecture design is based on maximizing fiber reinforcement in the axial direction with a minimum amount of fibers oriented in the hoop direction. Axial fiber reinforcement contributes to both bending and axial stiffness and strength of the shell, which is required to splice the damage portion of the wood pile. Hoop fiber reinforcement provides adequate integrity to the flexible shell with the required shear strength and mechanical fastener support. One CSM layer was placed on each face of the shell laminate to provide improved bonding to the substrate and to develop a resin rich area for environmental protection. The resulting laminate lay-up of the FRP composite shell is [CSM, 0, 90, 0, 0, CSM] (See Figure 3.8).

A low viscosity epoxy-based vinyl ester resin, Derakane 411-C50, was selected as the matrix for the composite shells (Dow 1999). The epoxy-based vinyl ester resin was selected because of its high flexibility and impact resistance, its lower cost compared to other resin systems, such as epoxies, and its good performance in harsh marine environments. This resin has a viscosity of 0.15 Pa.s and is well suited for SCRIMP^{TM}

processing. The high flexibility and impact resistance allows the manufactured part to easily absorb impact loads from approaching vessels.

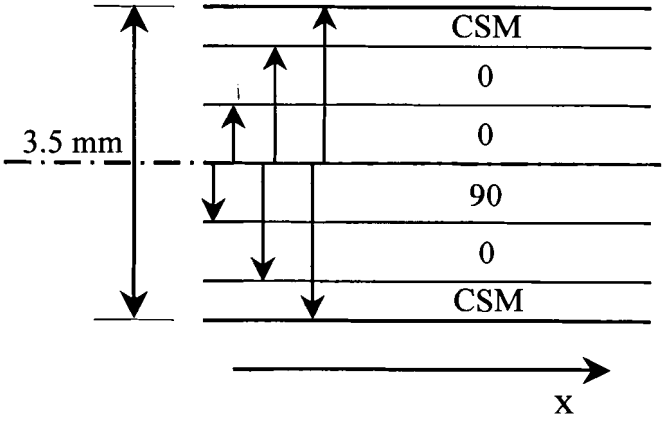

Figure 3.8 - FRP Composite Shell Laminate Lay-Up

3.5.2 Grouting Systems

The criteria used to select the grouting system were: (a) ability to be applied underwater, (b) pumping ability, (c) minimal shrinkage, (d) commercial availability, and (e) cost competitiveness. Research conducted on concrete columns suggests that the grout material used has fewer voids when pumped from the bottom up, rather than dropped from the top (Snow 2000). Two different types of grouting systems were selected and evaluated: (1) cement-based structural grout, and (2) expanding polyurethane chemical grout.

The cement-based grout can be pumped in place using conventional concrete pumps and cures underwater (Five Star 2001; NBEC 2000). This grout has minimal shrinkage and high compressive strength at early stages. The typical, one day,

compressive strength of this material at 23^0C is 35 MPa, while at twenty-eight days it reaches compressive strengths up to 52 MPa.

The expanding polyurethane chemical grout, trade name SikaFix HH, is a two-part material system: component A is the polyurethane and component B is an accelerator (Sika 1998). This grout is a fluent material and can be easily pumped to place. The curing reaction is triggered when the grout comes in contact with moisture, with less than one hour curing time. The polyurethane grout system results in a flexible layer with high-energy absorption capabilities. However, the polyurethane grout does not have any significant compression or bearing strength and, therefore, is non-structural. The cost of the polyurethane grout is relatively high compared to the cement-based grout.

3.5.3 Underwater Curing Adhesive

An underwater curing adhesive was required to bond the FRP composite shells together and provide "composite action". The selection criteria for the adhesive were: (a) ability to cure underwater, (b) ability to be applied underwater, (c) ability to bond well to vinyl ester composites, and (d) durability in waterfront environments (See Chapter 4). The adhesive selected was Hydrobond 500: an underwater curing two-part epoxy adhesive: part A is the epoxy resin and part B is the hardener (Superior Polymer 2000). Part A, which is modified Bisphenol-A Polyglycidyl Ether, is a viscous light amber liquid with mild odor that comes in various consistencies. Part B, which is a modified Polyamine, is a viscous liquid with a fishy odor and comes in various colors and consistencies. Blue color was selected for the pile repair application because it is visible through the FRP composite shells and, therefore, it was possible to visually inspect the

adhesive spread area between shells. For underwater applications, a paste consistency applied with a trowel is recommended. In the laboratory prototypes, the adhesive was applied around the circumference and along the length of the FRP composite cylindrical shells covering all the contact area between two shells.

3.5.4 Polymer Concrete Coating

A polymer concrete coating or overlay was required to develop friction between the FRP composite shell and the cement-based structural grout. The polymer concrete selected, trade name T-48, is a two-component low modulus polysulphide epoxy-based wearing course (TRANSPO 2000). Components A (resin) and B (hardener) are mixed in a 2:1 volume ratio. The selected polymer concrete is an impervious overlay that is typically used for restoring bridge decks and other pavements and applied with a thickness of 6 to 12 mm. (TRANSPO 2000) In the wood pile repair application a polymer concrete layer with a thickness of 3 mm was applied on the interior surface of the innermost shell. First, the epoxy was applied using rollers and then standard basalt sand was broadcast as the aggregate. The epoxy bonded well to the vinyl ester composite shell. The aggregate created a rough surface, which provided adequate interlocking with the cement-based grout. It was found that the shear strength at the interface between the cement-based grout and the innermost FRP composite shell was highly increased due to the polymer concrete coating (See Chapter 5).

3.6 Fabrication of FRP Composite Shells

The first manufacturing process used to fabricate the FRP composite cylindrical shells with the longitudinal slit was wet lay-up with vacuum bagging compaction. In this fabrication process the fabric reinforcement is impregnated with resin, placed on the mold, sealed using a plastic bag and compacted by drawing a vacuum. The vacuum pressure also removes part of the excess resin from the part into the breeder/bleeder layers. One problem found with this fabrication method was the limited pot life of the resin used, i.e., when long shells were manufactured the resin gelled before all of the fabric reinforcement layers were impregnated. This fabrication process delivered a composite shell with relatively low fiber volume content and a consolidated thickness of approximately 4.5 mm. The relatively high thickness of the consolidated part was an obstacle for installation, since the cylindrical shell lacked the required flexibility to let one worker open it around a wood pile.

To overcome the fabrication problems encountered, a variation of the Vacuum Assisted Resin Transfer Molding (VARTM) process, the licensed Seemann Composites Resin Infusion Process (SCRIMP^{TM}) (TPI 2001), was selected for fabricating the FRP composite cylindrical shells with the longitudinal slit. A polyvinyl chloride (PVC) pipe rated for 900 kPa internal pressure was used as a mold or tool. The fabric reinforcement was placed on the cylindrical mold dry (See Figure 3.9). Then, the fabric reinforcement was sealed with a tubular vacuum bag (See Figure 3.10).

Vacuum pressure of –102 kPa was applied with a vacuum pump and resin was infused through a resin pot. The pressure differential between the atmosphere and the applied vacuum allowed infusion of the resin into the fabric reinforcement lay-up. Once

the resin completely impregnated the fiber reinforcement, the vacuum pressure was reduced to –51 kPa until the resin gelled. The vacuum pressure debulked (compacted) the dry fiber reinforcement. After the resin gelled, vacuum pressure was removed and the part was allowed to cure. A cured partially exposed cylindrical shell is shown in Figure 3.11. The FRP composite shell was then removed by pulling open the longitudinal slit.

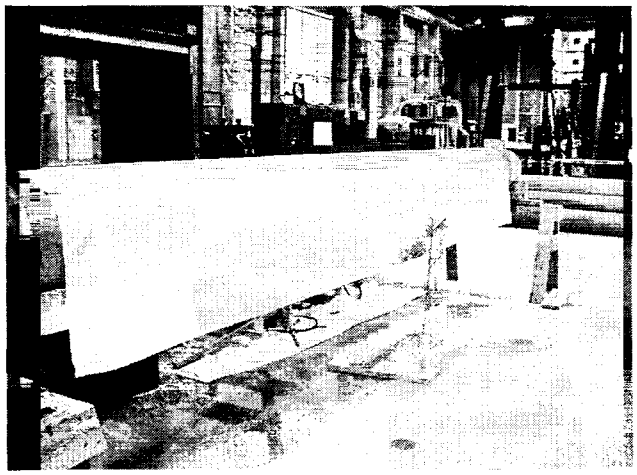

Figure 3.9 - Dry Fabrics and Peel Ply on the PVC Mold

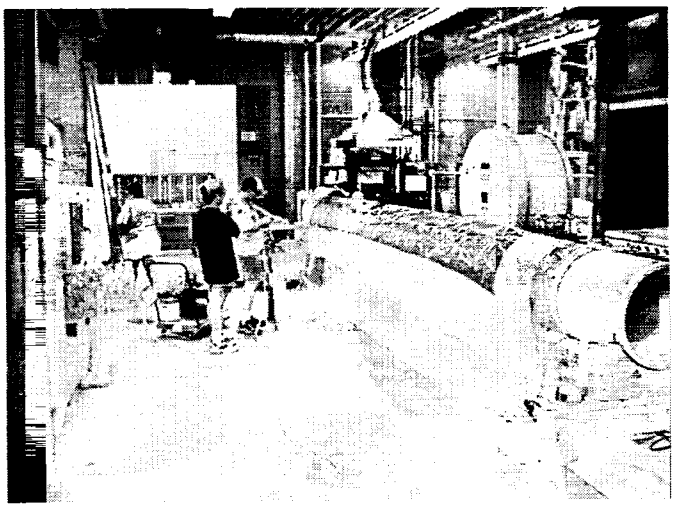

Figure 3.10 - Tube Vacuum Bag Placed over the System

The SCRIMP™ process delivered FRP composite shell with relatively high fiber volume content, and a consolidated thickness of approximately 3.3 mm. The shells fabricated by the SCRIMP™ process had adequate flexibility to be pulled open and placed around the wood pile prototypes.

Figure 3.11 – De-molding of Cured FRP Composite Shell

The FRP composite shields are expected to be exposed to ultraviolet radiation (UV), where the weathering effects are expected to be more important in the piles located on the perimeter of the waterfront facility. Weathering and UV protection of the FRP composite shells can be efficiently attained with a surface layer containing a pigmented gel coat or by incorporating an UV inhibitor as an additive to the polymer matrix (Haeberle et al. 2002).

3.7 Laboratory Prototypes - Fabrication

The feasibility of the repair method was demonstrated in the Laboratory by fabricating FRP composite shells and restoring "damaged" wood pile prototypes (See Figure 3.12).

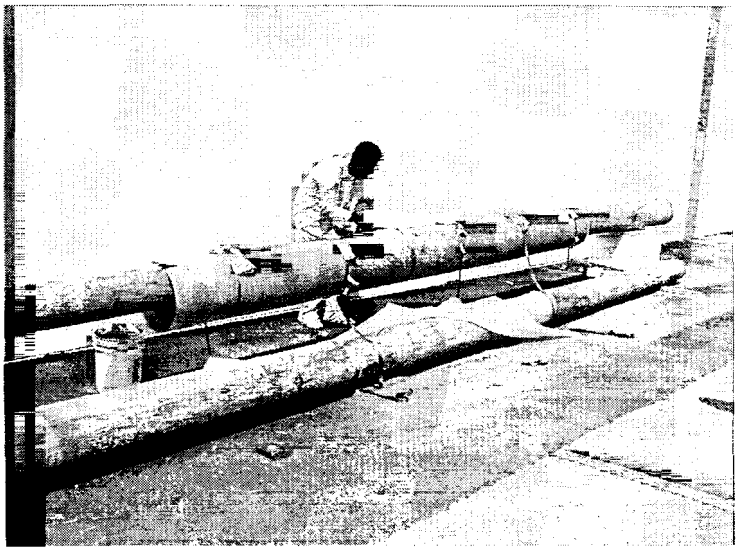

Figure 3.12 - Application of FRP Composite Shells to a Pre-Damaged Wood Pile

Marine borer damage was simulated by reducing the cross sectional area of the pile. The space between the wood core and the FRP composite shells was filled with a grouting system. Two different grouting materials were used: (1) Portland cement-based (inorganic) structural grout (See Figure 3.13); and (2) Polyurethane-based (organic) non-structural grout with shear connectors that transfer loads from the wood pile to the FRP composite shells (See Figure 3.14).

Laboratory prototypes were fabricated for two types of experiments: (1) Push-out tests by compression loading to characterize the interface response (wood/grout/FRP

composite) (Figure 3.15), and (2) Full-size bending tests to characterize the overall structural response (Figure 3.16).

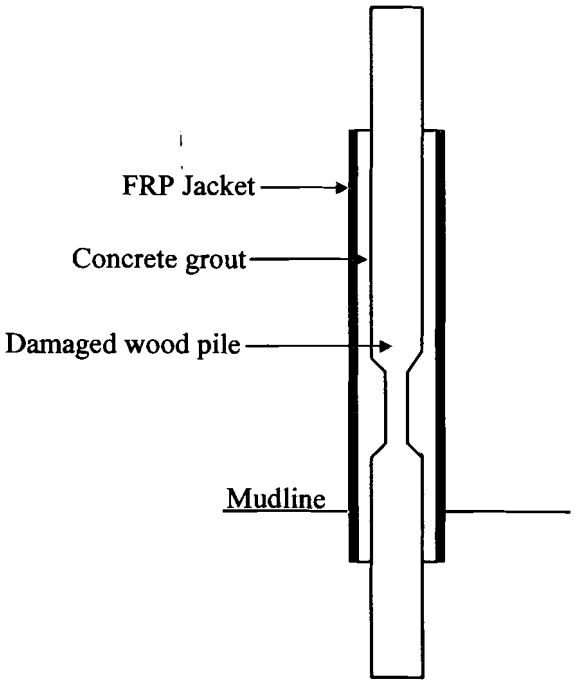

Figure 3.13 - Repair System B with the Cement-Based Grout

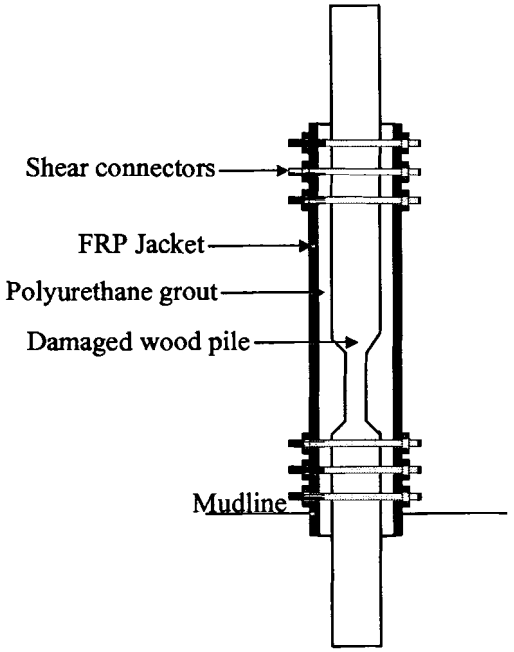

Figure 3.14 - Repair System C with the Polyurethane Grout and Shear Connectors

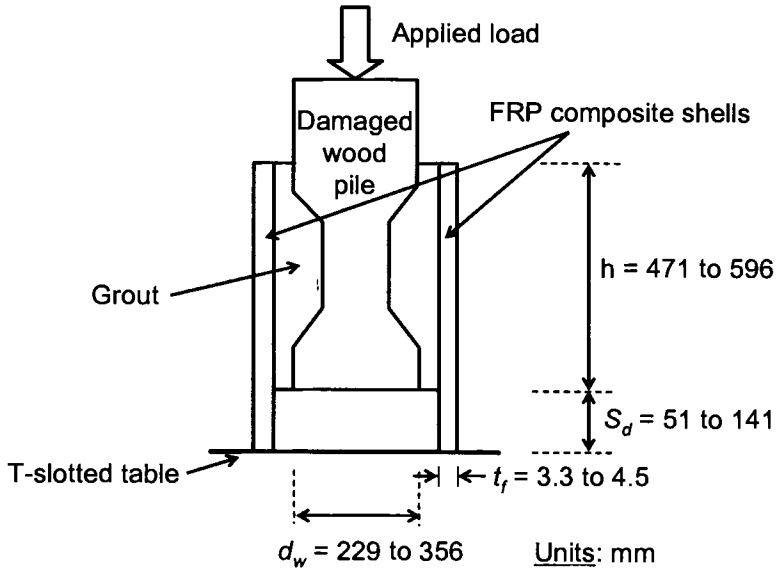

Figure 3.15 - Push-Out Test Configuration

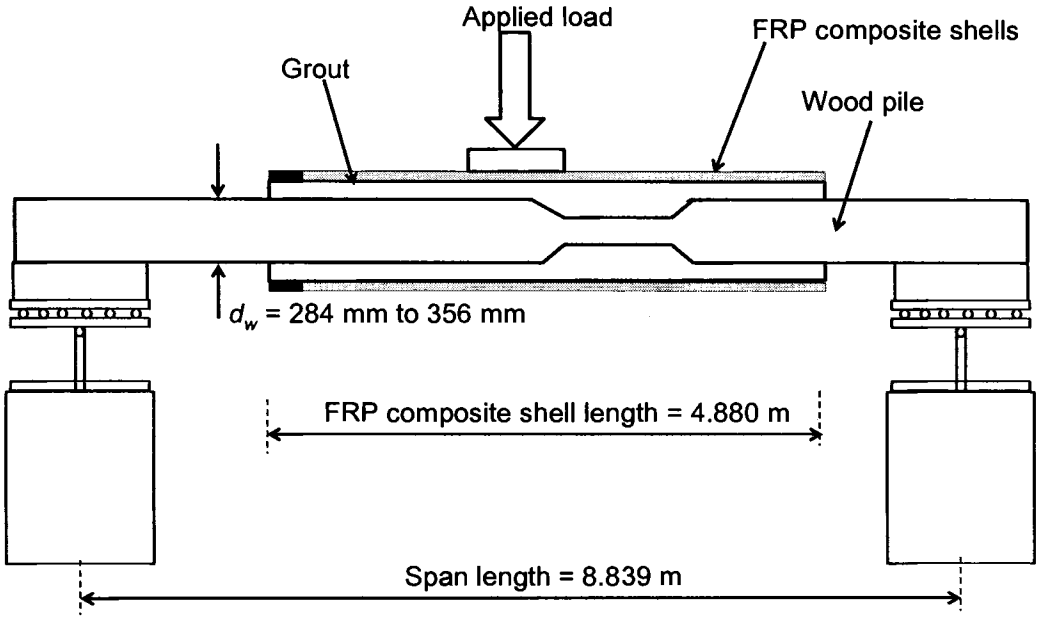

Figure 3.16 - Full Size Bending Test Configuration

3.8 Installation Procedure

To implement the repair method in waterfront applications, a possible step-by-step installation procedure was developed and is presented next.

3.8.1 Step 1: Clean the old wood pile

Wood piles usually have marine organisms growing on them. Even though good bonding between the grout and the wood core is not expected to be achieved, cleaning will be helpful. The marine organisms are organic matter and their presence creates voids in the grout, making it weaker and reducing the interlocking that is required for the repair system to work efficiently. Cleaning can be performed using a water jet without excessive pressure (US Army Corps of Engineers et al. 2001). Excessive pressure can cause more damage to the already vulnerable wood pile. Cleaning can also be achieved by scrapping off the marine organisms with a modified scraper that conforms to the shape of the wood pile (Hardcore Composites 1999).

3.8.2 Step 2: Place shear connectors at the wood-grout interface

If shear connectors, such as lag screws, at the wood-grout interface are required, then they have to be driven in the wood pile deep enough to be effective. The connectors need to extend as much as the thickness of the grout to serve as spacers.

3.8.3 Step 3: Position the first FRP composite shell around the wood pile

The longitudinal slit along the length of the FRP composite shell is opened and the shell is placed around the damaged wood pile.

3.8.4 Step 4: Apply adhesive on first shell

A coat of underwater epoxy adhesive is applied on the interior surface of the second shell and on the exterior surface of the first shell, if possible. The use of trowels is recommended to help spread the adhesive.

3.8.5 Step 5: Position the second shell

The second shell is slid around the first one with the longitudinal slits or gaps staggered (preferably 180°) to avoid lines of weakness. This step is repeated for additional shells staggering the longitudinal slits.

3.8.6 Step 6: Strap the shells together

It is necessary to use straps or other means to apply pressure on the FRP composite shells to hold them in place until the adhesive cures and also forcing any trapped water between them out. Straps should be spaced approximately at 0.6 m intervals for satisfactory pressure to be applied to the adhesive contact area.

3.8.7 Step 7: Drive the FRP composite shield to the required depth into mud line

After curing of the adhesive, the FRP composite shield can be driven into the mud line, which needs to be loosened. This can be achieved either by using a water jet that stirs and loosens the mud or by digging around the wood pile to the required depth and then backfilling the hole.

3.8.8 Step 8: Drill holes and place shear connectors

If shear connectors are required for the transfer of loads from the wood pile to the FRP composite shield, then holes need to be drilled and the shear connectors placed before grouting. This will ensure that any possible voids are filled by the grout and no possible entry points remain for marine borers to enter and damage the wood pile. If the holes are to be drilled underwater, then an air drill will be necessary. In the laboratory, regular steel threaded rods were used; however, in field applications galvanized steel rods should be used to avoid corrosion.

3.8.9 Step 9: Prepare grout and pump it into place

After the FRP composite shield is driven in the mud, then the grout material can be pumped. Grout needs to be pumped from the bottom up to avoid segregation.

3.9 Cost Analysis

To assess the commercial feasibility of the wood pile repair method a preliminary cost analysis was conducted. For this purpose, the cost of repairing full size wood piles in the laboratory was calculated. The cost was divided into the following items: (a) materials, (b) fabrication supplies and (c) labor for preparation and application. Material costs included the cost of the fiber reinforcement, resin and catalyst. The fiber reinforcement cost for a typical composite shell, which has a diameter of 394 mm and a length of 4.88 m, was $101. The fiber reinforcement cost included the CSM mat cost, $17 per shell, and the woven unidirectional fabric cost, $84 per shell.

The resin cost for a typical composite shell was $70 and the catalyst cost was $8. The cost of fabrication supplies per shell included peel ply, $40, release film, $25, distribution media, $16, plastic tubing, $8.5, bagging film, $12, sealant tape, $7, and vacuum line, $5.5. The labor cost to prepare materials, supplies and the mold for SCRIMP™ fabrication of one shell was based on the time required, three and a half hours, for two student workers to complete the task at a wage rate of $10 per hour. Therefore, the total cost for labor application was $70 per shell. The labor application cost was based on the time required for one student worker to mix the resin and infuse the part. In the laboratory one and a half hours were spent to complete the infusion process. Therefore, the total labor application cost was $15. The total cost for one shell was $378, where the cost items are summarized in Table 3.1.

Table 3.1 - Cost Items for FRP Composite Shells Fabricated in the Laboratory

Item	Cost per FRP Composite shell ($)
Fiber reinforcement	101
Resin	70
Catalyst	8
Fabrication supplies	114
Labor preparation	70
Labor application	15
Total	378

Note: The above prices are for shells having a diameter of 394 mm and a length of 4.88 m.

The total cost for repairing a typical wood pile with a diameter of 335 mm using 4.88 m long FRP composite shells can be determined by adding the cost of the underwater epoxy adhesive, $200, and the cement based grout with a thickness of 50 mm, $220. The labor cost for the application of the adhesive and the grout, $100, was estimated assuming that two and a half hours are required for four student workers to complete these tasks. The cost of any equipment needed, such as concrete mixing trucks and pumps is expected to exceed $200. The total cost for a typical wood pile repair was $1475 (approximately $1500), where the cost items are summarized in Table 3.2.

Table 3.2 - Cost Items for Wood Pile Repair with FRP Composite Shells

Item	# Items	Cost per item ($)	Total cost ($)
FRP composite shell	2	378	756
Adhesive	4 gal	50	200
Grout	20 bags	11	220
Labor	10 hrs	10	100
Equipment	/	/	200
Total			1476

Note: The above prices are for wood piles with a diameter of 335 mm repaired with 4.88 m long FRP composite shells.

It is worth noting that additional cost items such as the shear connectors and the polymer concrete coating are not included in this estimate. Some costs would be expected to decrease if multiple piles at the same site were reinforced. Actual worker rates will be higher than student worker labor rates assumed in this study; however it is expected that

fabrication and installation time will be reduced with practice and expertise partially compensating changes in the overall labor cost.

In the cost analysis of the repair method, no cost item for the extraction of the existing damaged wood pile is needed. This represents a cost saving compared to the alternative of pile removal, since the cost for extracting and disposing the old treated wood piles, including the disruption to the pier facility, is eliminated. The disturbance to the normal operation of the waterfront facility is expected to be minimal. Most of the repair work can take place beneath the pier facility; no heavy or large equipment is necessary to complete the task.

3.10 Conclusions and Recommendations

The study presented in this chapter allows the following conclusions to be drawn:

1. Lay-up of wet fabric reinforcement with vacuum bagging compaction proved to be an ineffective method for the fabrication of FRP composite shells.
2. The SCRIMP^{TM} fabrication process proved to be a satisfactory method for the fabrication of FRP composite shells.
3. The repair method is environmentally friendly since no new chemicals are introduced to the surrounding marine environment. The encasement with the FRP composite shield will also attenuate further leaching of chemicals from treated wood piles into the water.
4. The proposed FRP composite shield with the grouting system has a dual function: environmental protection and structural restoration of the wood pile.

5. The repair method can be cost competitive compared to damaged pile extraction and new pile installation in cases where disruption to the waterfront facility (e.g., pier or wharf) are of concern.

The following commentary and practical recommendations are proposed:

1. Modifications and improvements are expected to take place when the technology is implemented in the field.
2. For extended protection of wood piles in service without marine borer damage, the use of the polymer grout with only two FRP composite shells may be advantageous.
3. For structural restoration of wood piles with damage (e.g., necking with reduction in cross-sectional area), the use of the cement-based structural grout combined with polymer concrete overlay and the required number of FRP composite shells may provide the requisite load bearing capacity.
4. It should be noted that the labor rate used for determination of labor cost is low ($10 per hour) since it is the rate for a student worker. In real applications the rate is expected to be approximately $40-$50 per hour. The total time for a typical repair to be performed by professionals is expected to be less and therefore a portion of the cost will be balanced.

Chapter 4

Freeze-Thaw Resistance of FRP Composites Adhesive Bonds with Underwater Curing Epoxy

4.1 Abstract

A proposed method for the protection and structural restoration of wood piles developed at the University of Maine requires the field placement of FRP composite pre-manufactured shells around the piling. The FRP composite shells need to be attached with an underwater curing adhesive that produces a satisfactory structural bond. The adhesively bonded shells develop "composite action" when supporting loads. The main concern for durability of the adhesive bond is the resistance to freeze-thaw cycles. To assess adhesive bond durability, single lap shear tests were performed after exposure to freeze-thaw cycles. The experiments served to characterize the loss of adhesive bond strength between FRP composite coupons representative of the shell material. It was found that the adhesive strength of the underwater curing epoxy tested in this work is reduced 43 % after exposure to standard twenty freezing and thawing cycles.

4.2 Introduction

The climate of Maine and other states in the New England area imposes cycles of freeze-thaw during winter. The method for protection and structural restoration of wood piles presented in Chapter 3 requires field installation of FRP composite pre-manufactured shells around the piles. During field placement, FRP composite shells need

to be attached with an underwater curing adhesive that produces a satisfactory structural bond. The adhesively bonded shells need to develop "composite action" to serve as a load bearing structural component. The main concern for durability of the adhesive bond between the shells is the resistance to freeze-thaw cycles.

A procedure for exposure to freeze-thaw cycling of FRP composites bonded to concrete substrates was developed (ICBO 2001). This procedure was adapted to evaluate freeze-thaw exposure of four different FRP composite materials including an E-glass/vinyl ester composite fabricated by the SCRIMP™ process (Wood 2000). Standard tensile tests and short-beam shear tests were used to evaluate residual mechanical properties.

In this work, the available procedure for freeze-thaw cycling exposure (ICBO 2001) was adopted. To assess adhesive bond durability, single lap shear tests were performed after exposure to freeze-thaw cycles following the ASTM D5868 standard test procedure (ASTM 1995). The experiments were designed to allow the loss of adhesive bond strength between FRP composite coupons representative of the shell material used for wood pile restoration to be characterized. The objective of this chapter is to evaluate the residual adhesive shear strength of FRP composite specimens bonded with underwater curing epoxy after exposure to freezing and thawing cycles.

4.3 Materials and Methods

4.3.1 Composites Fabrication

FRP composite plates made of E-glass fiber reinforcement and a vinyl ester matrix were fabricated using the SCRIMP™ resin infusion process (TPI 2001). Unidirectional woven fabric reinforcement and chopped strand mat (CSM) layers were placed dry on a steel base mold and then sealed with a vacuum bag. The fiber architecture of the plates was: [CSM, 0, 90, 0, 0, CSM], which corresponds to the actual FRP composite shells used for wood pile restoration (See lay-up in Figure 4.1).

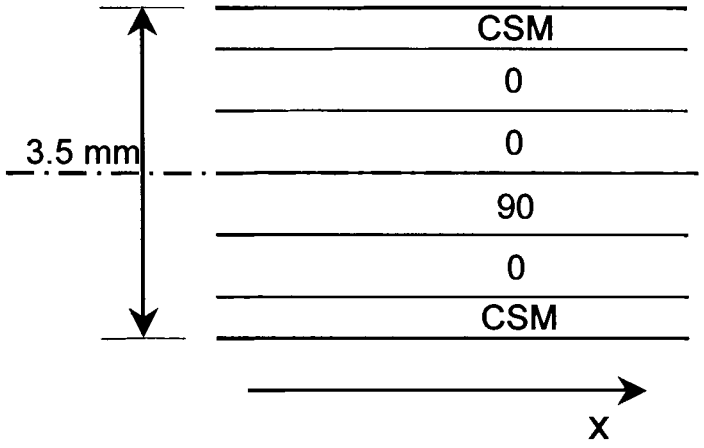

Figure 4.1 - Fiber Lay-up (cross-section) of FRP composite plates

The criteria for material selection and fiber lay-up are discussed in Chapter 3. It is worth noting that one CSM layer was added on each surface of the laminate to improve bonding properties and to create a resin rich area that may provide environmental protection. An Epoxy based vinyl ester resin was selected as the matrix for the composite shells (Dow 1999).

A vacuum pressure of –102 kPa was applied with a vacuum pump. The applied vacuum pressure not only debulked (compacted) the dry fiber reinforcement, but also removed all the entrapped air from the fiber lay-up. Once the required vacuum level was attained, resin was infused through a system of resin feed lines and flow distribution media. The pressure differential between the atmosphere and the applied vacuum allowed infusion of the resin into the fiber lay-up. After the resin impregnated the fiber reinforcement, the vacuum pressure was reduced to –51 kPa until the resin gelled. Once the resin gelled, the vacuum pressure was removed and the composite part was allowed to cure. From the manufactured FRP composite plates, pieces of 280 mm x 102 mm were cut using a precision wafering machine available in the laboratory (Figure 4.2).

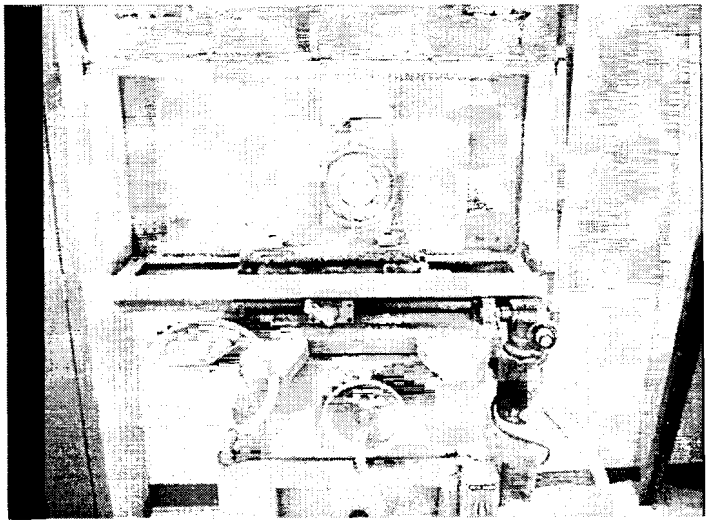

Figure 4.2 - Precision Wafering Machine

4.3.2 Adhesive Bonding

The FRP composite plate surfaces were wetted with water and then bonded together using an underwater curing epoxy adhesive, Hydrobond 500 (Superior Polymer 2000). This epoxy adhesive is specified for applications with a water temperature of at

least 5°C. The epoxy adhesive was applied on one plate and then the other plate was placed over the covered area creating an overlap of 25 mm. At the two edges, 25 mm wide strips, cut from the FRP composite plates, were bonded to compensate for the greater thickness created by the bond with the second plate. This also helped in aligning the specimen with the line of loading during the test. No preparation or cleaning of the plate surfaces was done prior to the application of the adhesive. The bonded plates were then placed under water for curing of the adhesive. A schematic of the bonded FRP composite plates is provided in Figure 4.3. The vertical dashed lines represent the location of the lap shear specimens cut from the FRP composite plates.

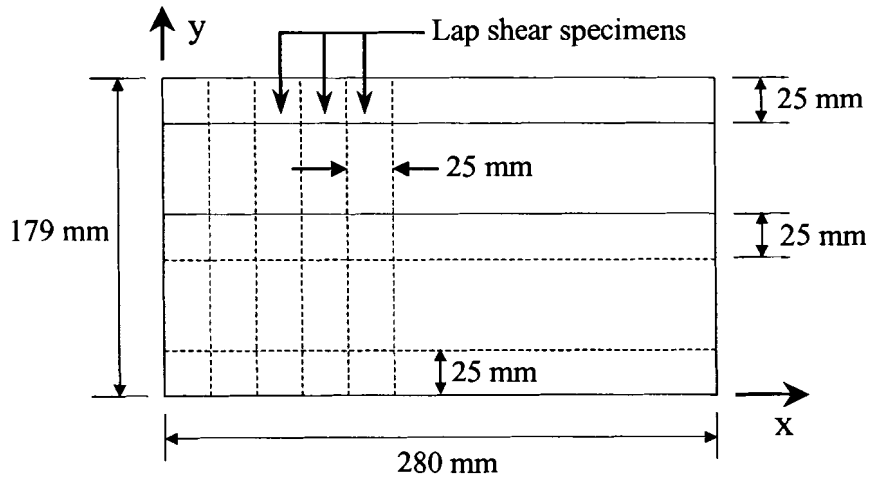

Figure 4.3 - Schematic of Adhesively Bonded FRP composite plates

4.3.3 Underwater Conditioning

The FRP composite specimens were placed in a tap water bath at a temperature of 38°C with an accuracy of ±0.5°C. In this way, the epoxy adhesive cured in an underwater environment. The water was heated by one submersible 250-watt heater and was circulated by a four-liter/min circulator pump (See Figure 4.4).

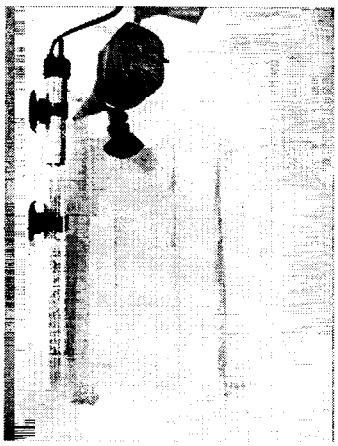

Figure 4.4 – Bonded FRP Composite Plates in the Hot Water Bath

The water was checked periodically with an electronic thermometer to verify that it was maintaining the proper temperature. The control coupons were removed from the water bath after 14 days, while the plates used for the freeze-thaw exposure were left for an additional seven-day period to complete the three weeks required by ICBO AC125 (ICBO 2001).

4.3.4 Freeze-Thaw Exposure

A minimum number of 20 freeze-thaw cycles is specified by ICBO AC125 (ICBO 2001). The specified cycles consist of a minimum of 4 hours in the freezer and a minimum of 12 hours in the hot water bath. In order to meet the ICBO AC125 requirements and have a repeatable daily schedule (i.e., 24 hour cycle), 8 hours in the freezer and 16 hours in the hot water immersion bath with a total of 20 cycles were selected. The heaters were set to maintain the immersion bath at 38°C and the freezer was set to −18°C, as specified by ICBO AC125. Before placing the plates in the freezer, a clean rag was used to dry the plates in order to remove the surface water. FRP composite

plates in the water bath and in the freezer are shown in Figure 4.4 and Figure 4.5, respectively.

Figure 4.5 – Bonded FRP Composite Plates in the Freezer

4.3.5 Single Lap Shear Test Evaluation

After conditioning and freeze-thaw exposure, the FRP composite plates were cut into coupons according to ASTM D5868 (ASTM 1995) using a precision wafering machine (Figure 4.2). The machine had a water pump system that watered the cutting blade to avoid excessive heat and to prevent FRP composite dust from getting airborne. The lap shear test coupon dimensions were 179 mm by 25 mm in agreement with ASTM D5868 (Figure 4.3). Lap shear test coupons are shown in Figure 4.6 and Figure 4.7.

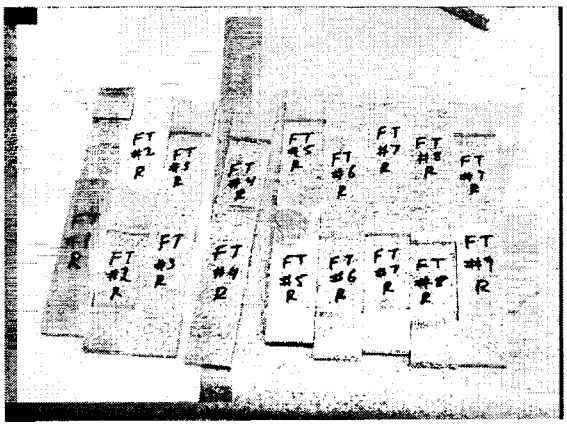

Figure 4.6 – Shear Lap Test Coupons

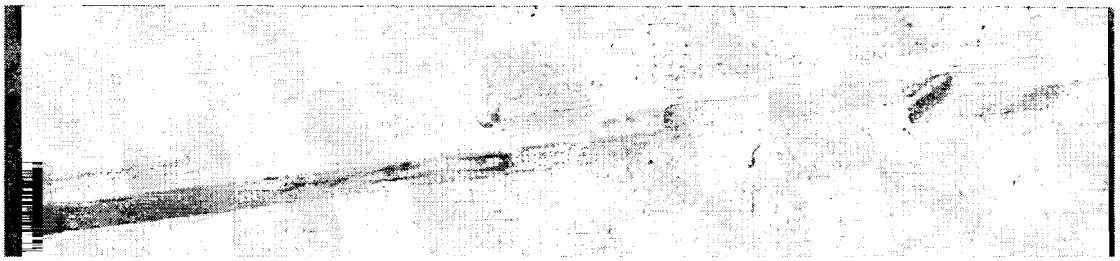

Figure 4.7 - Side View of a Lap Shear Test Coupon

The lap shear tests were conducted using a 100 kN servo-hydraulic loading frame (Instron 1998) in a controlled ambient environment with a temperature of 22°C and a relative humidity of 45% (See Figure 4.8). A total of 18 specimens were tested, 9 control and 9 exposed to freeze-thaw cycles. The specimens were loaded in tension in the displacement controlled mode at a rate of 13 mm per minute. The maximum applied load and the mode of failure were recorded.

Figure 4.8 - Lap Shear Test Setup

4.4 Results and Discussion

The standard practice for classifying adhesive failures in FRP composite joints was applied (ASTM 1994). Adhesive failure (ADH) is defined as: "rupture of the

adhesively bonded joint, such that the separation appears to be at the adhesive-adherend interface" (ASTM 1994). Cohesive failure (COH) is defined as: "rupture of an adhesively bonded joint, such that the separation is within the adhesive" (ASTM 1994).

Experimental data from single lap shear tests of control specimens is presented in Table 4.1.

Table 4.1 –Single Lap Shear Experimental Results for Controlled Specimens

Specimen	Width b (mm)	Length L (mm)	Overlap Area A_b (mm^2)	Maximum Load P (kN)	Apparent Shear Strength S (MPa)	Mode of Failure
1R	24.97	27.31	681.9	11.07	16.2	Adhesive
2R	27.18	27.05	735.2	12.30	16.7	Adhesive
3R	25.91	27.18	704.2	10.64	15.1	60 % Adhesive / 40 % Cohesive
4R	24.89	26.42	657.6	10.93	16.6	Adhesive
5R	24.71	26.42	652.8	10.31	15.8	90 % Adhesive / 10 % Cohesive
6R	24.71	26.04	643.5	9.64	15.0	Adhesive
7R	24.89	26.80	667.1	11.60	17.4	Adhesive
8R	24.84	26.42	656.3	11.02	16.8	Adhesive
9R	25.02	26.92	673.5	10.90	16.2	85 % Adhesive / 15 % Cohesive

The predominant mode of failure of the control coupons was adhesive failure, with minimal or no cohesive failures. Only one shear lap control specimen had a significant amount of cohesive failure. Typical adhesive failure from one of the control specimens is depicted in Figure 4.9.

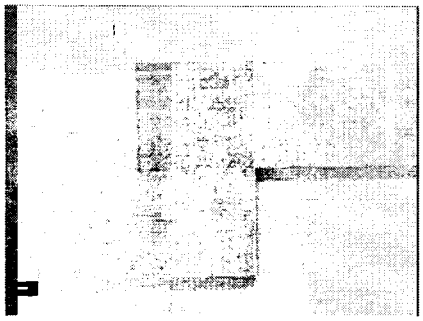

Figure 4.9 - Typical Adhesive Failures in Control Specimens

Experimental data from single lap shear tests of freeze-thaw exposed specimens are presented in Table 4.2. Most shear lap specimens demonstrated an adhesive mode of failure with a significant amount of cohesive failure. In some cases, cohesive failure accounted for 50 % of the total overlap bonding area. A typical shear lap specimen subjected to freeze-thaw cycles showing a combination of adhesive and cohesive failure is depicted in Figure 4.10.

The overlap bonding area, A_b, was calculated by multiplying the specimen width, b, by the overlap length, L (See Table 4.1and Table 4.2).

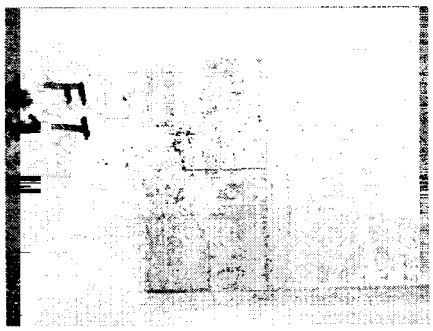

Figure 4.10 - Typical Adhesive-Cohesive Failures in Freeze-Thaw Specimens

Table 4.2 - Single Lap Shear Experimental Results for Freeze-Thaw Specimens

Specimen	Width b (mm)	Length L (mm)	Overlap Area A_b (mm^2)	Peak Load P (kN)	Apparent Shear Strength S (MPa)	Mode of Failure
1FT	24.89	26.42	657.6	6.07	9.2	Adhesive
2FT	25.60	25.55	654.1	6.07	9.3	50 % Adhesive / 50 % Cohesive
3FT	25.15	26.42	664.5	5.90	8.9	Adhesive
4FT	25.27	26.16	661.1	6.04	9.1	80 % Adhesive / 20 % Cohesive
5FT	25.65	25.27	648.2	6.19	9.6	60 % Adhesive / 40 % Cohesive
6FT	25.48	26.67	679.6	6.34	9.3	50 % Adhesive / 50 % Cohesive
7FT	24.94	26.16	652.4	5.71	8.7	80 % Adhesive / 20 % Cohesive
8FT	25.32	26.62	674.0	6.20	9.2	90 % Adhesive / 10 % Cohesive
9FT	25.35	25.83	654.8	6.08	9.3	80 % Adhesive / 20 % Cohesive

The apparent shear strength, S, of the adhesive bond was determined by dividing the peak load, P, by the overlap area, A_b, as follows

$$S = \frac{P}{A_b} \tag{4.1}$$

Comparative results for control and freeze-thaw exposed specimens are shown in Table 4.3. The mean shear strength for the control specimens was 16.2 MPa, while the respective value for the freeze-thaw specimens is 9.2 MPa. Therefore, there was a reduction in the mean shear strength after 20 freeze-thaw cycles of approximately 43%. From the values of the coefficient of variance (COV), it was observed that the test results had relatively low variability (e.g., COV of 4.9 % and 2.4 %, respectively).

Table 4.3 - Single Lap Shear Comparison

Type of Specimen	Control	Exposed to Freeze-Thaw Cycles
Composite Substrate	E-Glass / Vinyl Ester	E-Glass / Vinyl Ester
Adhesive	Underwater Epoxy	Underwater Epoxy
Conditioning	14-Day Water Immersion at 38°C	21-Day Water Immersion at 38°C and 20 Freeze-Thaw cycles
Mean Shear Strength	16.2 MPa	9.2 MPa
Standard Deviation (STD)	0.80 MPa	0.24 MPa
COV	4.9 %	2.4 %
Mode of Failure	Adhesive Failure	Mostly Adhesive with Significant Cohesive Failure

A statistical analysis of the apparent shear strength was performed using one-way analysis of variance (ANOVA) for the controlled and freeze-thaw exposed data sets. The analysis was conducted using the SYSTAT software package (SPSS 1999). The ANOVA analysis determined if the shear strength response was a function of freeze-thaw exposure. The model for a one-way ANOVA is represented symbolically as follows:

$$Y_n = B_o + B_1 \cdot X_n + \varepsilon_n \tag{4.2}$$

where

Y_n = observed apparent shear strength for the data sets

B_o, B_1 = coefficients of the model

X_n = code associated with the treatment under study (e.g., freeze-thaw cycles)

ε_n = random unit variation within the block of data.

The null hypothesis and alternative hypothesis are

$$\begin{aligned} H_0 &: B_1 = 0 \\ H_A &: B_1 \neq 0 \end{aligned} \tag{4.3}$$

Post hoc analysis of type Bonferroni was used for pair-wise comparisons with a confidence level of 95% ($\alpha = 0.05$). In order for the two data sets not to be significantly different, the p value, which is the probability of the coefficient B_1 to be zero, has to be greater than 0.05 ($p > 0.05$). In this case the two sets are statistically different and have a very low probability of overlap with a p value = 0.000.

It is speculated that the reduction in the bond shear strength is due to the presence of voids in the adhesive layer that facilitate water ingress. The void content in the adhesive layer is associated with the uneven spread of the adhesive on the FRP composite substrate combined with the lack of applied clamping pressure. During freezing, water

expansion in the voids and crevices deteriorates the epoxy adhesive bond line leading to a loss in cohesive strength.

4.5 Conclusions and Recommendations

The experimental study presented in this chapter allows the following conclusions to be drawn:

1. The shear strength of the Hydrobond 500 underwater curing epoxy studied is sensitive to freezing and thawing cycles.
2. Exposure to freeze-thaw cycles leads to a change in the mode of failure from predominantly adhesive type to combined adhesive/cohesive type.
3. The retention of mean shear strength after freeze-thaw exposure was only 57%. However, the residual shear strength (9.2 MPa) is still adequate to transfer shear stresses between FRP composite shells in wood pile repair applications as discussed in Chapter 5.
4. The relatively low COV obtained in the experiments indicates that repeatability of the fabrication process, the testing protocol and the shear strength measurement is satisfactory.
5. It is worth noting that in marine applications, where the adhesive layer is exposed to brackish or ocean water, the freezing point is lowered below 0°C due to the presence of salts. Therefore, the probability of exposure to freeze-thaw cycles for the same climate region may be reduced compared to fresh water. For this reason, the freeze-thaw cycling effect studied in this chapter is expected to be more critical in fresh water. However, it is unknown how salt water may affect the bond

or whether chemical interactions with the salt at lower temperatures may affect bond durability or curing.

The following practical recommendations are proposed:

1. In field applications of FRP composite shells around wood piles, closely spaced straps can be used to increase clamping pressure and, therefore, reduce voids in the adhesive layer.
2. Alternative underwater curing adhesives resistant to freeze-thaw cycles should be sought.
3. In the design of FRP composite bonded shells a knock-down factor for apparent shear strength needs to be introduced to account for the loss of strength that can occur during exposure to freeze-thaw cycles with certain adhesive systems.
4. The effect of increasing the number of freezing and thawing cycles (beyond the standard twenty cycles) on the strength of the underwater epoxy adhesive should be studied.

4.6 Notation

The following symbols are used in this chapter:

S	=	Bond shear strength
P	=	Peak load value
A_b	=	Overlap bonding area

Subscripts

b	=	Bond

Chapter 5

Experimental Characterization of FRP Composite-Wood Pile Interface by Push-Out Tests

5.1 Abstract

Structural restoration of spliced or damaged wood piles with FRP composite shells requires that shear forces be transferred between the wood core and the encasing composite shells. When a repaired wood pile is loaded, shear stress will develop between the wood pile and the FRP composite shell through the grouting material. Alternatively, shear force transfer is developed through shear connectors. The main objective of this chapter is to characterize the interfaces in wood piles repaired with FRP composites shells and grout materials. Two interfaces were characterized: (a) wood pile/grout material and (b) grout material/innermost FRP composite shell. A set of design parameters that control the response of both interfaces were identified: (a) Extent of cross-section reduction of wood pile due to deterioration (necking); (b) Type of grout material (cement-based or polyurethane); (c) Use of shear connectors, and (d) Addition of a frictional coating on the innermost shell. Push-out tests by compression loading were performed to characterize the interfaces and discriminate the effect of the design parameters. The outcome of the push-out tests was the evaluation of the load/slip non-linear response and the progressive failure mechanism. A set of repair systems that represent different combinations of the design parameters were fabricated and the interfaces evaluated. The general finding was that the combination of cement-based grout

and polymer concrete overlay on the innermost shell provided the most efficient shear force-slip response. Furthermore, normalized representations of shear stress transfer at the wood/grout/FRP composite interfaces and through shear connectors were developed to aid in the design process.

5.2 Introduction

Marine wood piles supporting waterfront structures are designed to support vertical gravity loads from the pier structure, top-side facilities, and from mobile equipment and vehicles. Horizontal loads due to wind pressure, wave action, ice formation and eventual vessel impact are exerted on wood piles and need to be considered in the design process. When extensive damage is imposed on the wood piles by marine organisms or mechanical action (e.g., drifting ice, floating debris or docking vessels) the ability of the wood piling system to support the vertical and horizontal design loads is compromised.

In structural restoration of wood piles with fiber reinforced polymer (FRP) composite shells, shear transfer capability between the wood core and the encasing composite shells is required to splice the damaged portion. When a wood pile repaired with FRP composite shells is subjected to bending moment, shear forces or axial forces, shear stress will develop between the wood pile and the FRP composite shell through the grouting material. Alternatively, shear force transfer between the wood pile and the FRP composite shells can take place at the discrete location of shear connectors when these are present. A representative test method is required to assess the shear force and deformation response between wood piles and FRP composite shells.

Push-out tests (British Standards Institution 1979; European Committee for Standardization 1997) are utilized to characterize shear force transfer and slip response in structural connections. For example, a push-out test configuration for shear connectors in steel-concrete composite beams was developed to assess the strength and load/slip characteristics of the connectors embedded in concrete (Menzies 1971). The test specimen configuration, effectively characterized the connection interface between the concrete slab and the steel girder. Push-out tests were also performed to investigate the feasibility of using a new type of steel shear connectors called perforbond rib in composite beams (Veldanda and Hosain 1992). The influence of the shape of the deck profile on the shear resistance of connectors (studs) used in composite construction was investigated through push-out tests (Lawson 1996). Push-out tests were performed to evaluate the strength and the load/slip characteristics of a new shear stud connector (Arroyo and Francois 1996). A push-out test setup applied to column-beam connections of FRP composite pultruded profiles was developed to evaluate adhesive and bolted joints (Lopez-Anido et al. 1999). A push-out test set up to investigate strength, stiffness, slip capacity and fatigue endurance of shear connections with a full-depth precast slab was presented (Shim et al. 2000). Alternatively, the load transfer mechanism between fiber-reinforced polymer (FRP) composite-glulam beams and concrete slabs using lag screws was studied using short-span bending tests (Brody et al. 2000). A test protocol for push-out tests of FRP composite bridge decks connected to supporting beams was proposed (Karbhari 2001).

The main objective of this chapter is to characterize the interfaces in wood piles repaired with FRP composites shells and grout materials. Two interfaces need to be

characterized: (a) wood pile/grout material and (b) grout material/innermost FRP composite shell. A set of design parameters that control the response of both interfaces were identified: (a) Extent of cross-sectional reduction of the wood pile due to deterioration; (b) Type of grout material; (c) Use of shear connectors, and (d) Addition of frictional coating on innermost shell. To discriminate the effect of the identified design parameters on the two interfaces, push-out tests by compression loading were performed (See Figure 5.1).

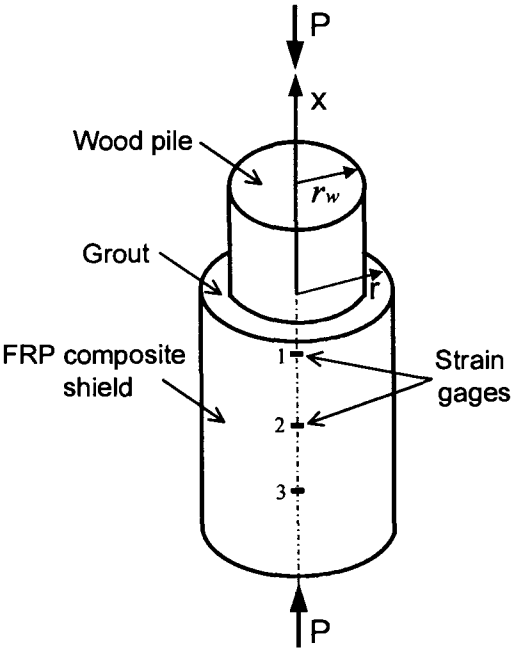

Figure 5.1 - Schematic of the Push-Out Specimens for Repair Systems A, B and D

The expected outcome of the push-out tests was the characterization of the load/slip non-linear response and the progressive failure mechanism. For this reason a set of repair systems that represented different combinations of the design parameters were fabricated and the interfaces evaluated through push-out tests. Results of this work were also expected to be used in the development of phenomenological models of shear stress

transfer at the wood/grout/FRP composite interfaces and through shear connectors as a means to predict the structural response of a wood pile repaired with FRP composite shells, as shown in Chapter 7.

5.3 Repair Systems Studied

Five different repair systems (A, B, C, D and E) that represent relevant combinations of the proposed design parameters were investigated. Two specimens were fabricated and evaluated for each repair system with the exception of repair system E where only one specimen was available. Wood pile sections made of copper chromated arsenate (CCA) treated southern yellow pine were encased with prefabricated FRP composite shells using different variations of the design parameters identified. A total of nine specimens were fabricated and evaluated by conducting push out tests (Table 5.1).

Table 5.1 - Design Parameters Evaluated through Push-Out Tests

Repair system	Wood pile	Grout	Shear connectors	PC coating	# Specimens
A	Intact	Cement	No	No	2
B	Damaged	Cement	No	No	2
C	Intact	Polyurethane	Yes	No	2
D	Intact	Cement	Yes	No	2
E	Intact	Cement	No	Yes	1

Dimensions and configuration of the specimens fabricated and evaluated are provided in Table 5.2. The specifics of each repair system are provided in the following sub-sections.

Table 5.2 - Specimen Configuration and Dimensions

Repair system specimen	Length of wood prototype (mm)	Diameter of wood prototype, $2 \cdot r_w$ (mm)	Length of FRP shield, h (mm)	Number of shells in FRP shield	Thickness of grout t_g (mm)	Number of threaded rods
A1	680	229	521	2	57	0
A2	768	254	610	2	63	0
B1	864	235	737	2	57	0
B2	851	254	737	2	51	0
C1	648	330	546	2	20	3
C2	762	318	648	2	13	3
D1	610	248	499	2	46	3
D2	800	317	648	2	46	3
E1	660	356	635	2	38	0

5.3.1 Repair System A

This system consists of an intact (undamaged) wood pile section encased with FRP composite shells and a structural cement-based grout. The cement-based grout (Five Star 2001; NBEC 2000) was selected based on the performance requirements for a wood pile repair system, as discussed in Chapter 3. This system helped evaluate the effect of necking damage because the results obtained were compared with the results of system B. Undamaged wood pile sections are shown in Figure 5.2(a). A wood section encased with FRP composite shells and a cement-based grout is shown in Figure 5.2(b).

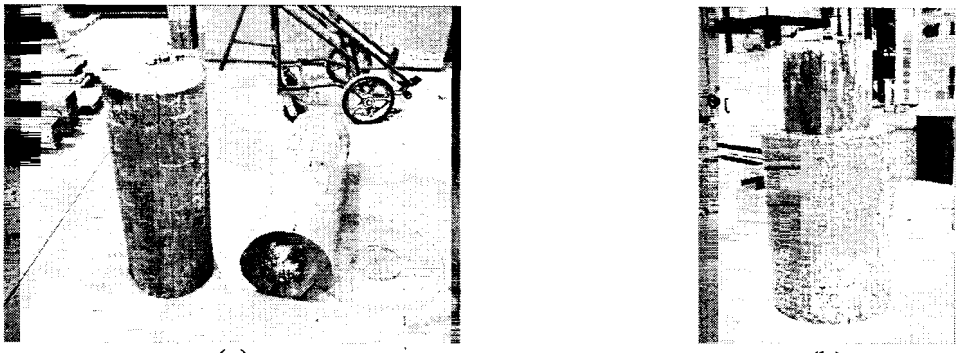

(a) (b)

Figure 5.2 - (a) Undamaged Wood Pile Sections, (b) Undamaged Wood Pile Section with FRP Composite Shells and Cement-Based Grout (Repair System A)

A schematic of the repair system A is depicted in Figure 5.3.

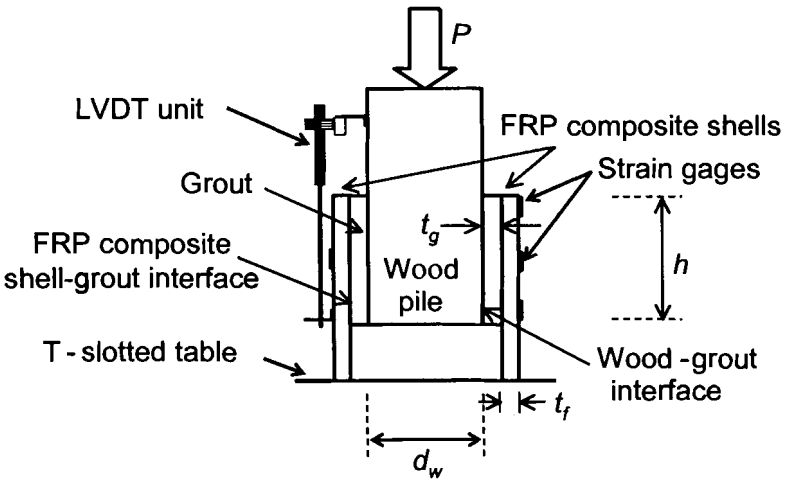

Figure 5.3 - Schematic of Test Set-Up for Repair System A

5.3.2 Repair System B

Repair system B consists of a damaged (approximately 62 % reduction in cross sectional area) wood pile section encased with FRP composite shells and a structural cement-based grout. This cross-section reduction simulated Gribble damage or necking

(See Chapter 2). A damaged wood pile section before repair is shown in Figure 5.4(a). The wood pile after repair is shown in Figure 5.4(b).

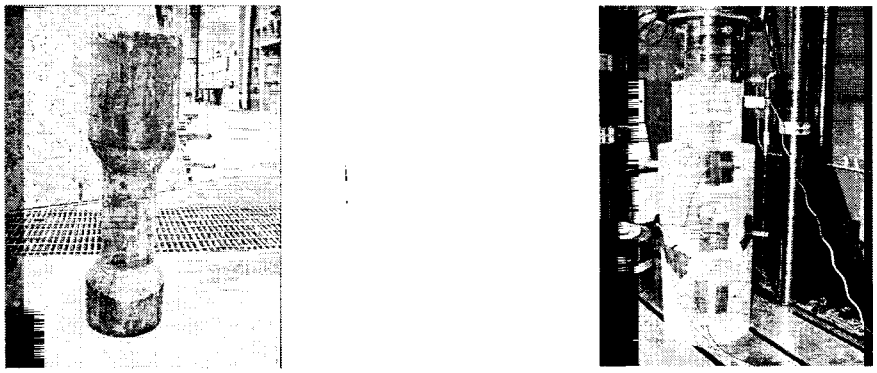

(a) (b)

Figure 5.4 - (a) Damaged Wood Pile Section (62% reduction), (b) Damaged Wood Pile Section with FRP Composite Shells and Cement-Based Grout (Repair System B)

A schematic of the repair system B is shown in Figure 5.5.

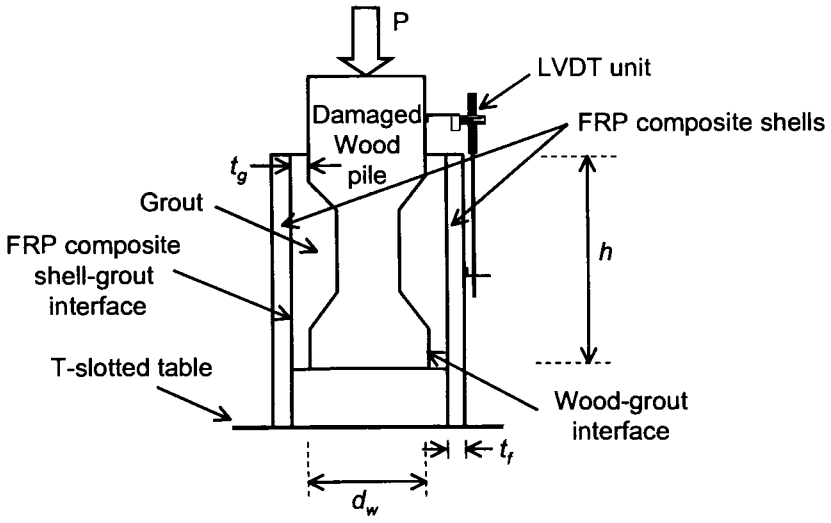

Figure 5.5 - Schematic of Test Set-Up for Repair System B

5.3.3 Repair System C

Repair system C consists of an intact (undamaged) wood pile section encased with FRP composite shells, a no-structural polyurethane grout and shear connectors. The

polyurethane grout, trade name SikaFix HH (Sika 1998), was selected based on the performance requirements for a wood pile repair system, as discussed in Chapter 3. A close up picture of the repair system after failure is provided in Figure 5.6(a). The threaded rod arrangement is shown in Figure 5.6(b).

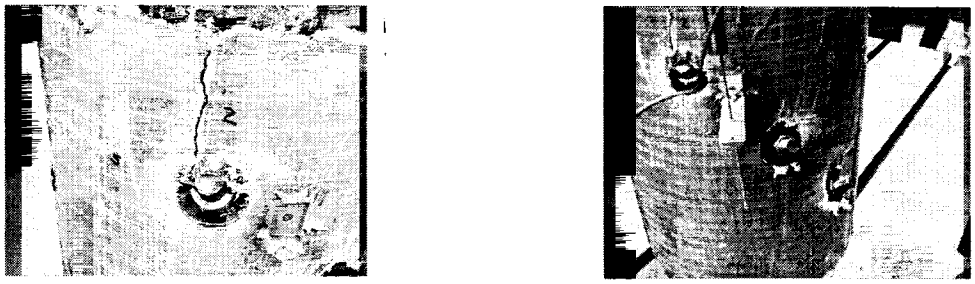

(a) (b)

Figure 5.6 - (a) Failed Wood Pile Section with FRP Composite Shell, Polyurethane Grout and Threaded Rods (Repair System C), (b) Threaded Rod Arrangement

5.3.4 Repair System D

Repair system D consists of an intact (undamaged) wood pile section encased with FRP composite shells, a cement-based grout and shear connectors. A picture of the repair system is provided in Figure 5.7.

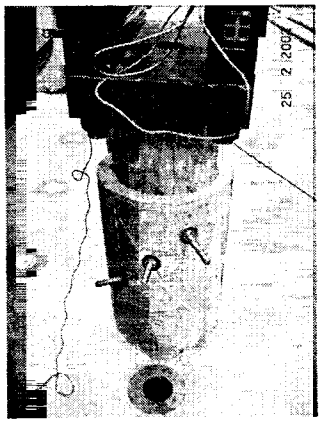

Figure 5.7 - Undamaged Wood Pile Section Encased with FRP Composite Shell, Cement-Based Grout and Threaded Rods (Repair System D)

A schematic applicable to both repair systems C and D is shown in Figure 5.8.

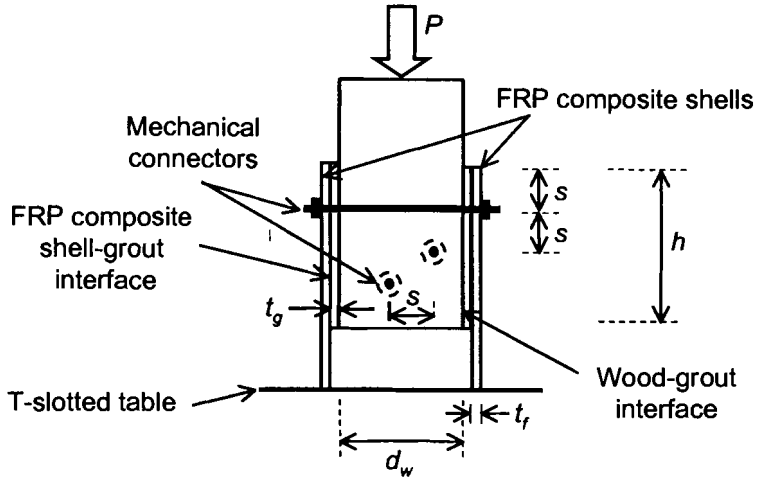

Figure 5.8 - Schematic of Test Set-Up for Repair Systems C and D

5.3.5 Repair System E

Repair system E consists of an intact (undamaged) wood pile section encased with FRP composite shells, a cement-based grout and polymer concrete coating on the interior surface of the innermost shell. The polymer concrete coating or overlay, trade name T-48 (TRANSPO Industries 2000), was selected based on the performance requirements for a wood pile repair system, as discussed in Chapter 3. The total thickness (epoxy resin and aggregates) of one layer of the coating was approximately 3 mm. The polymer concrete coating applied on the interior surface of a shell is shown in Figure 5.9(a). The repair system E is depicted during testing in Figure 5.9(b).

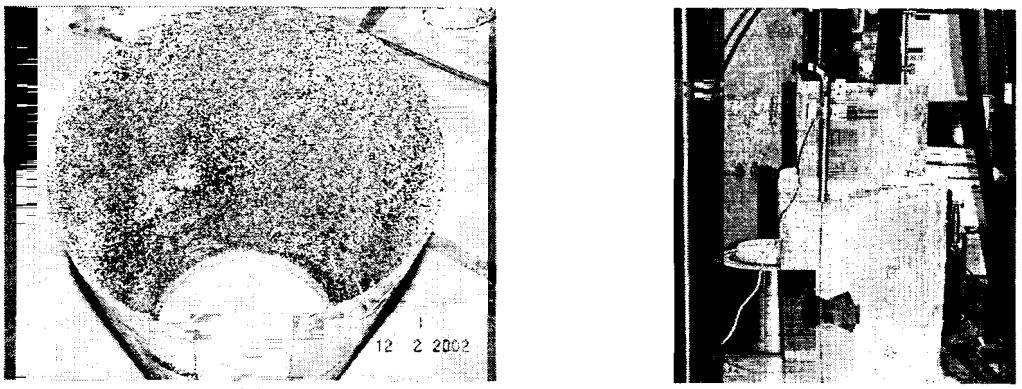

(a) (b)

Figure 5.9 - (a) Applied Polymer Concrete Overlay on the Innermost Shell, (b) Undamaged Wood Pile Section with FRP Composite Shell, Cement-based Grout and Polymer Concrete Coating (Repair System E).

5.4 Specimen Fabrication

Cylindrical FRP composite shells with a longitudinal opening or slit were fabricated in the laboratory using the licensed Seemann Composites Resin Infusion Molding Process (SCRIMP^{TM}) (TPI 2001). A detailed description of the materials and process used in the shell fabrication are presented in Chapter 3. A total of 18 FRP composite shells were fabricated for the push-out tests as shown in Figure 5.10.

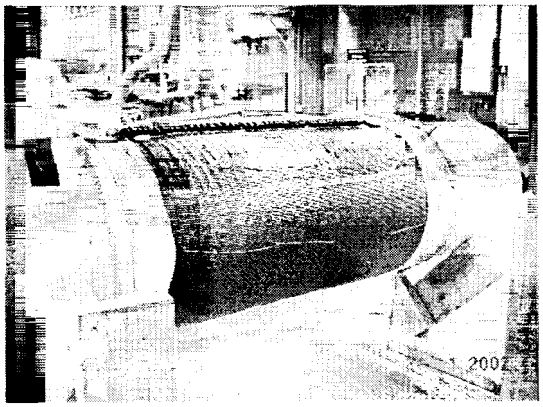

Figure 5.10 - Cylindrical Shell Fabrication Setup showing Resin Flow through Distribution Media

Two consolidated shells were bonded together with an adhesive to form the FRP composite shield or jacket that encased the wood pile section. The underwater curing epoxy adhesive, trade name Hydrobond 500 (Superior Polymer 2000), was selected based on the performance requirements for a wood pile repair system, as discussed in Chapter 3. Durability of this underwater epoxy adhesive to freeze-thaw cycles was studied in Chapter 4. The longitudinal gaps were staggered at an angle of 180° to avoid lines of weakness in the FRP composite shield.

The space between the wood pile and the FRP composite shield was filled with a grouting material. Grouting was conducted with the specimens placed upside down, since it was easier to support the relatively light FRP composite shield than the wood pile on a wood form with sealing. The spacing needed for the push out test at the bottom between the FRP composite shield and the wood pile was easily adjusted by vertically adjusting the wood form. The wood form also provided support until the grouting materials cured. After curing, the form was removed. For the cement-based structural grout at least three days were allowed for curing before testing to develop satisfactory strength gain (NBEC 2000).

5.5 Push Out Test Method

5.5.1 Set Up and Procedure

The push-out tests were conducted using a 500 kN Instron servo hydraulic testing system with a T-slotted table (See Figure 5.1). One of the repair systems, which exceeded 500 kN load capacity, was tested on a 1400 kN Instron actuator mounted on a loading frame. The tests were conducted in load control mode, i.e., a constant load rate was

applied independently of the amount of relative displacement between the wood pile and the FRP composite shield. Load control mode was selected because the repair systems had no relative movement between the wood pile and the FRP composite shield until the shear strength of the interface between the cement-based grout was exceeded. If the displacement mode was applied, then the load needed to exceed the shear strength of the interface would be reached in a very short period of time and it would be difficult to determine the real shear strength of the interface. A loading rate that allowed the test to be completed between 10 and 20 minutes was selected depending on the specific repair system. The first specimens tested, A1, C1 and D1, were loaded at a rate of 17 kN/min. The rest of the specimens were loaded at a rate of 27 kN/min. Loading was applied in cycles using a dual ramp generator (i.e., loading and unloading of the specimen as a single step) available from the controller of the servo-hydraulic testing system (Instron 1998). The maximum load and loading rate are specified in the first ramp and the unloading rate and minimum load in the second ramp. Typically, five or six loading cycles were applied for each specimen to evaluate residual displacement or slip. If the relative displacement between the wood pile and the FRP composite shield recovered after unloading, the system was considered linear elastic. The push-out tests were conducted in an environmentally controlled room, with an ambient temperature of 22 ± 1°C and a relative humidity of 45 ± 1 %.

The compression load was applied to the wood pile, and it was transferred to the grouting material and the FRP composite shield through shear stresses at the interfaces and shear force, depending on the repair set-up, at the connectors (See Figure 5.3, Figure

5.5 and Figure 5.8). The FRP composite shield and grouting material were supported by the T-slotted table of the testing system.

5.5.2 Instrumentation

Linear Variable Differential Transducer (LVDT) units were used to measure the relative movement (slip) between the wood pile and the FRP composite shield. One LVDT unit was mounted on the wood pile with a reference point, bonded aluminum angle, on the FRP composite shield. A schematic of the test set-up with the LVDT unit mounted for repair system B is shown in Figure 5.5. All test data was collected using Lab View 6.0 software and data acquisition system (National Instruments 2000).

On some of the specimens, with the cement-based grout, strain gages (type CEA-06-250UW-350) were surface mounted on the FRP composite shield (Measurements Group 1997). Three strain gages were bonded on one side at three different locations to determine hoop strains along the length of the FRP composite shield (See Figure 5.1). Another strain gage was bonded on the opposite side of the shield at the same height as the middle gage to determine whether bending stresses were present due to load eccentricity. The test set up with the LVDT unit and attached strain gages for one specimen of repair system D is shown in Figure 5.11.

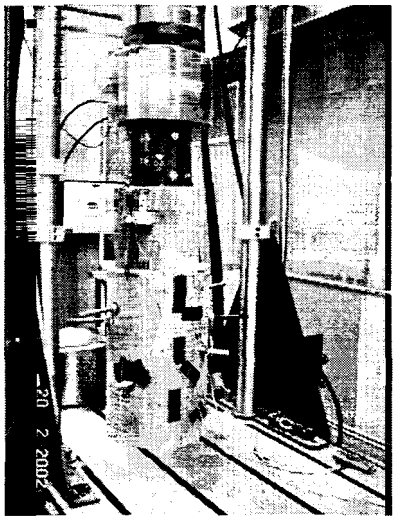

Figure 5.11 - Test Set-Up of Specimen Repaired with System D.

5.6 Results and Discussion

In the case of repair systems with cement-based structural grout (A, B, D and E), the wood pile/grouting and grouting/FRP composite shell interfaces were characterized. The effect of necking damage on the behavior of the system was also evaluated. In the case of the polyurethane grout (repair system C) shear force transfer by shear connectors was characterized. The shear transfer response with the combination of structural cement-based grout and shear connectors was also evaluated (repair system D). For all repair systems the load-displacement curves were obtained.

A summary of experimental results obtained from the 9 specimens evaluated is presented in Table 5.3.

Table 5.3 - Summary of Push Out Tests by Compression Loading

Repair system specimen	Slip compressive load P_0 (kN)	Ultimate compressive load P_P (kN)	Reach available maximum displacement?	Mode of failure
A1	90.9	288.7	Yes	Grout – FRP interface
A2	118.1	295.2	No	Grout – FRP interface At ultimate: Wood – Grout interface
B1	167.8	315.8	Yes	Grout – FRP interface
B2	146.9	433.4	Yes	Grout – FRP interface
C1	126.0	370.8	No	FRP crushing by shear connectors
C2	144.0	364.8	No	FRP crushing by shear connectors
D1	182.9	453.4	Yes	Signs of FRP crushing by shear connectors
D2	261.9	529.5	No	FRP crushing by shear connectors
E1	180.5	402.3	Yes	Wood – Grout interface

The mode of failure for repair systems A and B was failure of the structural grout-FRP composite interface (Figure 5.12). The addition of a polymer concrete coating in repair system E provided interlocking between the grout and the innermost FRP composite shell and forced the failure to occur at the wood-grout interface at a much higher load level (Figure 5.13).

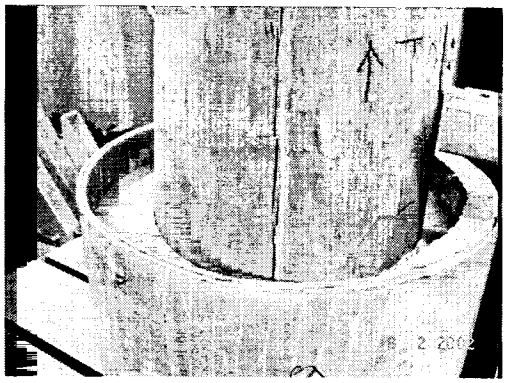

Figure 5.12 - Failure at the Interface between FRP Composite Shield and Cement-Based Grout

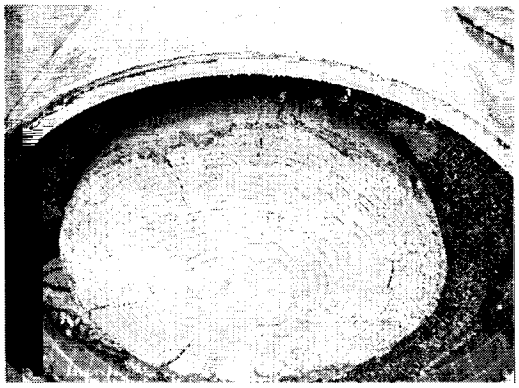

Figure 5.13 - Failure at the Interface between Wood Pile and Cement-Based Grout

The hour-glass shape (necking) of the pre-damaged wood pile in repair system B prevented the wood–grout interface from breaking since for such a failure to occur it would be necessary to shear through the concrete. Repair systems C and D employed shear connectors for transfer of shear forces to the FRP composite shield. Although these repair systems employed different grout materials, the mode of failure was similar: crushing of the FRP composite shield at the bolt location (See Figure 5.14).

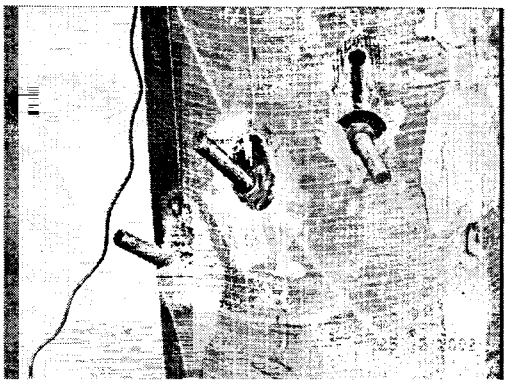

Figure 5.14 - Crushing of FRP Composite Shield by the Shear Connectors

An increase in the peak load of approximately 44% for repair system D compared to repair system C was attributed to the contribution of the cement-based grout.

To compare the performance of the different repair systems the results were normalized by computing the apparent interface shear strength (See Table 5.4).

Table 5.4 - Normalized Experimental Results for Repair Systems A, B, D and E

Repair system specimen	Interface	Interface overlap contact area (m^2)	Slip interface apparent shear strength τ_0 (kPa)	Ultimate interface apparent shear strength τ_P (kPa)
A1	Grout - FRP	0.4782	190	-
A2	Grout - FRP	0.5623	210	-
A2	Wood -Grout	0.3749	-	780
B1	Grout – FRP	0.7233	232	-
B2	Grout – FRP	0.6800	216	-
D1	Grout – FRP	0.4800	381	-
D2	Grout – FRP	0.6310	415	-
E1	Wood -Grout	0.4247	425	-

The apparent slip-shear strength of the grout-FRP composite interface, τ_0, was calculated by dividing the vertical compressive load, P_0, at the onset of relative displacement (slip) by the interface overlap contact area as follows

$$\tau_0 = \frac{P_0}{2 \cdot \pi \cdot r \cdot h} \tag{5.1}$$

where r is the inner radius of the FRP composite shield (Figure 5.1) and h is the height of the overlap interface (Figure 5.3). The apparent ultimate-shear strength of the grout-FRP composite interface, τ_p, was calculated as

$$\tau_P = \frac{P_P}{2 \cdot \pi \cdot r \cdot h} \tag{5.2}$$

Similarly the slip and ultimate apparent shear strength of the wood-grout interface, τ_0 and τ_p, respectively, were calculated as

$$\tau_0 = \frac{P_0}{2 \cdot \pi \cdot r_w \cdot h} \tag{5.3}$$

$$\tau_P = \frac{P_P}{2 \cdot \pi \cdot r_w \cdot h} \tag{5.4}$$

where r_w is the radius of the wood pile as shown in Figure 5.1. The normalized load displacement responses of repair systems A, B, D and E are depicted in Figure 5.15 through Figure 5.18.

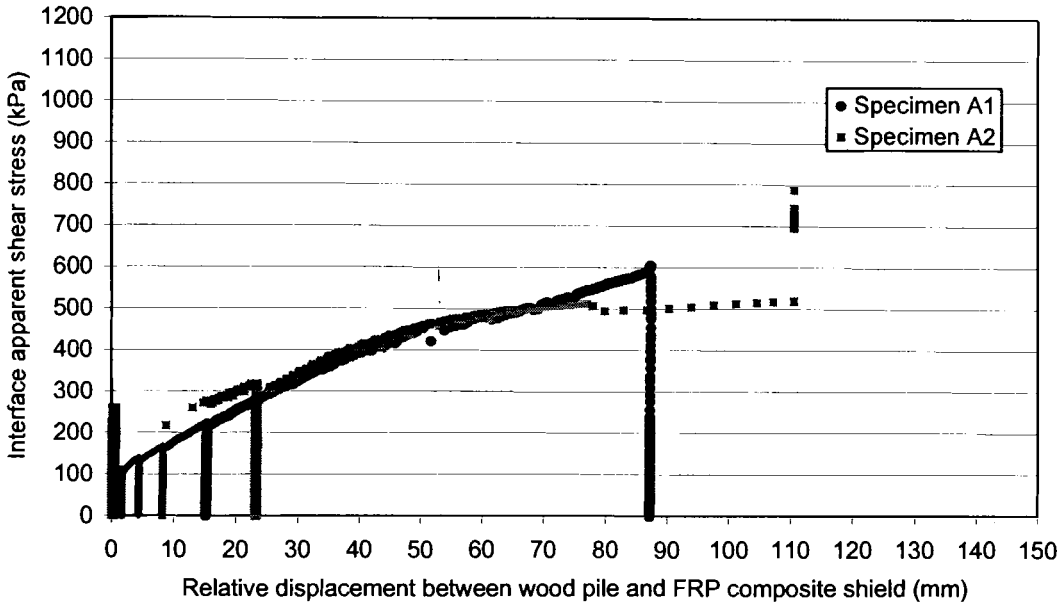

Figure 5.15 - Load-Displacement Response for Repair System A

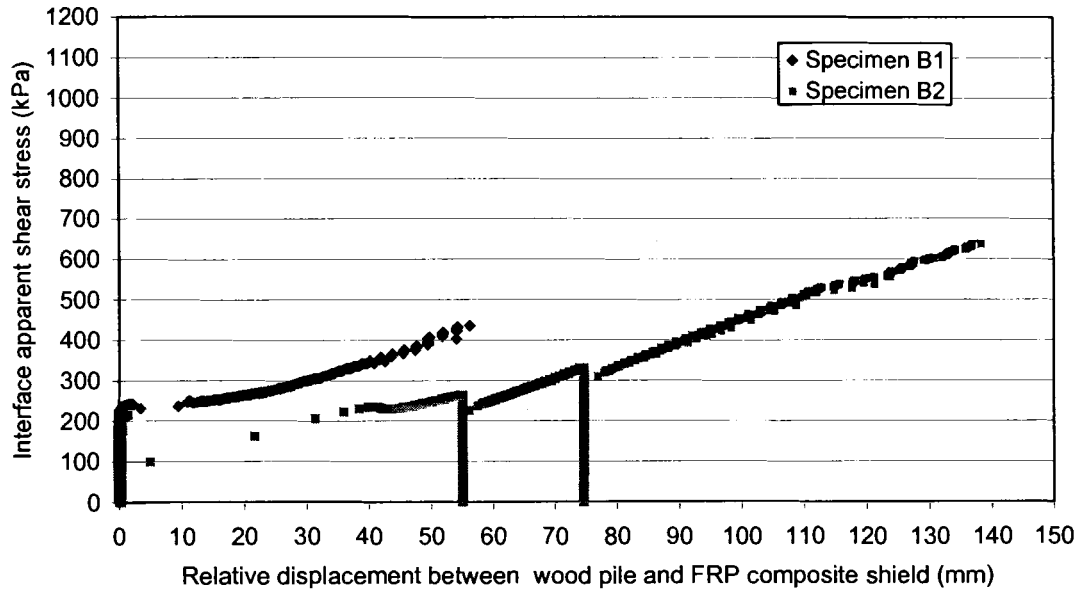

Figure 5.16 - Load-Displacement Response for Repair System B

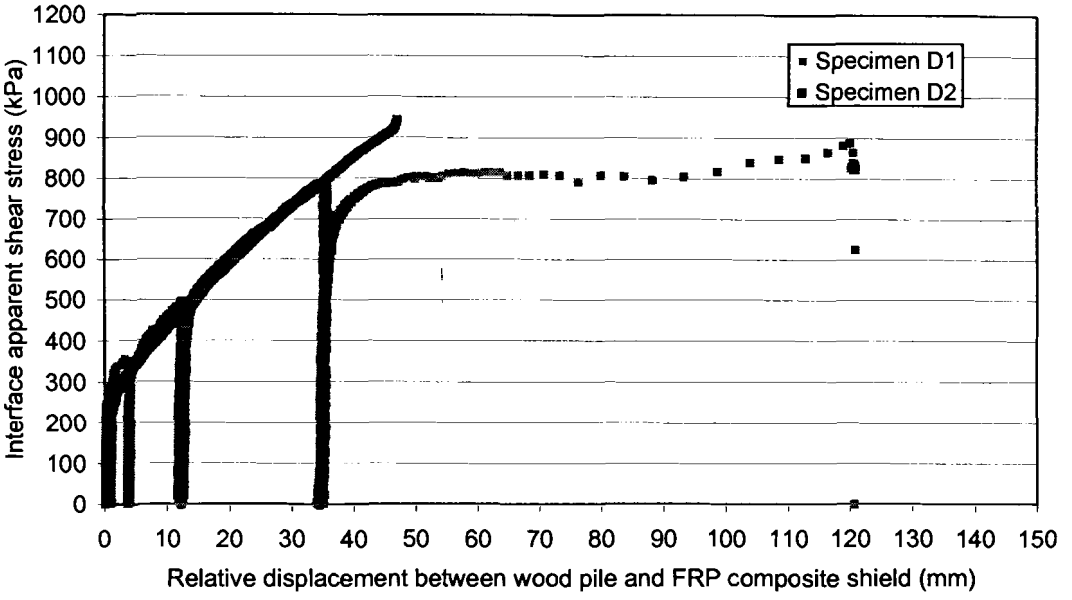

Figure 5.17 - Load-Displacement Response for Repair System D

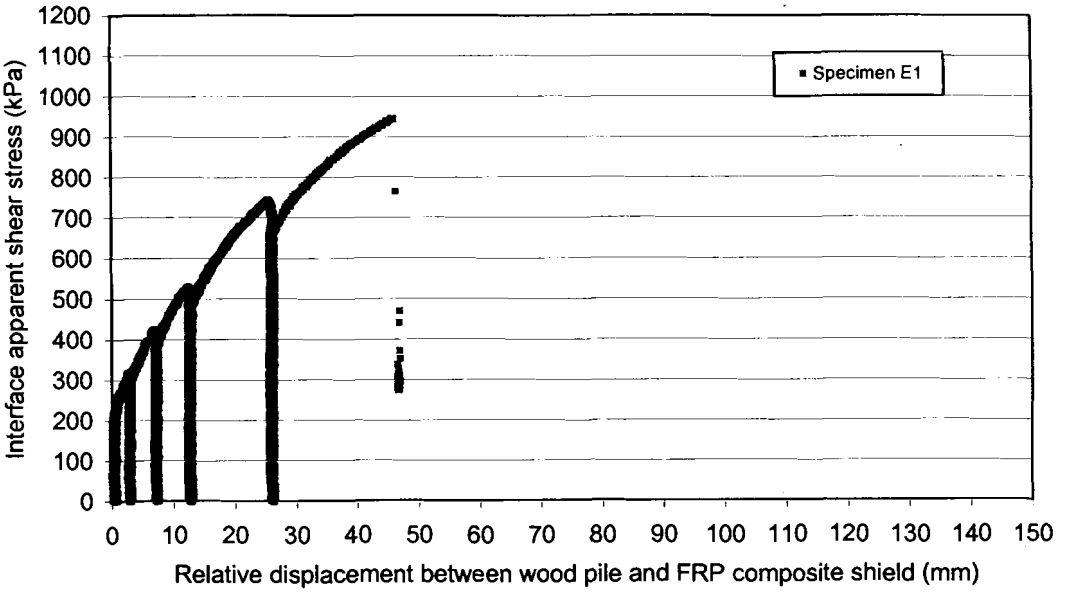

Figure 5.18 - Load-Displacement Response for Repair System E

For repair system C, the slip and ultimate interface shear force per bolt, S_0 and S_P, respectively, were computed as:

$$S_0 = \frac{P_0}{n} \tag{5.5}$$

$$S_P = \frac{P_P}{n} \tag{5.6}$$

where n is the number of shear connector rods. Shear force per rod versus displacement response for repair system C (n = 3) is shown in Figure 5.19.

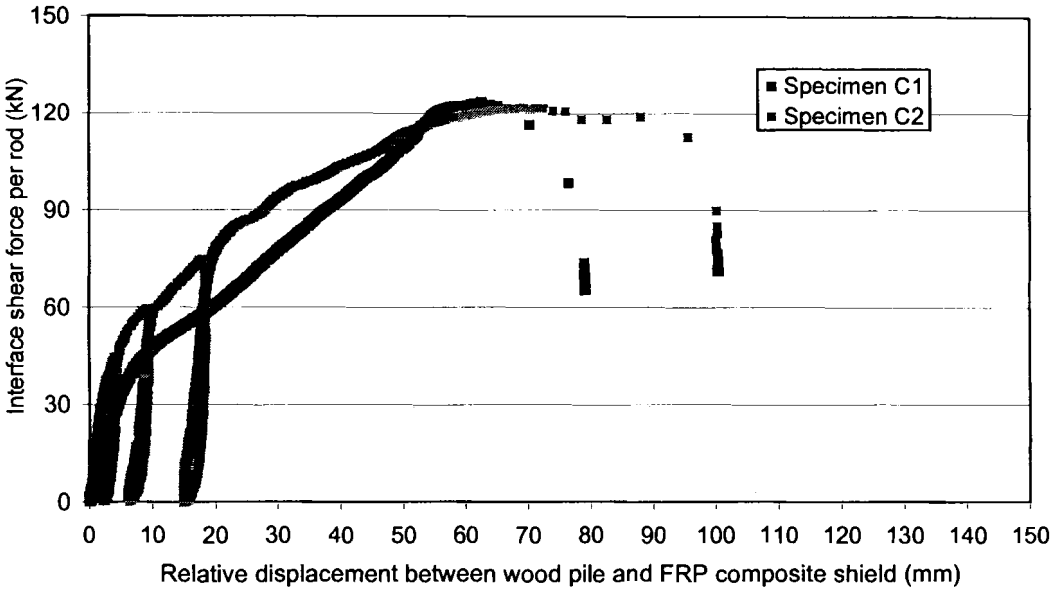

Figure 5.19 - Load-Displacement Response for Repair System C

Each 19 mm diameter threaded rod was able to transfer approximately S_P = 122 kN of force before crushing of the FRP composite shield. The required length for FRP composite shells can be calculated by multiplying the number of rods, n, by the rod

spacing, s, as shown in Figure 5.8. The end distance adopted was equal to the rod spacing (s = 102 mm) (See Figure 5.8).

The hoop strain profile along the height of the FRP composite shield for repair systems A and B was evaluated by bonding strain gages at different locations (See Figure 5.1 and Table 5.5).

The strain profiles for repair system A (specimen A1) and B (specimen B2) are depicted in Figure 5.20 and Figure 5.21, respectively.

Table 5.5 – Hoop Strains on Outer FRP Composite Shell

Repair system specimen	Wood pile	Strain gage #	Strain gage location		Slip load level		Ultimate load level	
			Distance from shell bottom (mm)	Hoop angle (degrees)	P_0 (kN)	Hoop strain ε_θ (με)	P_P (kN)	Hoop strain ε_θ (με)
A1 (h = 521 mm)	intact	1	445	0	90.9	1179	288.7	1929
		2	279	0		664		1798
		3	114	0		372		1374
		4	279	90		935		2001
B2 (h = 737 mm)	damage	1	673	0	146.9	191	433.4	-103
		2	432	0		74		5
		3	190	0		234		2750

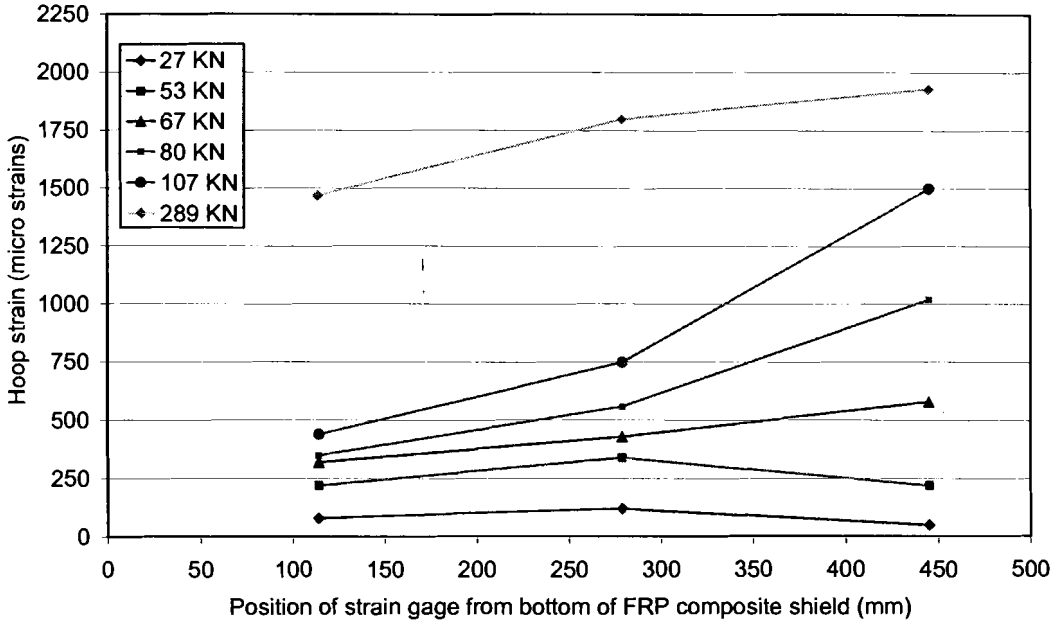

Figure 5.20 – Hoop Strain Distribution on outer FRP Composite Shell for Different Load Levels for Repair System A (Specimen A1)

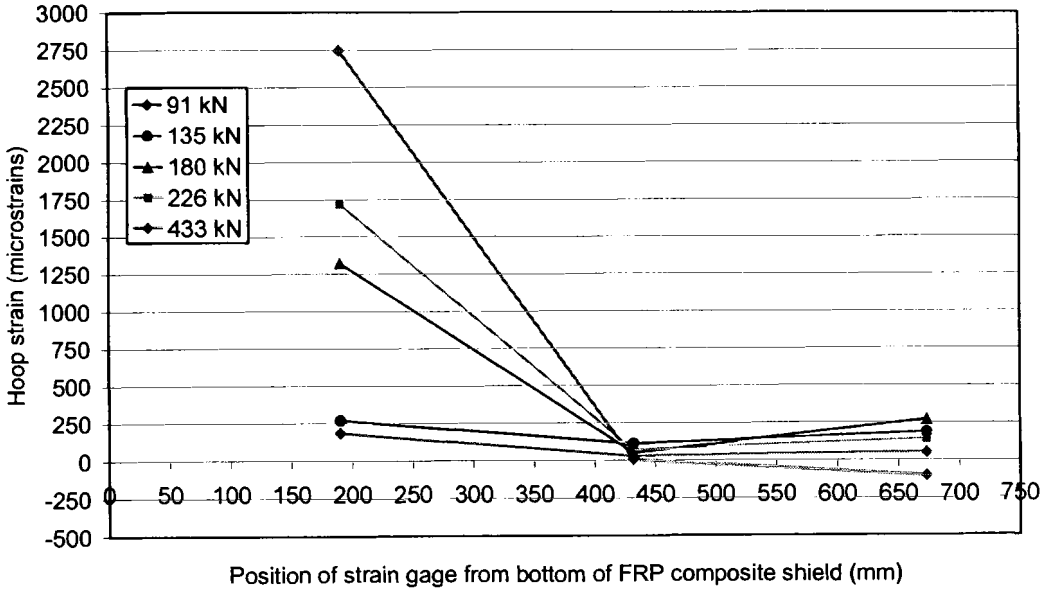

Figure 5.21 - Hoop Strain Distribution on outer FRP Composite Shell for Different Load Levels for Repair System B (Specimen B2)

In the case of specimen A1 (undamaged wood pile), an almost uniform strain distribution was observed for initial loading (See Figure 5.20). When slip developed at the interface between the grout and the innermost FRP composite shell, hoop strains increased markedly with the height (i.e., the upper portion of the shell was subjected to greater hoop strain). By correlating the center strain gages at opposite circumferential locations, strain gages 2 and 4, a strain difference that was attributed to unavoidable load eccentricity was observed (See Figure 5.22).

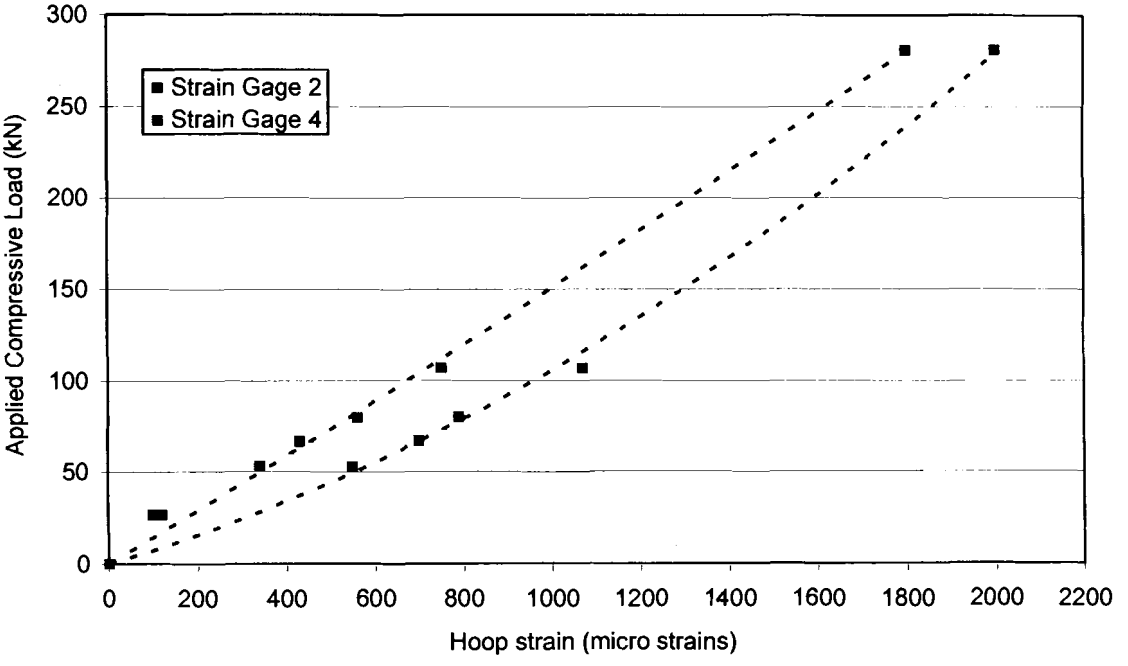

Figure 5.22 – Hoop Strain versus Applied Compressive Load at Opposite Circumferential Locations for Specimen A1

In the case of specimen B2 (damaged wood pile), an almost uniform strain distribution was also observed for initial loading (See Figure 5.21). When slip developed at the interface between the grout and the innermost FRP composite shell, hoop strain increased markedly in the lower strain gage. It is speculated that the observed hoop strain peak toward the bottom of the shell was due to an increase in interior confinement. Since

the wood pile specimen was tapered with the higher diameter on the top, the vertical movement of the pile produced a wedge effect on the grouting material that increased interior confinement pressure on the FRP composite shield. It is assumed that the increase in interior confinement on the bottom portion of the shield was favored by the interlocking between the wood pile with necking and the grout, which differentiates the specimen B2 response with respect to the specimen A1 response. The maximum hoop strain recorded, 2750 micro strains for specimen B2, did not produce failure of the FRP composite material.

The apparent interface shear stress versus slip response was represented by step-wise linear curves, as shown in Figure 5.23 and Figure 5.24.

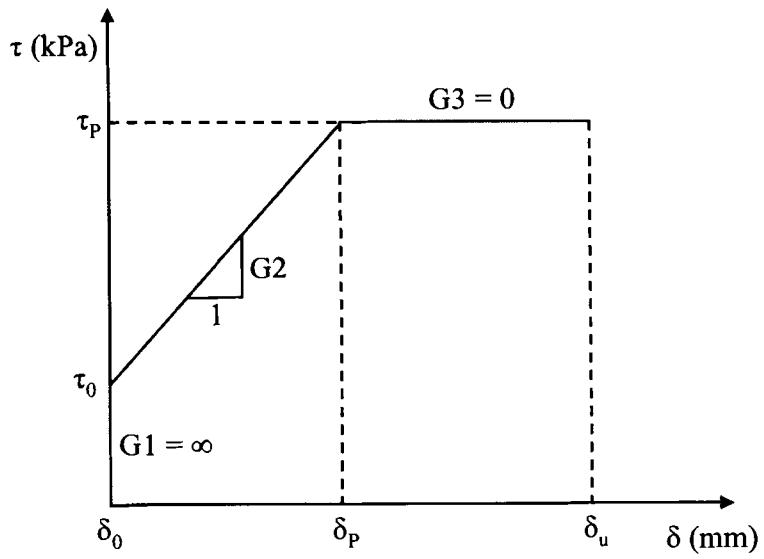

Figure 5.23 – Shear Stress-Slip Preliminary Design Chart for Repair Systems A, D and E

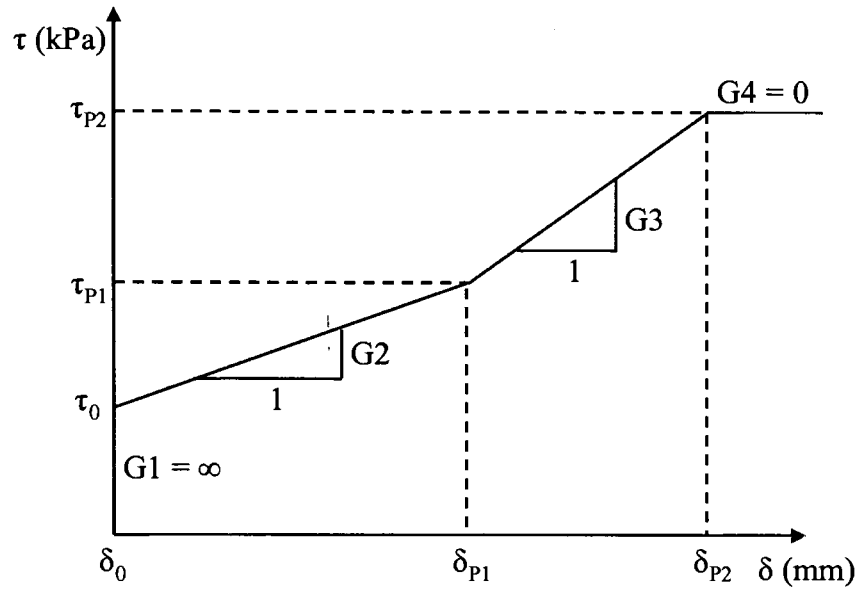

Figure 5.24 - Shear Stress-Slip Preliminary Design Chart for Repair System B

Similarly, the interface shear force per rod versus slip response was represented in Figure 5.25.

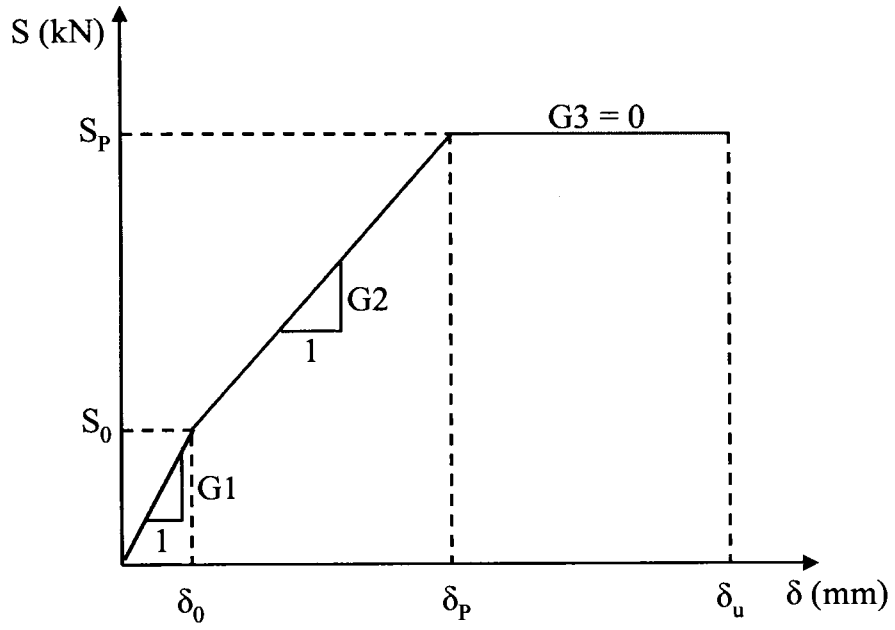

Figure 5.25 - Shear Force per Rod-Slip Preliminary Design Chart for Repair System C

The interface parameters that define the shear stress-slip and shear force-slip step-wise linear curves for each repair system are summarized in Table 5.6.

Table 5.6 - Design Parameters for Repair Systems

Syst.	Interf.	δ_0 (mm)	τ_0 (kPa)	S_0 (kN)	$G1$ (kPa /mm)	δ_P (mm)	τ_P (kPa)	S_P (kN)	$G2$ (kPa / mm)	δ_u (mm)	$G3$ (kPa/ mm)
A	grout-FRP	0	190	-	∞	61	500	-	5.4	112	0
B	grout-FRP	0	210	-	∞	57	440	-	1.9	NA	7.0
C	grout-FRP	6	-	45	23	58	-	122	4.7	90	0
D	grout-FRP	0	370	-	∞	37	810	-	14.7	120	0
E	wood -grout	0	390	-	∞	47	1000	-	16	NA	NA

5.7 Proposed Design Method

The step-wise linear curves for shear stress-slip and shear force-slip can be conveniently used as preliminary guiding charts in combination with Table 5.6, as follows: (1) For repair systems A, D and E (undamaged wood pile) apply curve in Figure 5.23; (2) For repair system B (damaged wood pile) apply curve in Figure 5.24; and (3) For repair system C (undamaged wood pile with shear connector rods) apply curve in Figure 5.25.

The preliminary or putative design process is illustrated for repair system E by computing the height of the overlap interface, h, which corresponds to the FRP composite shell length. The following design data is considered: r_w = 140 mm and t_g = 50 mm. The required vertical load to be transferred through the repair is: P = 160 kN, with a safety factor $SF = 2$ to prevent slip.

From Table 5.6, the repair system E shear strength corresponding to slip at the wood-grout interface is: τ_0 = 390 kPa. Substituting $P_0 = SF \cdot P$ in Eq. (5.3) and solving for h results in

$$h = \frac{SF \cdot P}{2 \cdot \pi \cdot r_w \cdot \tau_0} \tag{5.7}$$

The required shell length is h = 933 mm. Based upon the preliminary test data, this design will result in a safety factor for interface ultimate shear strength of:

$$\frac{SF \cdot \tau_P}{\tau_0} = \frac{(2) \cdot 1000\ kPa}{390\ kPa} = 5.2$$

It should be cautioned that additional replicate specimens should be tested before actual design curves and values can be recommended in work beyond the scope of this thesis.

5.8 Conclusions and Recommendations

Based on the results presented in this chapter the following conclusions are drawn:

1. The proposed push out test method served to characterize the shear versus slip response of the wood-grout and grout FRP composite interfaces.

2. Damaged in the wood pile in the form of necking, which simulates Gribble attack as discussed in Chapter 2, provided interlocking with the grout increasing the interface slip shear strength.
3. The application of the polymer concrete coating layer on the interior surface of the innermost shell prevented slip at the grout-FRP composite interface in our tests.
4. The cement-based grout provided lateral support to the rod-FRP composite bolted connection compared to the polyurethane grout, which resulted in higher interface ultimate shear strength.

The following commentary and proposed practical recommendations are offered:

1. Design of the FRP composite shell shall be based on the interface slip shear strength as illustrated in the example presented.
2. The use of the polymer concrete coating (overlay) on the interior surface of the inner shell is recommended.
3. The use of shear studs or other shear connectors, such as lag screws, embedded in the wood pile and extending through the thickness of the cement-based grout, but not through the FRP composite shield, is recommended. These connectors can increase the wood-grout interface slip strength and also serve as spacers.
4. In field repair of wood piles, it is recommended that the pile surface be cleaned with water or a scraper to eliminate the presence of marine organisms that may affect the interface properties.

5.9 Notation

The following symbols are used in this chapter

h	=	Height of the overlap interface (FRP composite shell length)
n	=	Number of shear connector rods
P	=	Applied compressive load
P_0	=	Slip vertical compressive load
P_P	=	Ultimate vertical compressive load
r	=	Inner radius of FRP composite shield
r_w	=	Radius of wood pile
s	=	Spacing of shear connector rods
SF	=	Safety factor
S_0	=	Slip interface shear force per rod
S_P	=	Ultimate interface shear force per rod
t_f	=	Thickness of FRP composite shield
t_g	=	Thickness of grout
ε_θ	=	Strain in FRP composite shield in the hoop direction
τ_0	=	Slip interface apparent shear strength
τ_P	=	Ultimate interface apparent shear strength

Subscripts

w	=	Wood pile
f	=	FRP composite shield
g	=	grout
θ	=	Hoop direction

Chapter 6

Experimental Characterization of FRP Composite-Wood Pile Structural Response by Bending Tests

6.1 Abstract

A special prefabricated Fiber Reinforced Polymer (FRP) composite shield or jacket was developed to repair wood piles in the field. Two types of load-transfer mechanisms between the wood pile and the FRP composite shield were developed and tested: (1) cement-based structural grout; and (2) steel shear connectors with an expanding polyurethane chemical grout. The objective of this chapter is to characterize the structural response of full-size pre-damaged wood piles repaired with the FRP composite shield system. A three-point bending test procedure was used to simulate the response of a pile subjected to lateral loads. The load-deformation response, deflected shape profile, relative longitudinal displacements (slip), strain distribution, ultimate bending moment capacity and mode of failure were evaluated. Wood piles were pre-damaged by reducing approximately 60% of the cross-section over a portion of the pile. It was found that a pre-damaged wood pile repaired using the FRP composite shield with cement-based grout exceeded the bending capacity of a reference wood pile. The repair system using the FRP composite shield with steel shear connectors and polyurethane grout did not fully restore the bending capacity of a reference wood pile; however it can be used for marine borer protection when wood damage is not critical.

6.2 Introduction

6.2.1 Background

Wood piles have been traditionally used in many marine locations for piers and one to two story waterfront buildings, especially when loose granular materials are present. Locally available wood piles provide a low-cost foundation system. Untreated wood piles are subjected to deterioration from marine borers, fungi and other sources as discussed in Chapter 2. For this reason many wood piles have been treated in the past with preservatives, like creosote or chromated copper arsenate (CCA). With time, preservatives will be leached from the wood, and thus deterioration will begin in treated wood piles similar to that of untreated wood piles.

When wood piles deteriorate, the conventional repair is to dismantle the pier, extract the deteriorated piles, drive new piles and rebuild the pier over the new piles. In addition, treated extracted piles may need special disposal. For some facilities, especially when buildings sit on piers, extraction of all piles and driving of new piles can be difficult and costly. In these cases repair becomes a viable alternative. Repairs are possible since the portion of the pile below the mudline is normally fully intact. The major deterioration occurs in the portion of the pile in the inter-tidal zone and in the splash zone (above high-tide). The repair system can also reduce the rate of future deterioration by introducing a barrier that protects the wood pile from marine borer attacks.

6.2.2 Structural Integrity

Structural wood piles are designed to withstand driving forces, axial gravity loads from the pier structure (sometimes tensile loads) and lateral loads imposed by wind pressure, wave action, ice formation or vessel docking impact. Lateral loads impose bending moments and shear forces on the pile.

When a wood pile has deteriorated, it typically loses cross-section and thus loses capacity to sustain design loads. In this chapter only the capacity for lateral loading of a repaired pile will be covered. The lateral capacity has the most unknows in repair. Driving stresses are not a repair concern. The capacity for compressive vertical loading is related to the cross-sectional area, and tensile vertical loading is less common.

The test method for piles subjected to lateral loads requires the driving of the wood pile into the ground followed by application of a lateral or a combination lateral and axial load as per ASTM D3966 (ASTM 1990). However, in the repair case, a pile will not be re-driven and all the work is conducted above the ground surface, thus the structural integrity of the repaired pile is most important.

Thus it is possible to evaluate a repaired wood pile by conducting a bending test with controlled loading and support conditions. In (EDM 1995) a repair system for wood poles was evaluated by conducting bending tests in accordance to ASTM D1036 (EDM 1995). Decay damage was simulated by mechanically modifying the wood pole section at the ground line.

6.2.3 Objective of the Chapter

The objective of this chapter is to characterize the structural response in bending of full-size pre-damaged wood piles repaired with a specially developed FRP composite shield. The FRP composite shield was designed to fit around installed wood piles in the field. Two types of repair system were designed, installed and tested: (1) An FRP composite shield with cement-based grout between the shield and the wood pile; and (2) An FRP composite shield with shear connectors through the pile and shield and with polyurethane grout between the wood and the shield.

A three-point bending test procedure was used to test the response of a pile subjected to lateral loads The proposed test set-up was designed using ASTM D1036 (ASTM 1999b), a standard test procedure for poles, as a guide. The load-deformation response, deflected shape profile, relative longitudinal displacements (slip), strain distribution, ultimate bending moment capacity and the mode of failure were evaluated.

6.3 Materials and Methods for Pile Repair

6.3.1 Pile Prototype Specimens

Commercial piles were utilized for all testing. Nine meter long, class B, southern yellow pine wood piles treated with CCA preservative were selected (ASTM 1999a). Intact piles were tested to compare to repaired damaged piles. Damaged piles were obtained by cutting the pile to a reduced cross-section near the center of the pile.

Pre-damage to three wood piles was achieved by reducing the diameter of the cross section over a segment of length L_d = 900 mm from the center span toward the pile

tip. The reduction in radius simulated the type of *Limnoria* damage found in a field inspection of the Portland, Maine harbor (See Chapter 2). A 62% reduction of the total cross sectional area was applied in the laboratory to simulate *Limnoria spp.* necking damage. The extent of pre-damage was selected based on the requirement that any wood piles losing 50% of their cross sectional area or more be replaced (U.S. Army 1978).

Two wood piles were used as reference and control specimens. The reference wood pile (IW) was tested undamaged or intact. The control wood pile (DW) was pre-damaged prior to the bending test. The specimen selection served to: 1) quantify the bending stiffness and strength increase resulting from the proposed repair systems by comparing with the reference pile, IW; and 2) establish if the capacity of a damaged wood pile, DW, can be restored with the proposed repair systems.

Cylindrical fiber reinforced polymer (FRP) composite shells or sleeves with a longitudinal opening or gap along their length were fabricated using the licensed Seemann Composites Resin Infusion Molding Process (SCRIMP^{TM}) (TPI 2001). These especially constructed shells can be applied over existing damaged piles in the field. Two FRP composite shells with a thickness of approximately 3.3 mm were used in encasing each of two pre-damaged wood piles, B and C, as presented in Chapter 3. The two fabricated shells were bonded together with an adhesive to form the FRP composite shield or jacket that encased the wood pile section. An underwater curing epoxy adhesive, trade name Hydrobond 500 (Superior Polymer 2000), was selected based on the performance requirements for a wood pile repair system, (See Chapter 3). Durability of this underwater epoxy adhesive to freeze-thaw cycles was tested (See Chapter 4). The longitudinal gaps of each shell were staggered at an angle of 180° to avoid lines of

weakness in the FRP composite shield. The space between the wood and the FRP composite shells was filled with one of the grouting systems (See Figure 6.1).

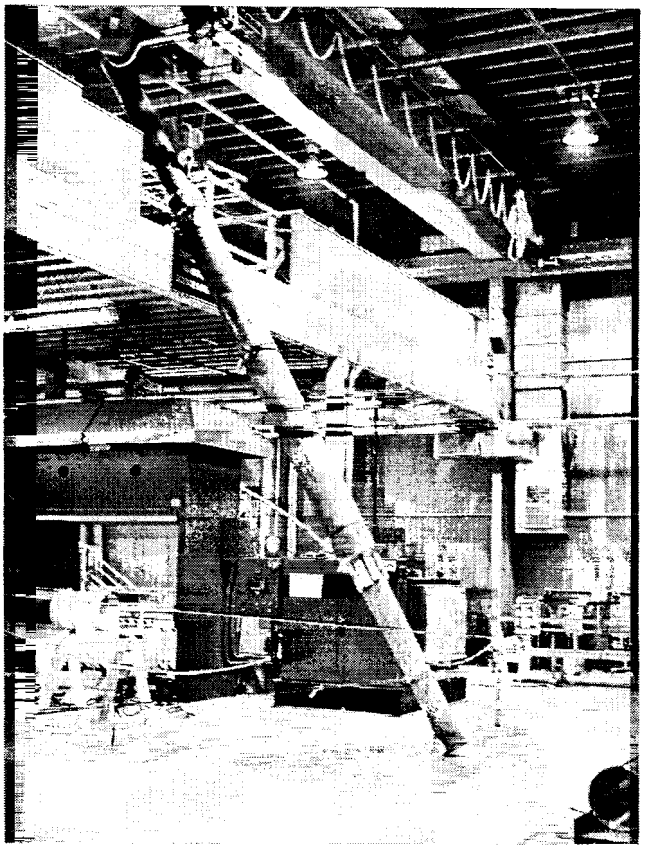

Figure 6.1 - Wood Pile with FRP Composite Shield during Grouting Operation

The first repair system, B, used a cement-based underwater structural grout (Five Star 2001) with a specified compressive strength at 28 days of 51.7 MPa to provide contact between the FRP composite shield and the wood pile, as well as to complete the isolation of the damaged wood portion from marine borers. The second repair system, C, used shear connectors (steel threaded rods) through the shield and the pile to transfer shear forces and used an expanding polyurethane non-structural grout (Sika 1998) to complete the isolation of the damaged wood portion from marine borers. Both repair

systems used two adhesively bonded shells to encapsulate the pre-damaged full-size wood pile using the repair method outlined in Chapter 3.

The cement-based grout used in repair system B was placed from the bottom up to avoid segregation of the materials and air entrapment. A concrete mixer was applied to prepare the grout mix, and a 50 mm diameter discharge hose was used for filling the space. The thickness of the grout was approximately 60 mm. In the grouting operation for the polyurethane chemical grout used for repair system C, the two-part grout was mixed according to the supplier specifications and pumped from the bottom of the repaired section using a paint pot and pressurized air. As the mixture reacted with water, it expanded to fill the space between the wood pile and the inner FRP composite shell with a final thickness of approximately 13 mm. Four steel threaded rods with a diameter of 19 mm were used at each end of the FRP composite shield as shear connectors in repair system C. The steel threaded rods were spaced along the pile axis approximately 102 mm and rotated approximately 30° in the circumferential direction.

A summary of the four pile specimens tested is summarized in Table 6.1. The wood piles, graded according to ASTM D25 (ASTM 1999a), had variable diameters and taper as shown in Table 6.2.

Table 6.1 Wood Pile Systems Configuration

System	Wood pile	FRP Composite Shield	Grout	Shear Connectors	Pile length, (L) m	Span length, (L_s) m
Intact Reference (IW)	Intact	N.A.	N.A.	No	9.14	8.84
Damaged Control (DW)	Pre-damaged	N.A	N.A.	No	9.14	8.84
Repair system B	Pre-damaged	Yes	Cement-based	No	9.14	8.84
Repair system C	Pre-damaged	Yes	Poly-urethane	Yes	9.14	8.84

Table 6.2 Wood Pile Systems Pre-Damage and Bending Test Results

System	Diameter at butt, mm	Diameter at tip, mm	Diameter at load point, mm	Diameter damaged section, mm	Cross-section reduction, %	Peak load, kN	Max. deflection at mid-span, mm
Intact Reference (IW)	363	305	340	N/A	0	79.0	204
Damaged Control (DW)	356	305	308	186	63	8.1	179
Repair system B	362	240	284	182	62	115.5	197
Repair system C	365	267	315	197	61	52.0	158

6.3.2 Three-Point Bending Test Method

To test the structural response of the repaired wood piles, three point bending tests were performed using ASTM D1036 (ASTM 1999b) for wood poles as a guide. The simply-supported test method was selected to simplify the experimental setup. The wood piles were supported at the butt and the tip, and the load was applied at the center.

The span length between the two end supports was $L_S = 8.84\ m$, while the total length of the piles was $L = 9.14\ m$. Each steel end support had a roller mounted on a hinge that was resting on a concrete block (See Figure 6.2 and Figure 6.3), which provided enough space under the pile to accommodate deflection.

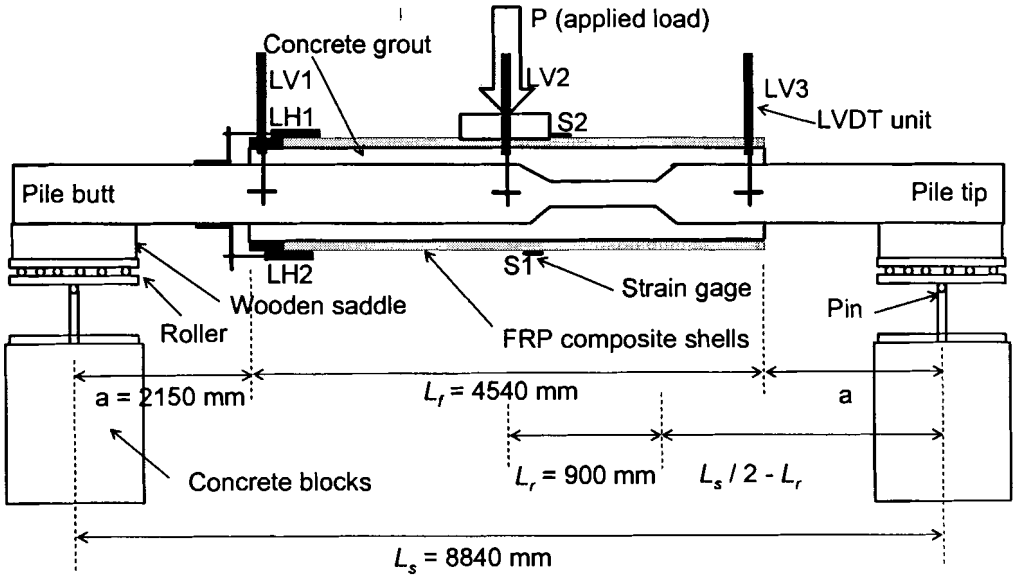

Figure 6.2 Schematic of test set-up for repair system B.

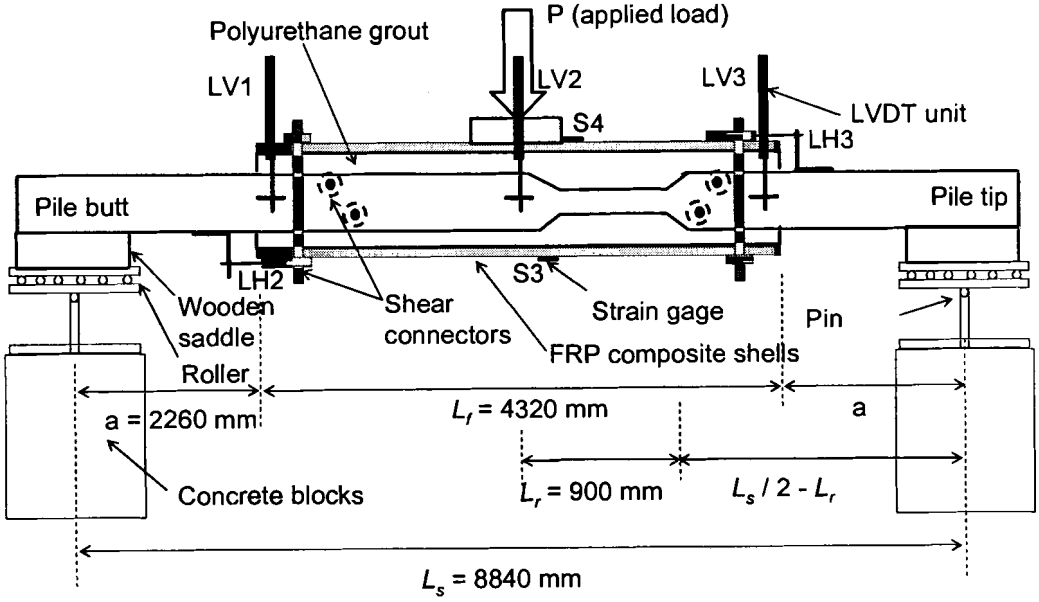

Figure 6.3 Schematic of test set-up for repair system C.

Since the wood piles are circular in cross-section, wooden saddles and straps were placed on top of the end supports to avoid lateral movements (See Figure 6.4). Another saddle with a length of 305 mm was used at mid-span for load transfer from the actuator to the pile without slippage. Load was applied with an Instron servo-hydraulic actuator mounted underneath the structural floor using a steel frame placed on top of the wooden saddle, which resulted in a stable loading configuration (See Figure 6.5).

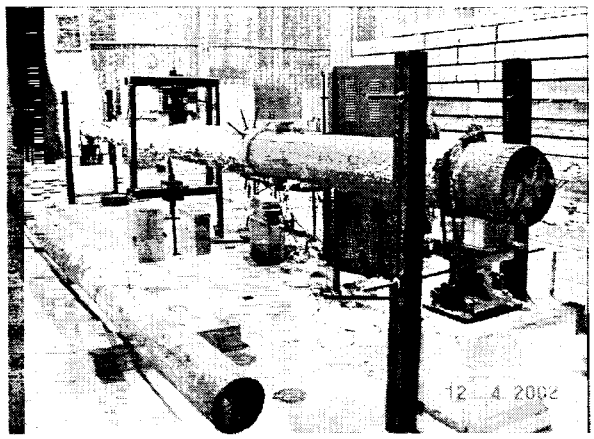

Figure 6.4 Test set-up for repair system C.

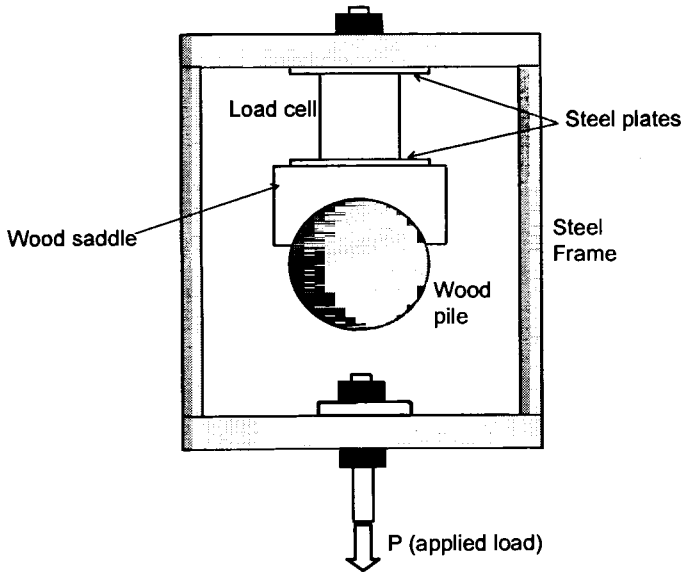

Figure 6.5 - Schematic of Loading Device.

Testing was conducted in a displacement control mode with a constant deflection rate. The peak or maximum load was anticipated based on a beam structural model presented in Chapter 7. Loading was applied in cycles with increasing amplitude to assess residual deformation. A dual ramp generator available from the Instron control software was used to apply a constant deflection rate. Load cycles that represented 10, 20 and 40% of the expected failure load were applied to each specimen. Finally, the pile specimen was loaded to failure, which is defined by the peak load. After the failure load was reached, the repaired specimens, B and C, were reloaded to evaluate the behavior of the system after it was load damaged.

Vertical deflections were measured at three different locations along the length of the pile using Linear Variable Differential Transducer (LVDT) units to obtain the deflected shape. Deflections were measured at mid-span, and at the two ends of the FRP composite shield. Horizontal movement (slip) between the wood pile and the FRP composite shield was measured on the top and bottom at the ends of the encasing shield using LVDT units. Strain gages (CEA-06-250UW-350) were bonded (Measurements Group 1997) on the top and bottom of the FRP composite shield, in the longitudinal direction, to monitor strains during the test (See Figure 6.2 and Figure 6.3). Lab View 6.0 (National Instruments 2000) was used to collect deflections, load and strain data.

6.4 Results and Discussion

6.4.1 Intact Reference Pile (IW)

The reference wood pile, IW, was tested intact to provide the baseline response. The load-deflection response of the reference pile was linear to failure, as shown in Figure 6.6. The peak load reached by the reference pile was 79 kN. The wood pile under bending failed in tension at the mid span location where the load was applied. After failure, re-loading was not possible for the reference pile.

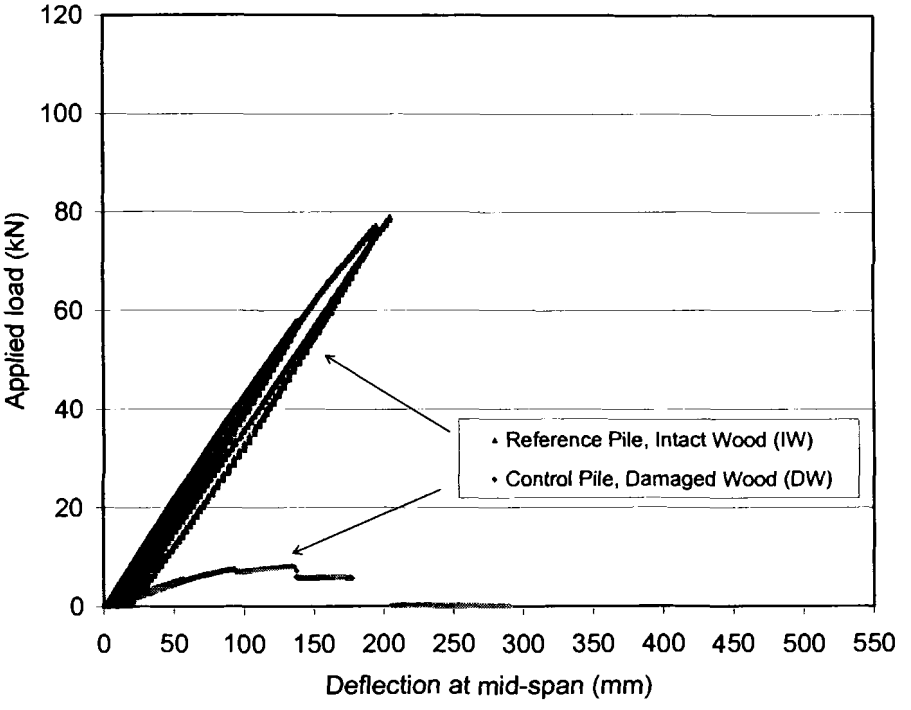

Figure 6.6 Load-deflection response for intact reference pile (IW) and damaged control pile (DW).

6.4.2 Pre-Damaged Control Pile (DW)

The control pile, DW, was pre-damaged with its cross sectional area reduced by 63%. This pile was tested to characterize the behavior of a damaged wood pile. The load-deflection response of the control pile is shown in Figure 6.6. The peak load corresponding to the control pile was 8.2 kN. The 63% reduction in cross sectional area diminished the wood pile bending capacity to one-sixth of the intact reference pile (IW) value. Under bending, the damaged control pile failed in tension at the damaged section. After failure, re-loading was not possible for the control pile.

6.4.3 Repair System B (FRP Composite Shield/Cement Grout)

A pre-damaged pile with its cross-sectional area reduced by 62% over a portion of the pile was repaired using system B (FRP Composite Shield/Cement Grout). The response of the repair system B was linear to failure (See Figure 6.7).

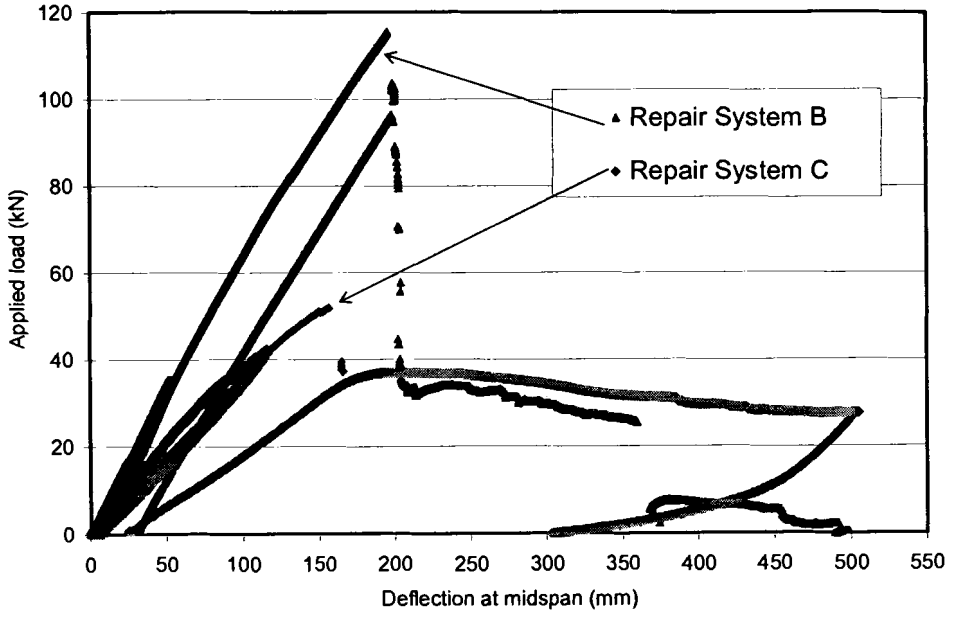

Figure 6.7 Load-deflection response for repair systems B and C.

Under bending, the wood pile failed at a peak load of 115 kN (see Table 6.2) in tension at the end of the FRP composite shield, as shown in Figure 6.8(a).

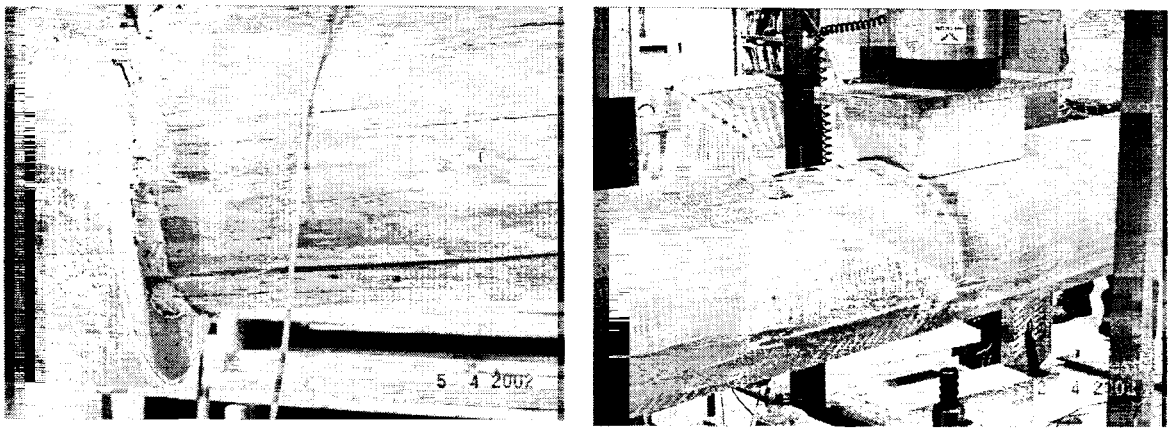

(a) (b)

Figure 6.8 Failure modes: (a) Tension failure in wood pile at shield end (repair system B); (b) Compression failure in FRP composite shield (repair system C).

After unloading, approximately 15% of the total deflection was not recovered, which was attributed to damage accumulation. The specimen was reloaded after failure (See second loading curve depicted in Figure 6.7). The re-loading curve was also linear with approximately the same load-deflection slope as the peak loading curve. Failure occurred in the wood pile outside the segment encased with the FRP composite shield. It was hypothesized that the FRP composite shield restored enough bending capacity to the wood pile pre-damaged section to prevent failure at this location.

Two LVDT units (LH1 and LH2) that measured the horizontal differential movement (slip) between the wood pile and the FRP composite shield were located close to the end of the shield, as shown in Figure 6.2. Load-slip curves are presented in Figure 6.9. Positive slip, which was measured on the bottom side, indicates that the wood

surface moved out of the shield, and thus the shield was subjected to tension stresses. The negative slip at the top indicates that the shield was subjected to compressive stresses.

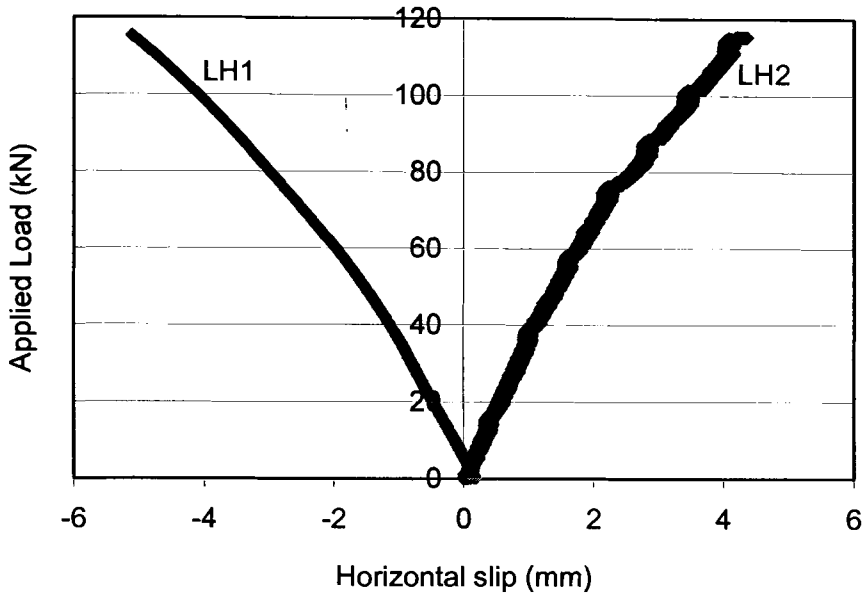

Figure 6.9 Load–slip response for repair system B (load cycle to failure).

The maximum slip value recorded was approximately 5 mm for both LVDTs. The load-slip curve indicates that there is partial interaction between the wood pile and the FRP composite shield. Since top and bottom slip values are similar, this indicates that the FRP composite shield bent about the same neutral axis as the wood pile. Having the two components, shield and wood pile, bending about one single neutral axis validates the design basis that the repaired pile under lateral loads behaves as a beam system.

During re-loading, a shear crack initiated at the edge of the FRP composite shield and started propagating in the FRP composite shield towards mid-span (Figure 6.10). The crack was located at the position where the slit of the inner shell was placed. The load capacity of the repaired system was drastically reduced when the crack initiated. After the

crack reached mid-span, the wood pile section at the pre-damaged location failed. This was attributed to the observation that the pre-damaged wood pile section had no load bearing contribution from the cracked FRP composite shield. This secondary failure of the wood pile diminished the ability of the system to further support any significant lateral loads.

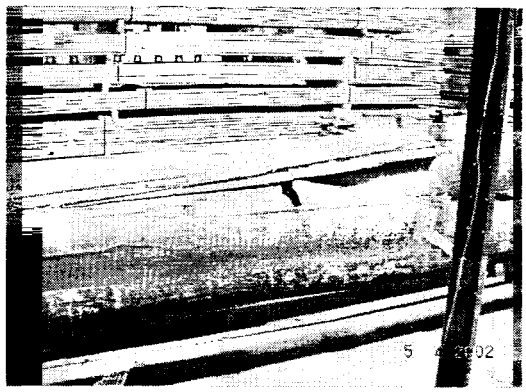

Figure 6.10 - Crack Propagation from Edge of FRP Composite Shield (Repair System B)

6.4.4 Repair System C (FRP Composite Shield/Shear Connectors/Polyurethane Grout)

A pre-damaged pile with its cross-sectional area reduced by 61% over a portion of the pile was repaired using system C (FRP Composite Shield/Shear Connectors/Polyurethane Grout). The load-deflection response of system C was linear up to failure, as shown in Figure 6.7. The peak load for the pile specimen was 52 kN. At the peak load, the FRP composite shield failed in compression in the axial direction at mid-span (end of wood saddle), as depicted in Figure 6.8 (b). This damage was attributed to the observation that the compressible polyurethane grout did not provide load bearing

support between the wood pile and the FRP composite shield. Approximately 16% of the total deflection was non-recoverable (inelastic).

The pile specimen was re-loaded after reaching the peak load. The pile was able to support approximately 70% load of the peak load during reloading with a lower load-deflection slope. As more damage was introduced to the FRP composite shield, the load capacity of the system was reduced (see Figure 6.7). The flexibility of the system using shear connectors was illustrated by the fact that the pile was loaded until reaching the maximum stroke of the servo-hydraulic actuator (500 mm) without catastrophic failure.

Maximum relative horizontal movement (slip) between the wood pile and the FRP composite shield measured with two LVDT units (LH2, and LH3) is presented in Figure 6.11. The maximum horizontal slip recorded was approximately 5 mm for the bottom LVDT (LH2), and less than half of that value for the top LVDT (LH3). The difference in horizontal slip at the top and the bottom indicates that the FRP composite shield does not bend about the same neutral axis as the wood pile does.

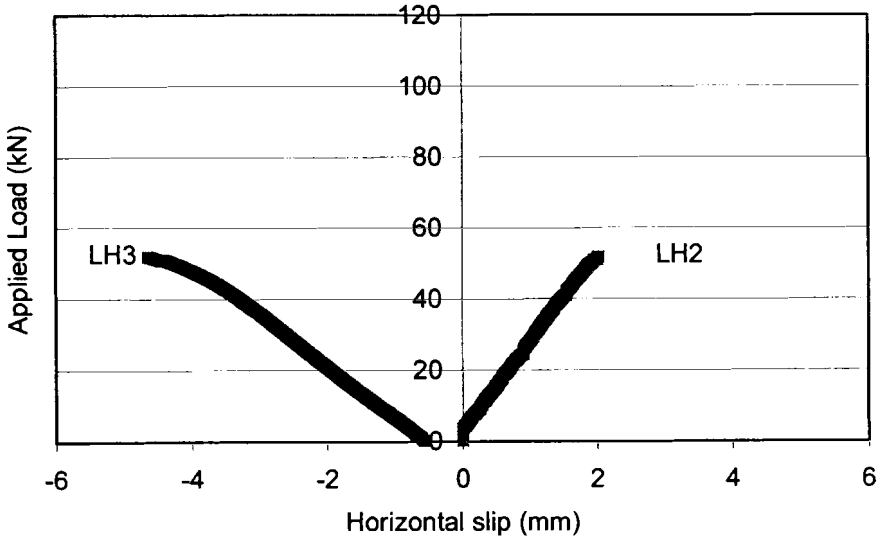

Figure 6.11 Load–slip response for repair system C (load cycle to failure).

The observed failure mode, localized FRP composite compression failure, also supports the observation that the shield does not behave in beam bending with the wood pile.

6.4.5 Deflected Profile Assessment

The deflected profiles at peak load for all pile systems are depicted in Figure 6.12. It was found that the repair system B with the cement-based grout resulted in a maximum mid-span deflection of 196 mm, which is similar to the corresponding value for the reference intact wood pile IW, 205 mm. The repair system B resulted in a decrease in curvature in the maximum bending moment region compared to the reference and control piles (i.e., smoother change in deflection slope along the pile axis). This is a consequence of the increase in bending stiffness over the repaired length of the pile.

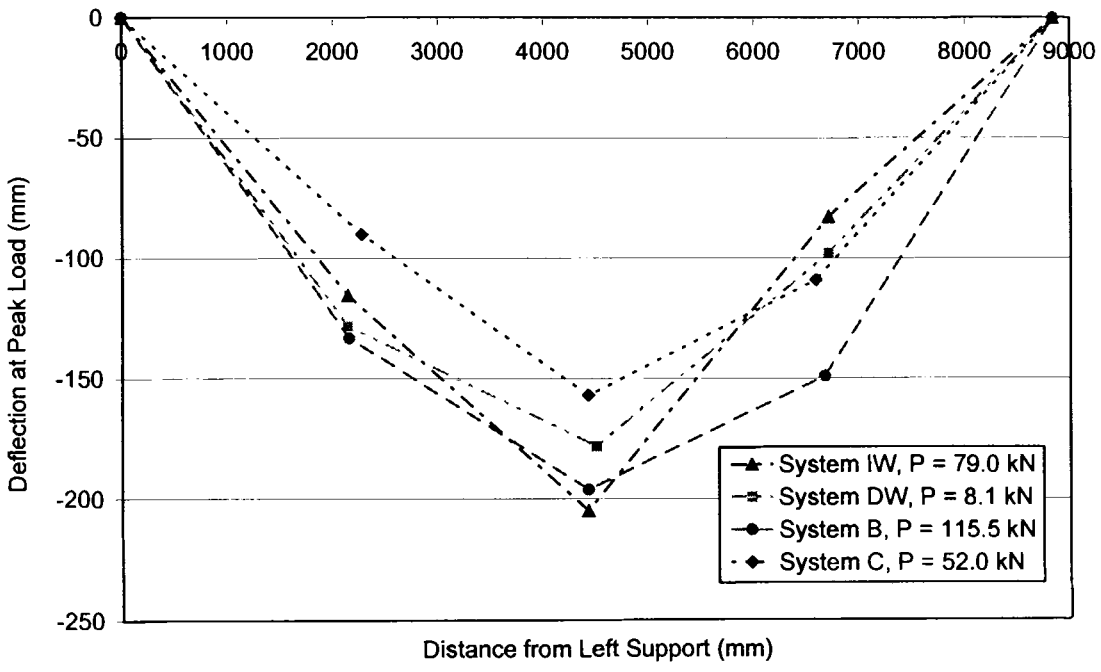

Figure 6.12 Deflected shape at peak load for all pile systems.

6.4.6 Strain Distribution in the FRP Composite Shield

Longitudinal strains at the top and bottom of the FRP composite shield were monitored during the load test for repair systems B and C. Load-strain distribution for both repair systems are presented in Figure 6.13 (see Figure 6.2 and Figure 6.3 for strain gage locations). The axial strains at peak load for the repair system with the cement-based grout, B, were –3800 micro strains on the top and 6700 micro strains on the bottom of the FRP composite shield. Axial strains at peak load for the repair system with the steel shear connectors, C, were –2760 micro strains on the top and 2710 micro strains on the bottom of the FRP composite shield.

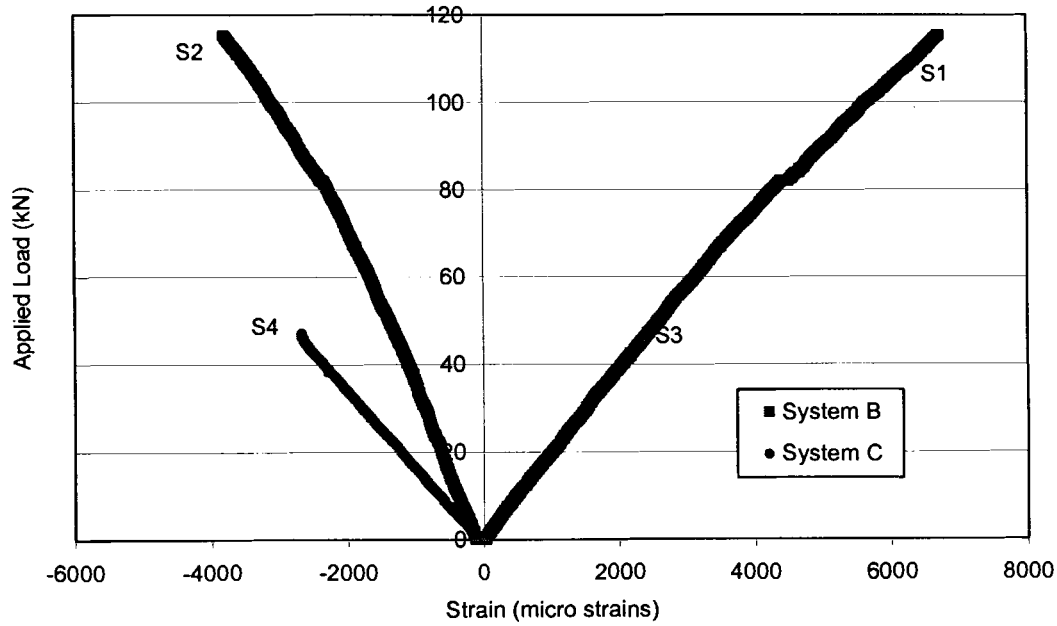

Figure 6.13 Load-strain response for repair systems B and C.

The difference in axial strains between the two repair systems was attributed to the different load transfer mechanisms and flexibility. The cement-based grout in repair system B transferred stresses between the FRP composite shield and the wood pile resulting in higher strains before failure compared to repair system C. In repair system C,

the flexibility resulting from using the steel shear connectors between the shield and the wood pile was much greater than the repair system B with the cement-based grout system. The polyurethane grout did not contribute to reducing the overall flexibility in repair system C.

6.5 Load and Deflection Normalized Parameters

To provide a meaningful comparison among the different piles evaluated (with different diameters and taper) the experimental load-deflection response was normalized. The expression for the maximum deflection of a simply supported beam with constant cross-section is considered for normalizing load and deflection values, as follows:

$$\Delta = \frac{P \cdot L_s^3}{48 \cdot E_w \cdot I_w} \tag{6.1}$$

where $(E_w I_w)$ is the product of the modulus of elasticity by the moment of inertia of the wood pile at the design section. The design section is defined as the section of the wood pile at mid-span. The value of E_w was obtained from the timber poles and piles supplement of the LRFD Manual for Engineered Wood Construction. (AF&PA 1996) The moment of inertia of the circular cross section was calculated as follows:

$$I_w = \frac{\pi \cdot d_w^4}{64} \tag{6.2}$$

where d_w is the design diameter of the wood pile. Rearranging equation (6.1) results in

$$\frac{\Delta}{L_S} = \frac{1}{48} \cdot \frac{P \cdot L_S^2}{E_w \cdot I_w} \tag{6.3}$$

From this equation, the applied load, P, was normalized by the bending stiffness and the span length, as follows:

$$p = \frac{P \cdot L_s^2}{E_w \cdot I_w} \tag{6.4}$$

where p is the normalized (dimensionless) applied load. Similarly, the deflection at mid-span was normalized by dividing by the span length, as follows

$$\delta = \frac{\Delta}{L_S} \tag{6.5}$$

where δ is the normalized (dimensionless) deflection.

The normalized load-deflection response for all four specimens is shown in Figure 6.14. The normalized maximum load and deflection for all pile specimens is summarized in Table 6.3.

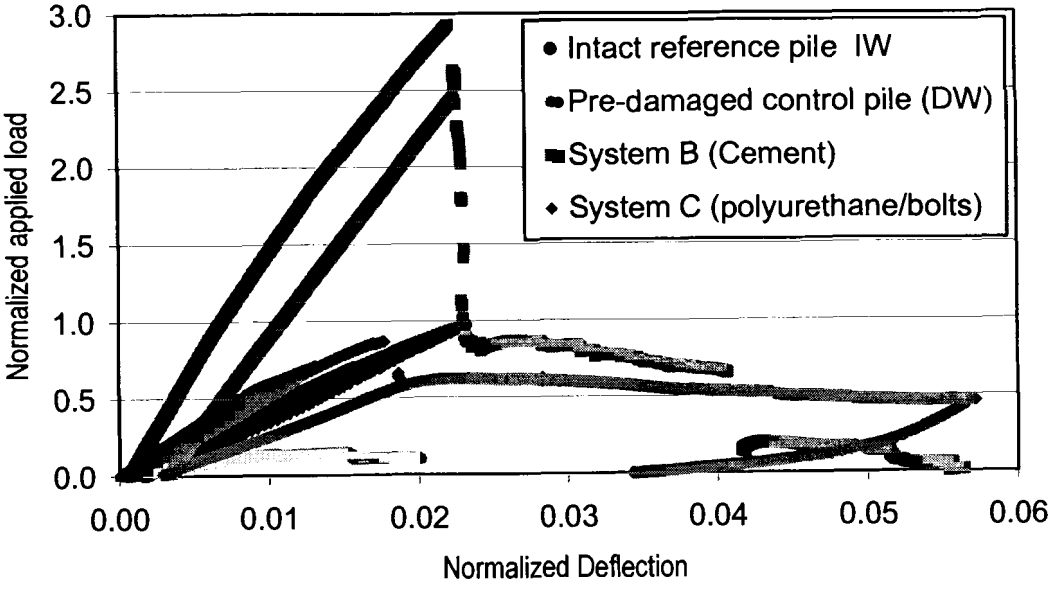

Figure 6.14 - Normalized Load-Deflection Responses for all Wood Pile Systems

The normalized load capacity of the damage specimen, DW, was approximately 15% of the intact reference wood pile, IW. Repair system B exhibited the highest load-deflection slope of all the tested pile systems due to the stiffness and quasi-integral response provided by the cement-based grout. For example, repair system B had a normalized peak load of 2.93 and a normalized maximum deflection at mid-span of 0.022, while repair system C with a normalized peak load of 0.87 had a normalized maximum deflection of 0.018. Bending of the shear connectors in repair system C with the non-structural polyurethane grout resulted in a relatively flexible response.

Table 6.3 Normalized Load and Deflection

System	Span length, (L_s) m	MOE, (E_w) GPa	Moment of inertia, (I_w) 10^{-4} m^4	Normalized peak load	Normalized max. deflection
Intact Wood (IW)	8.84	9.65	6.56	0.97	0.023
Damaged Wood (DW)	8.84	9.65	4.42	0.15	0.021
Repair system B	8.84	9.65	3.19	2.93	0.022
Repair system C	8.84	9.65	4.83	0.87	0.018

6.6 Conclusions

Based on the results presented in this chapter the following conclusions are drawn:

1. A reduction in cross-sectional area of approximately 60% on a portion of the wood pile length decreased the wood pile bending capacity to one-sixth of the intact value. This demonstrated the importance of repairing damaged wood piles.
2. Use of FRP composite shells with slit openings can be applied over damaged piles and can serve as part of a system to fully restore the bending strength of a damaged wood pile.
3. A pre-damaged wood pile with approximately 60% reduction in cross-section on a portion of the length was repaired using the FRP composite shield with cement-based structural grout. It exceeded the bending capacity of an intact reference wood pile.
4. A pre-damaged wood pile with approximately 60% reduction in cross-section on a portion of the length was repaired using the FRP composite shield with shear connectors and polyurethane grout. It only restored the bending capacity to two-thirds of an intact reference wood pile.
5. Transfer of stresses from the FRP composite shield to the wood pile is better accomplished using cement-based grout than with more flexible steel shear connectors. The bending strength of the FRP composite shield/cement grout repair system is more than double the bending strength of the FRP composite shield with steel shear connectors repair system.
6. The FRP composite shield combined with grouting provides a strong impervious containment of a damage pile section. Currently existing systems of repair do not

have impervious containment or the containment shell does not have sufficient strength. Impervious containment of the damaged pile section discourages further marine borer damage to the pile.

6.7 Notation

The following symbols are used in this chapter:

a	=	Distance from support to FRP composite shield
d_w	=	Wood pile design diameter at the mid-span section
E_w	=	Modulus of elasticity of the wood pile
I_w	=	Moment of inertia of the wood pile
L	=	Total pile length
L_r	=	Pre-damaged length
L_f	=	FRP composite shield length
L_s	=	Simply-supported span length
P	=	Lateral load applied on the wood pile
p	=	Normalized (dimensionless) applied load
δ	=	Normalized (dimensionless) deflection
Δ	=	Maximum deflection of a simply supported beam

Subscripts

w	=	Wood

Chapter 7

Design of FRP Composite Shield for Repairing Damaged Wood Piles

7.1 Abstract

A beam design model was developed to predict stiffness and strength properties of wood piles restored with a Fiber Reinforced Polymer (FRP) composite shield or jacket. Two types of load-transfer mechanisms between the wood pile and the FRP composite shield were studied: (1) cement-based structural grout; and (2) steel shear connectors with an expanding polyurethane chemical grout. The design model accounts for wood pile damage by reducing the cross-section over a portion of the pile length. Laminate analysis was applied to estimate FRP composite elastic and strength properties. The model allows computation of shear forces at the interfaces between three different materials (wood pile, grout, and FRP composite shield) present in a repaired wood pile. The beam model was correlated with experimental results from three-point bending tests of pre-damaged wood piles repaired with FRP composite shields. The model was applied to predict the maximum bending loads, modes of failure and mid-span deflections of pre-damaged and repaired wood piles. It was found that the proposed model equations have reasonable accuracy and they can be used as a design tool to determine the FRP composite reinforcement needed to restore the structural capacity of a damaged wood pile. The proposed beam model can be applied to various boundary conditions representative of actual piles in waterfront structures (e.g., fixed-free supports).

7.2 Introduction

7.2.1 Background

Structural wood piles installed in waterfront facilities are designed to withstand axial gravity loads from the pier structure (sometimes tensile loads) and lateral loads imposed by wind pressure, wave action, ice formation or vessel docking impact. Lateral loads impose bending moments and shear forces on the pile. When a wood pile has deteriorated, it typically loses cross-section and thus loses capacity to sustain design loads.

A special prefabricated Fiber Reinforced Polymer (FRP) composite shield or jacket was developed to repair installed wood piles in the field (See Chapter 3). Two types of repair system were designed, installed in full-size pre-damaged wood piles and tested in bending (See Chapter 6): (1) An FRP composite shield with cement-based grout between the shield and the wood pile; and (2) An FRP composite shield with shear connectors through the pile and shield and with polyurethane grout between the wood and the shield.

7.2.2 Objective

The objective of this chapter is to present a beam design model to predict the bending response of full-size pre-damaged wood piles repaired with an FRP composite shield. Two types of load-transfer mechanisms between the wood pile and the FRP composite shield are studied: (1) cement-based structural grout; and (2) steel shear connectors with an expanding polyurethane chemical grout. The proposed model

accounts for wood pile damage by reducing the cross-section over a portion of the pile length.

7.3 Material Properties and Cross-Section Dimensions

7.3.1 Repair Systems

Cylindrical FRP composite shells or sleeves with a longitudinal opening or gap along their length were fabricated using the licensed Seemann Composites Resin Infusion Molding Process (SCRIMP^{TM}) (TPI 2001). These especially constructed shells can be applied over existing damaged piles in the field.

The first repair system, B, used a cement-based underwater structural grout (Five Star 2001b) to provide contact between the FRP composite shield and the wood pile, as well as to complete the isolation of the damaged wood portion from marine borers. The second repair system, C, used shear connectors (steel threaded rods) through the shield and the pile to transfer shear forces and used an expanding polyurethane non-structural grout (Sika 1998) to complete the isolation of the damaged wood portion from marine borers. Both repair systems used two adhesively bonded shells to encapsulate the pre-damaged full-size wood pile using the repair method outlined in Chapter 3.

7.3.2 FRP Composite Shell

7.3.2.1 Materials and Fabrication Process. Two FRP composite shells with a thickness of approximately 3.3 mm were used in encasing each of two pre-damaged wood piles for both repair systems B and C. The two fabricated shells were bonded

together with an underwater curing epoxy adhesive (Superior Polymer 2000) to form the FRP composite shield or jacket that encased the wood pile section.

A unidirectional woven E-glass fabric with a weight of 880 g/m^2, trade name VEW 260, was selected as the primary continuous reinforcement for the FRP composite shell. Chopped Strand Mat (CSM) weighing 305 g/m^2, trade name MAT 113, was used as secondary non-continuous and randomly oriented reinforcement on the surfaces. The proposed fiber architecture for the FRP composite shell consisted of three layers of unidirectional continuous fabric reinforcement in the longitudinal or axial direction (0°), one layer of unidirectional continuous fabric reinforcement in the hoop or circumferential direction (90°), and two outer CSM layers (See Figure 7.1).

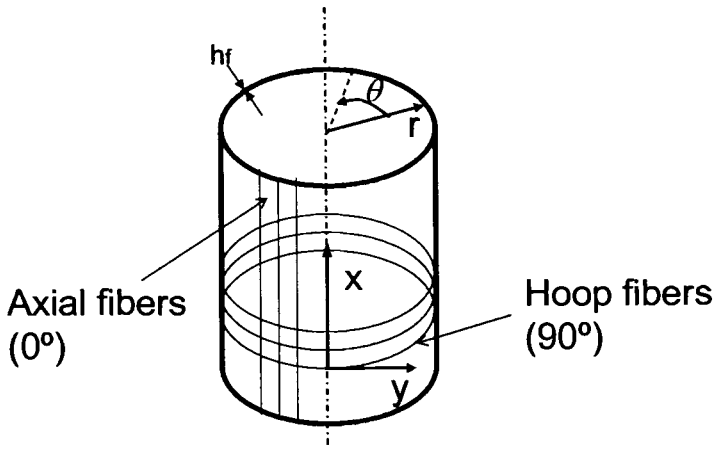

Figure 7.1 - FRP Composite Shell: Geometry and Continuous Fiber Directions

The fiber architecture design is based on maximizing fiber reinforcement in the axial direction with a minimum amount of fibers oriented in the hoop direction. Axial fiber reinforcement contributes to both bending and axial stiffness and strength of the shell, which is required to splice the damage portion of the wood pile. Hoop fiber reinforcement provides adequate integrity to the flexible shell with the required shear

strength and mechanical fastener support. One CSM layer was placed on each surface of the shell laminate to provide improved bonding to the substrate and to develop a resin rich area for environmental protection. The resulting laminate lay-up of the FRP composite shell is [CSM, 0, 90, 0, 0, CSM] (See Figure 7.2). An epoxy-based vinyl ester resin, Derakane 411-C50, was selected as the matrix for the composite shells (Dow Chemical 1999). This resin has a viscosity of 0.15 Pa.s and is well suited for SCRIMP™ processing.

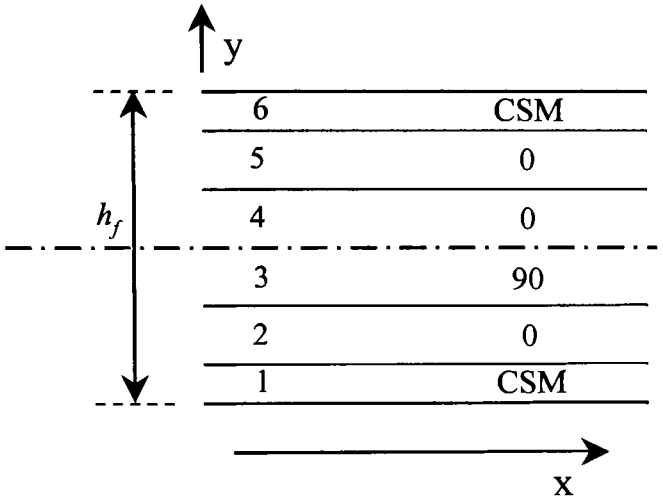

Figure 7.2 - FRP Composite Shell Laminate Lay-Up

7.3.2.2 Lamina Elastic Properties. Micromechanics equations were used to determine the elastic properties of each lamina modeled as a composite with fibers with a resin matrix. The thickness of each lamina or layer was determined from Equations (7.1) and (7.2). The weight fraction of the CSM was set at 0.50 based on prior experience.

$$t_{csm} = w_{csm} \cdot \left(\frac{\frac{1}{W_{csm}} - 1}{\rho_m} + \frac{1}{\rho_f} \right) \tag{7.1}$$

where, ρ_f is the density of the fibers, ρ_m is the density of the matrix. t_{csm} is the thickness of the CSM lamina in millimeters and w_{csm} is the weight per unit area of the CSM in g/m^2.

$$t = (h_f - t_{csm}) \cdot \frac{w}{w_{dir}} \tag{7.2}$$

where, t is the thickness of the lamina in millimeters, h_f is the thickness of the cured composite shell in millimeters, w is the weight per unit area of the lamina in g/m^2, and w_{dir} is the weight per unit area of the continuous directional fibers in the fabric. The fiber volume fraction, V_f, for each individual lamina was then calculate as

$$V_f = \frac{w}{\rho_f \cdot t} \tag{7.3}$$

The properties of each lamina such as the modulus of elasticity, Poisson's ratio and inplane shear modulus were determined based upon the properties calculated previously. These properties were calculated for each unidirectional lamina with respect to its material reference axes.

Assumed properties of the composite constituents, fiber and the resin matrix, are reported in Table 7.1.

Table 7.1 - Fiber Reinforcement and Resin Matrix Properties

Property	E-Glass Fiber (Barbero 1998)	Vinly Ester Resin Matrix (Dow Chemical 1999)
Elastic modulus, E	72.3 GPa	3.4 GPa
Poisson's ratio, ν	0.22	0.38
Density, ρ	2.54 g/cm^3	1.12 g/cm^3

The computed fiber volume fraction for each composite lamina is reported in Table 7.2.

Table 7.2 - Laminate Lay-up and Fiber Reinforcement

Layer #	Fiber Reinforcement	Fiber orientation angle	Fiber weight (g/m^2) (BTI 2000)	Fiber volume fraction (%)
1	CSM	random	305	32
2	Unidirectional	0	880	45
3	Unidirectional	90	880	45
4	Unidirectional	0	880	45
5	Unidirectional	0	880	45
6	CSM	random	305	32

Elastic properties of a composite lamina were calculated using micromechanics equations. Rule of Mixture (ROM) and Halpin-Tsai equations were used to predict lamina elastic moduli in both material directions (E_1, E_2), Poisson's ratio (v_{12}) and in plane shear modulus (G_{12}) (Mallick 1993) (Barbero 1998). The longitudinal elastic modulus was calculated using the following rule of mixtures equation:

$$E_1 = E_f \cdot V_f + E_m \cdot V_m \tag{7.4}$$

where the matrix volume fraction $V_m \approx 1 - V_f$ assuming that the composite laminate has negligible void content.

The transverse elastic modulus was obtained using the Halpin-Tsai semi-empirical formula

$$E_2 = E_m \cdot \left[\frac{1+\zeta \cdot \eta \cdot V_f}{1-\eta \cdot V_f} \right] \tag{7.5}$$

where η and ζ are empirical parameters, as follows:

$$\eta = \frac{\frac{E_f}{E_m} - 1}{\frac{E_f}{E_m} + \zeta} \tag{7.6}$$

It is assumed that $\zeta = 2$ for circular fibers.

Since a CSM lamina has short fibers, which are randomly distributed between 0° and 180°, the modulus of elasticity, is approximated by Equation (7.7) as an equivalent isotropic material (Barbero 1998).

$$E_{csm} = \frac{3}{8} E_1 + \frac{5}{8} E_2 \tag{7.7}$$

where, E_1 and E_2 are values of a unidirectional lamina calculated with the same fiber volume fraction as the CSM lamina. Other lamina elastic properties, G_{12} and ν_{12}, are computed in a similar manner.

The computed elastic moduli in material coordinates of the composite lamina are reported in Table 7.3.

Table 7.3 – Elastic Moduli of Composite Lamina

Modulus in material coordinates	Units	CSM (Layers 1 & 6)	Unidirectional fiber reinforcement (Layers 2, 3, 4 &5)
E_1	GPa	13.6	34.4
E_2	GPa	13.6	10.0

7.3.2.3 Laminate Elastic Parameters. The FRP composite shell was modeled as a laminate using classical lamination theory (Barbero 1998). The inplane compliance matrix, [α], was determined as follows

$$[\alpha] = [A]^{-1} \tag{7.8}$$

where [A] is the inplane stiffness matrix. Finally, the inplane laminate moduli were calculated. The laminate longitudinal and transverse modulus of elasticity in global coordinates, x and y, were computed as

$$E_x = \frac{1}{h_f \alpha_{11}} \tag{7.9}$$

$$E_y = \frac{1}{h_f \alpha_{22}} \tag{7.10}$$

The computed longitudinal and circumferential elastic moduli of the FRP composite shell are shown in Table 7.4.

Table 7.4 – Longitudinal and Circumferential Elastic Modulus of FRP Composite Shell

Property	Units	Value
E_x	GPa	25.4
E_y	GPa	15.6

7.3.3 Cement-Based Grout Properties

The cement-based grout compressive strength at twenty-eight days was specified as f'_c = 51.7 MPa (Five Star 2001a). The cement-based grout elastic modulus (E_c) was calculated based on the following equation for normal weight concrete (Nawy 2000):

$$E_c = 4700 \cdot \sqrt{f'_c} \quad \text{where } f'_c \text{ in MPa} \tag{7.11}$$

For the specifie value of f'_c the resulting modulus is E_c = 33.8 GPa. It should be noted that the confinement effect of the FRP composite shield on the grout properties was neglected (Kshirsagar et al. 2000). The calculated modulus therefore would represent a conservative value, and the authors felt this was appropriate given the need for a conservative design in practice.

7.3.4 Wood Pile Properties

A procedure to generate member design resistance for wood piles based on the Load and Resistance Factor Design (LRFD) method was applied (AF&PA 1996b). Wood pile bending strength, F_b, and modulus of elasticity (MOE), E_w were obtained from the Manual for Engineered Wood Construction (AF&PA 1996c). For a cantilever pile the

design diameter can be determined using the equation for a tapered circular column given in Section 4.3.4 of the ASCE Standard 16-95 (AF&PA 1996a):

$$D_w = D_1 + X \cdot (D_1 - D_2) \tag{7.12}$$

where D_1 and D_2 are the tip and but diameters respectively. The value of X can be calculated as follows, Table 4.3-1 of (AF&PA 1996a):

$$X = 0.12 + 0.18 \cdot (\frac{D_1}{D_2}) \tag{7.13}$$

This expression is valid for the case of an inverted "flagpole" pile with the small end (tip) fixed and the large end (butt) free. If the end conditions are different, then other cases in Table 4.3-1 of (AF&PA 1996a) should be considered.

The design moment of inertia of the intact portion of the wood pile, I_w, was calculated as follows:

$$I_w = \frac{\pi \cdot D_w^4}{64} \tag{7.14}$$

Then, the moment capacity, M_w, of the intact wood portion is calculated using the following equation:

$$M_w = F_b \cdot \frac{I_w}{c} \tag{7.15}$$

where F_b is the bending strength and c is the distance of the extreme wood fiber from the neutral axis.

Properties of the damaged wood pile section were based on the reduced diameter, D_{red}. The reduced moment of inertia, I_{red}, and the corresponding moment capacity of the damaged section, M_{red}, are calculated by substituting the properties of the reduced section in Equations (7.14) and (7.15), respectively.

It should be noted that the proposed beam design model neglects the taper of the wood pile. However, the definition of the design diameter attempts to account for the typical cross-section variation in wood piles. This is a simplification consistent with the objective of developing a simple design model.

7.4 Beam Design Model

7.4.1 Beam Model of Wood Pile Encased with FRP Composite Shield

A practical beam model to predict the response of pre-damaged and repaired wood piles under bending loads was developed. The geometric input data required are span length, wood pile diameters at butt, tip and load point, grout thickness and FRP composite shield thickness. The bending stiffness, $(EI)_{cs}$, of the repaired FRP composite-wood pile section before any damage is imposed to any of the materials (wood, grout and FRP composite), was determined as follows

$$(EI)_{cs} = \iint y^2 \cdot E_i \cdot dA \tag{7.16}$$

where y is the vertical distance from a horizontal line passing through the center of the cross-section to the point of interest, E_i is the modulus of elasticity of each materials and dA is the differential of cross-sectional area (See Figure 7.3). Since the FRP composite shield and the wood pile are assumed to be concentric, polar coordinates are introduced as depicted in Figure 7.3

$$y = r \cdot \sin\theta \tag{7.17}$$

where r is the radius and θ is the angle. Then, the differential area results in

$$dA = r \cdot dr \cdot d\theta \tag{7.18}$$

where dr is the differential radius and $d\theta$ is the differential angle.

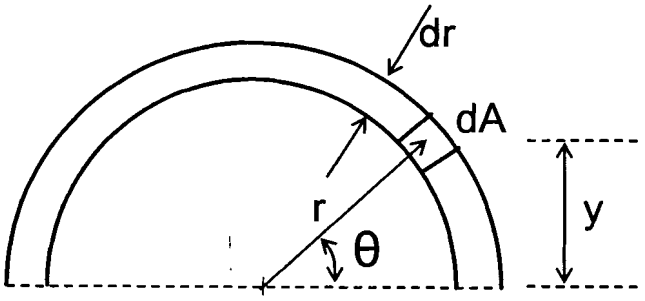

Figure 7.3 - Partial Cross-Section Schematic of Wood Pile and FRP Composite Shield

Substituting y and dA into equation (7.16)

$$(EI)_{cs} = \int_0^{r_f} \int_0^{2\pi} (r\sin\theta)^2 E_i \, r \, d\theta \, dr \tag{7.19}$$

Integrating over the radii of the different materials the stiffness of the repaired composite section can be expressed as

$$(EI)_{cs} = \frac{\pi}{4}\left(r_w^4 \cdot E_w + (r_c^4 - r_w^4)\cdot E_c + (r_f^4 - r_c^4)\cdot E_x\right) \tag{7.20}$$

where r_w is the outer radius of the wood pile, r_c is the outer radius of the cement-based grout, and r_f is the outer radius of the FRP composite shield.

Force equilibrium of a section cut from the FRP composite shield with length Δx is considered based on the free body diagram shown in Figure 7.4. The section is cut on one side of the neutral axis of the beam; therefore the only external loads applied are axial stresses at both ends and shear stresses at the interface with the cement-grout material.

The differential of axial force, ΔF_x, acting on ends of the FRP composite shield is computed by integrating bending stresses over the FRP composite shield cross-section, as follows

$$\Delta F_x = F_{x+\Delta x} - F_x = \frac{\Delta M}{(EI)_{cs}} \cdot \int_{r_c}^{r_f} \int_{0}^{\pi} E_x \cdot r^2 \cdot \sin\theta \cdot d\theta \cdot dr \tag{7.21}$$

where ΔM is the change in applied bending moment over the length Δx.

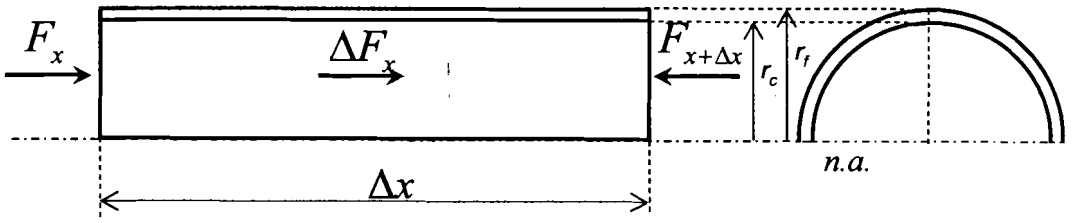

side view cross-section

Figure 7.4 - Section of FRP Composite Shield

After solving the double integral, the expression of ΔF_x results in:

$$\Delta F_x = \frac{2}{3} \cdot \frac{E_x \cdot (r_f^3 - r_c^3)}{(EI)_{cs}} \cdot \Delta M \tag{7.22}$$

The average shearing force at the interface between the FRP composite shield and the cement-based grout can be computed as the differential force over the contact area of the interface, as follows

$$\tau_{xr}^{f} = \frac{\Delta F_x}{\pi \cdot r_c \cdot \Delta x} = \frac{2}{3} \frac{E_x \cdot (r_f^3 - r_c^3)}{(EI)_{cs} \cdot \pi \cdot r_c} \cdot V \tag{7.23}$$

where the shear force is $V = dM/dx \cong \Delta M/\Delta x$ for a section of infinitesimal length (Gere 2000).

Following a similar approach the average shear stress at the interface between the wood and cement-based grout interface can be determined as follows:

$$\tau_{xr}^{c} = \frac{2}{3} \cdot \frac{E_x \cdot (r_f^3 - r_c^3) + E_c \cdot (r_c^3 - r_w^3)}{(EI)_{cs} \cdot \pi \cdot r_w} \cdot V \tag{7.24}$$

It should be noted that since the FRP composite shield and the wood pile bend about the same neutral axis only the average shear stresses computed in equations (7.23) and (7.24) develop at the interface.

The FRP composite shield is not fully effective at the two edges. Shear stresses need to develop at the interface over a length to fully develop axial stresses in the FRP composite shield. The length over which the FRP composite shield becomes effective is known as the development length.

7.4.2 Application to Three-Point Bending Configuration

7.4.2.1 Computation of Development Length. In this application, the wood pile was treated as a simply supported beam partially reinforced along the length with a concentrated load applied at midspan. A segment with a length L_f was reinforced with an FRP composite shield (See Figure 7.5). The beam design model was applied to predict maximum bending moments, average shear stresses at the interfaces, deflections at mid-span and mode of failure.

The diameter at the point of load was considered to be the design diameter, D_w, and it was used to calculate cross sectional properties such as moment of inertia, I_w, of the intact portion of the wood pile.

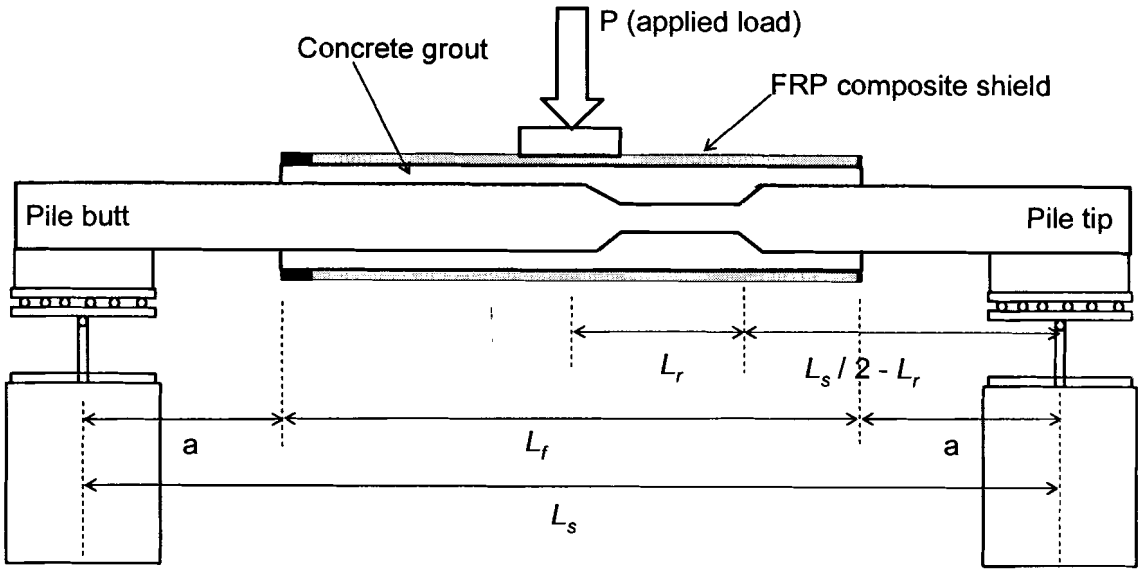

Figure 7.5 Three-Point Bending Experimental Setup

The bending moment, M, for a simply supported beam at a distance $x=a+l_{df}$ from the left support is

$$M = \frac{P}{2} \cdot (a + l_{df}) \tag{7.25}$$

where, a is the distance between the support and the edge of the FRP composite shield and, l_{df} is the development length of the FRP composite shield. Over the development length, the resultant of shear stresses at the interface should be equal to the axial force in the FRP composite shield when the section is fully effective, as follows:

$$\tau_0 \cdot l_{df} \cdot \pi \cdot r_c = F_{x=a+l_{df}} \tag{7.26}$$

where τ_0 is the apparent slip-shear strength of the grout-FRP composite interface, which was obtained from push-out tests (See Chapter 5). Substituting the known parameters in equation (7.26) the expression for the development length is obtained:

$$l_{df} = \frac{F_{x=a+l_{df}}}{\tau_0 \cdot \pi \cdot r_c} = \left(\frac{3 \cdot \tau_0 \cdot (\pi) \cdot r_c \cdot (EI)_{cs}}{P \cdot a \cdot E_x \cdot (r_f^3 - r_c^3)} - 1 \right)^{-1} \tag{7.27}$$

A similar procedure is followed to determine the development length for the cement-based grout (l_{dc}) as follows:

$$l_{dc} = \frac{F_{x=a+l_{dc}}}{\tau_0 \cdot \pi \cdot r_w} = \left(\frac{3 \cdot \tau_0 \cdot (\pi) \cdot r_w \cdot (EI)_{cs}}{P \cdot a \cdot \left(E_x \cdot (r_f^3 - r_c^3) + E_c \cdot (r_c^3 - r_w^3)\right)} - 1 \right)^{-1} \tag{7.28}$$

where, τ_0, is the apparent shear strength of the wood-grout interface, which was obtained from push-out tests (See Chapter 5).

In the case of the shear connectors (repair system C) the development length was determined by considering that the total force transferred by shear connectors should be equal to the axial force in the FRP composite shield, as follows:

$$P_p \cdot n = P_p \cdot \frac{l_{db}}{s} = F_{x=a+l_{db}} \tag{7.29}$$

where P_p is the force transferred by each shear connector obtained from push-out tests, n is the number of shear connectors, l_{db} is the development length of the FRP composite shield for repair system B (see Chapter 5) and s is the spacing of the shear connectors. Then, the development length becomes:

$$l_{db} = \frac{F_{x=a+l_{db}}}{\frac{P_p}{s}} = \left(\frac{3 \cdot \frac{P_p}{s} \cdot (EI)_{cs}}{P \cdot a \cdot \left(E_x \cdot (r_f^3 - r_c^3) + E_c \cdot (r_c^3 - r_w^3)\right)} - \frac{1}{a} \right)^{-1} \tag{7.30}$$

7.4.2.2 Ultimate Moment Capacity. The moment capacity of the FRP composite shield is determined as

$$M_{fu} = \frac{I_f}{r_f} \cdot F_{xc} = \frac{\pi}{4} \cdot (r_f^4 - r_c^4) \cdot \frac{F_{xc}}{r_f} \tag{7.31}$$

where I_f is the moment of inertia of the FRP composite shield, r_f is the distance of the extreme FRP composite shield fiber from the neutral axis and F_{xc} is the longitudinal compressive strength of the FRP composite shield. For the FRP composite shield considered, F_{xc} was estimated as 280 MPa.

The ultimate moment capacity of the repaired section is computed as the sum of the moment capacity of the FRP composite shield and the moment capacity of the wood pile. This approach assumes that both materials reach the ultimate moment capacity simultaneously. It should be noted that this is an approximation that only provides an upper bound for the moment capacity of the repair wood pile. However, if an accurate characterization of the moment capacity of the FRP composite shield and the wood pile is available, then the corresponding ultimate values can be utilized.

A graphical representation of the ultimate moment capacity of the wood pile repair with system B (cement-based grout) and the applied moment along the length of the pile is shown in Figure 7.6. The damaged segment corresponds to the drop observed in the moment capacity. The point at which the applied moment exceeds the moment capacity is the point at which the repaired wood pile fails. In the example shown in Figure 7.6 the wood pile fails at the edge of the FRP composite shield and the failure occurs in the wood. This response was verified by experimental results (See Chapter 6).

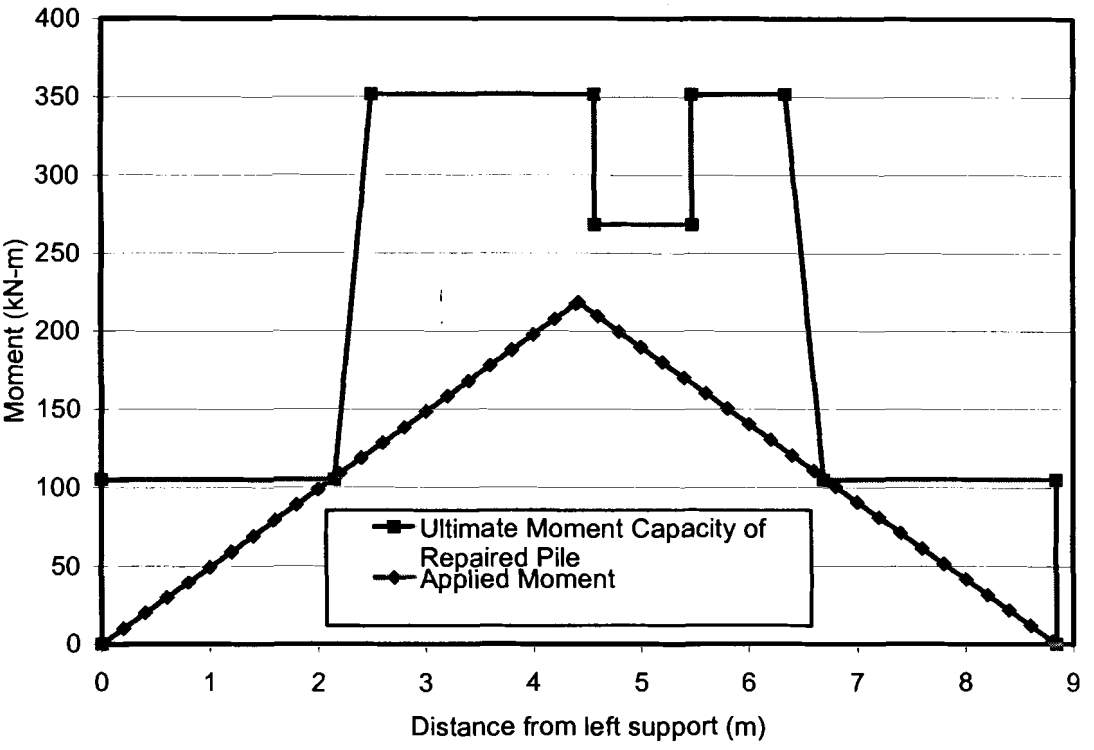

Figure 7.6 - Moment Capacity of Repaired Pre-Damaged Wood Pile and Applied Moment for Simply Supported Beam (Repair System B)

In the case of the repair system C with shear connectors and polyurethane grout, it was found experimentally (see Chapter 6) that the FRP composite shield fails due to local buckling. This mode of failure was attributed to the inability of the polyurethane grout to provide lateral support to the FRP composite shield. To account for this type failure, the moment capacity of the FRP composite shield was determined based on buckling of thin-walled circular cylinders under applied bending moment (Barbero 1998):

$$M_{fu} = K \cdot E_x \cdot r_f \cdot \frac{h_f^2}{1-\nu_{xy}^2} \tag{7.32}$$

where $K=0.72$ is a constant that can be obtained from theory or experiments, and $\nu_{xy} = 0.34$ is the assumed Poisson's ratio of the FRP composite shield (Barbero 1998). It

should be noted that this equation is only applicable to quasi-isotropic laminates (Barbero 1998); therefore it is an approximation to use this equation for the laminate considered for the FRP composite shield.

The moment capacity of the repaired wood pile with shear connectors, and the applied moment along the length of the pile are shown in Figure 7.7.

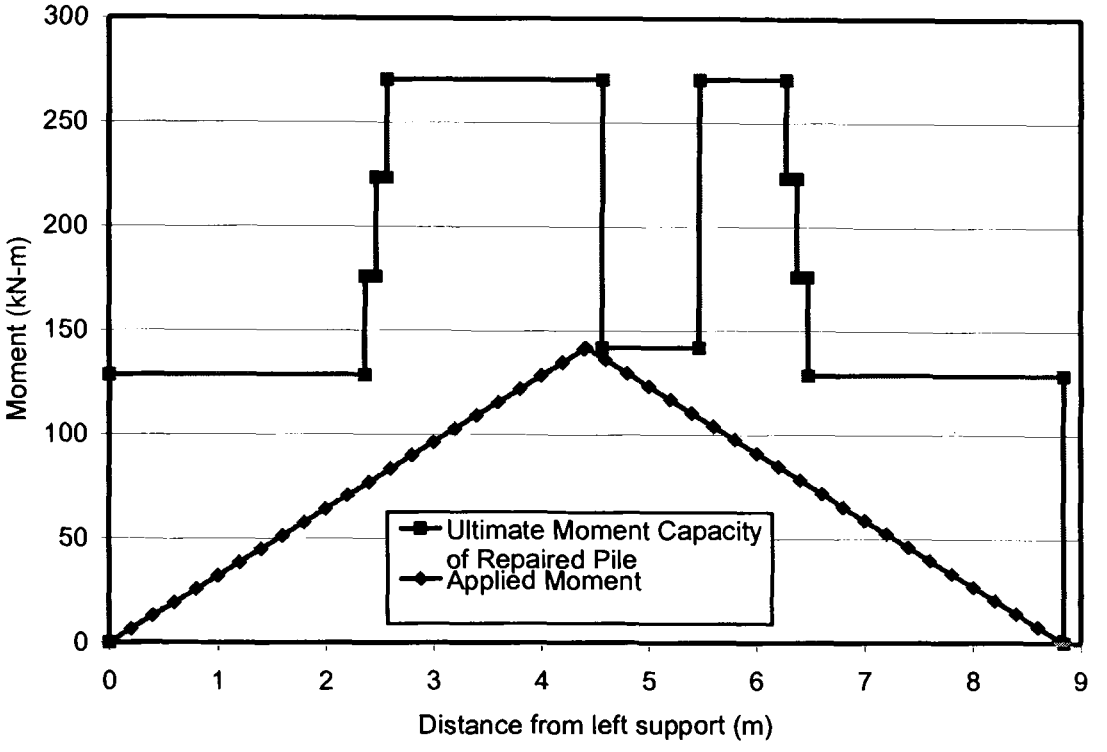

Figure 7.7 - Moment Capacity of Repaired Pre-Damaged Wood Pile and Applied Moment for Simply Supported Beam (Repair System C)

Failure was predicted at one end of the damaged section close to the beam midspan. This predicted failure location was in agreement with the predicted failure location in the bending tests (see Chapter 6).

7.4.2.3 Computation of Beam Deflections. The principle of virtual work was applied to calculate the midspan deflection. This approach accounts for the difference in stiffness of the pre-damaged and repaired wood pile along the length.

$$\Delta_{max} = \int \frac{M \cdot m}{EI} \cdot dx \tag{7.33}$$

where M is the applied moment, m is the virtual moment or unit moment, and EI is the product of the elastic modulus and the moment of inertia at each section.

7.4.3 Installed Wood Pile Application

7.4.3.1 Cantilever Column Configuration. A typical installed wood piles was modeled as a cantilever column. The point of fixity was assumed to be at a given depth below the mud line, D_{fix} (See Figure 7.8) (Alpin and Lepper 2000; U.S. Navy 2000). End boundary conditions were assumed as follows: (a) Top end condition: Rotation fixed, translation free, and (b) Bottom end condition: Rotation fixed, translation fixed. If different end conditions exist, then the appropriate changes can be done to the model to account for that. The wood species considered was southern yellow pine (SYP).

The cantilever column was modeled similarly to the simply supported beam with the major change being the moment distribution from the applied load, as follows

$$M = P \cdot x \tag{7.34}$$

where P is the applied load at the free end and x is the distance from the free end. The shear force in the cantilever column is equal to the applied concentrated load, P.

The moment considered in the cantilever column model, for development length calculations, was the moment at a distance a_2+l_{df} from the fixed end (See Figure 7.8).

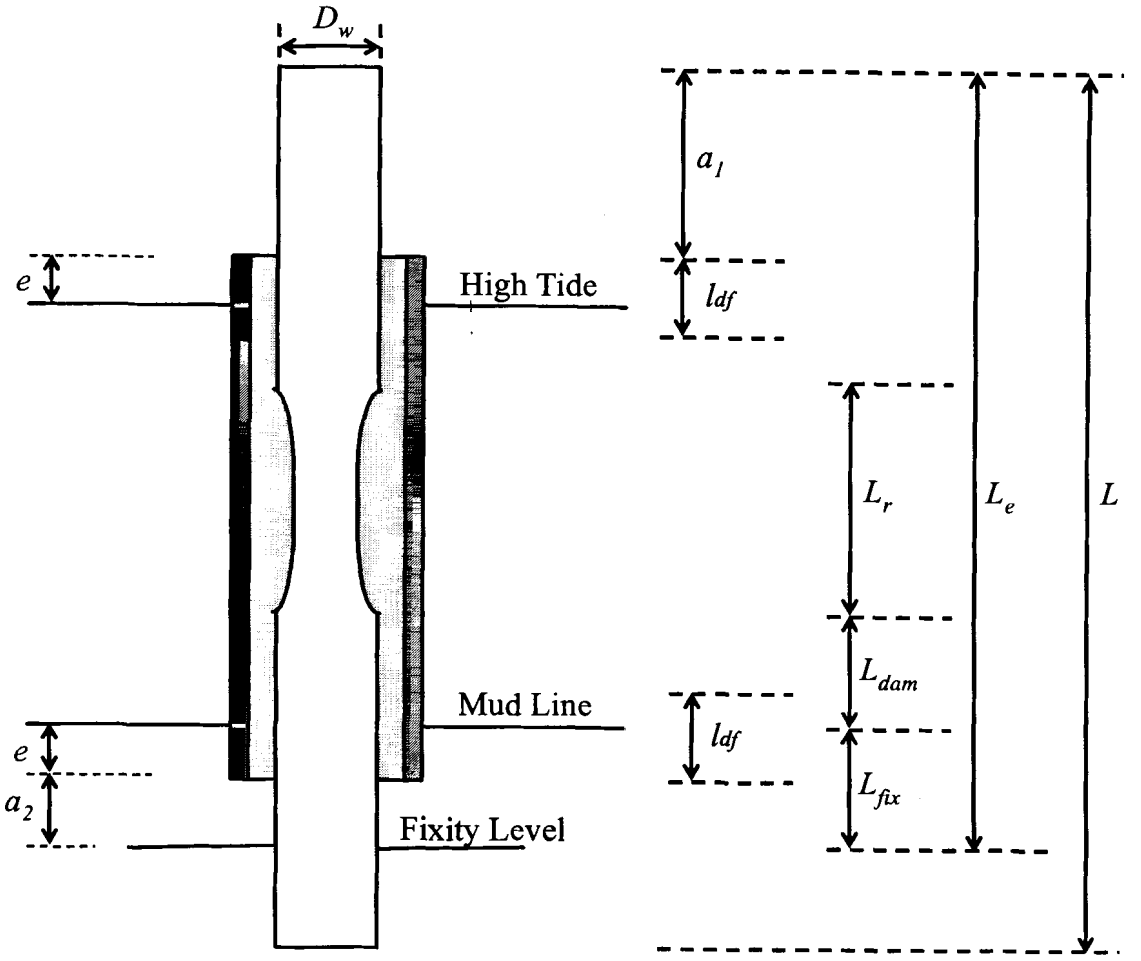

Figure 7.8 - Schematic of Cantilever Model of Typical Wood Pile

7.4.3.2 Design Example. The beam equations were applied to design the FRP composite shield to repair a typical damaged wood pile with a total length $L = 12.2\ m$, diameter at tip $D_1 = 300\ mm$, and diameter at butt $D_2 = 370\ mm$. The embedment length of the pile into the soil was $L_{emb} = L - L_e + L_{fix} = 6.1\ m$. The point of fixity was assumed to be at a depth from the mud line $L_{fix} = a_2 + e = 1.5\ m$ as shown in Figure 7.8 (Alpin and Lepper 2000; U.S. Navy 2000). The wood pile was damaged over a length $L_r = 800\ mm$ (70 % loss of cross sectional area) and the bottom of the damaged area was located at a distance $L_{dam} = 700\ mm$ from the mud line. The FRP composite shield encased the wood pile from a distance $e = 600\ mm$ below the mud line to a distance from the top of the pile

(butt) $a_1 = 1.83\ m$. The total length of the FRP composite shield was $L_f = 4.9\ m$. The wood pile was repaired using both systems B and C and the design solutions are compared.

The design diameter was calculated using equations (7.12) and (7.13). The elastic properties of the FRP composite were calculated using the equations based on laminate analysis. The cement based grout elastic modulus was determined from equation (7.11). Wood pile properties were calculated based on the equations provided. The beam design model was applied to the wood pile assuming a cantilever column configuration. The results from the design example are shown in Table 7.5.

Table 7.5 - Results from Design Example

Repair System	Ultimate load, kN	Development length, mm	Free end displacement at ultimate load, mm	Mode of failure
B (cement-based grout)	13.5	451	577	Wood tension failure at fixed location
C (shear connectors)	13.5	306	825	Wood tension failure at fixed location

The moment capacity of the wood pile repaired with system B (cement-based grout) and the applied moment are shown in Figure 7.9.

The moment capacity of the wood pile repaired with system C (shear connectors) and the applied moment are shown in Figure 7.10.

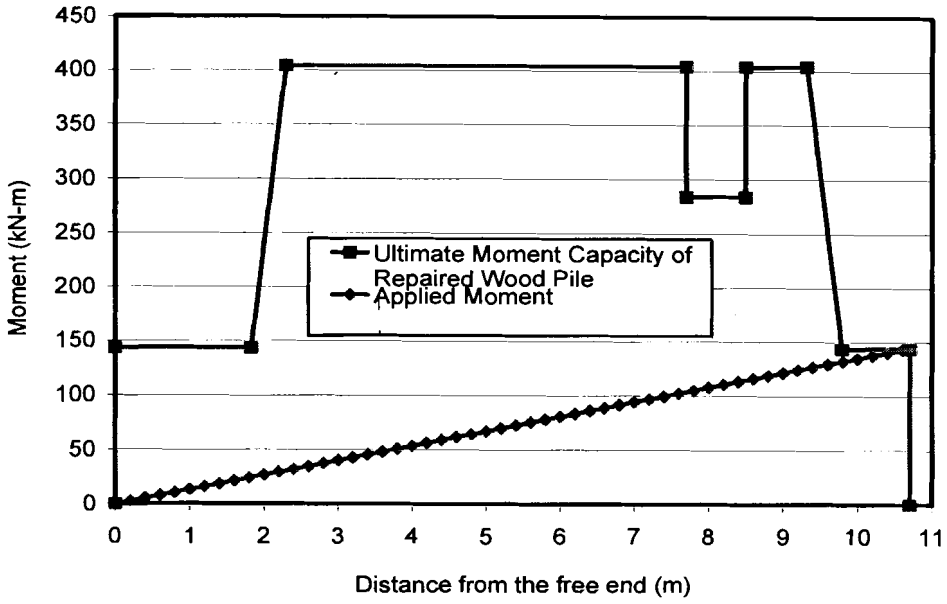

Figure 7.9 - Moment Capacity of Repaired Damaged Wood Pile and Moment at Peak Load for Cantilever Beam Model (Repair System B)

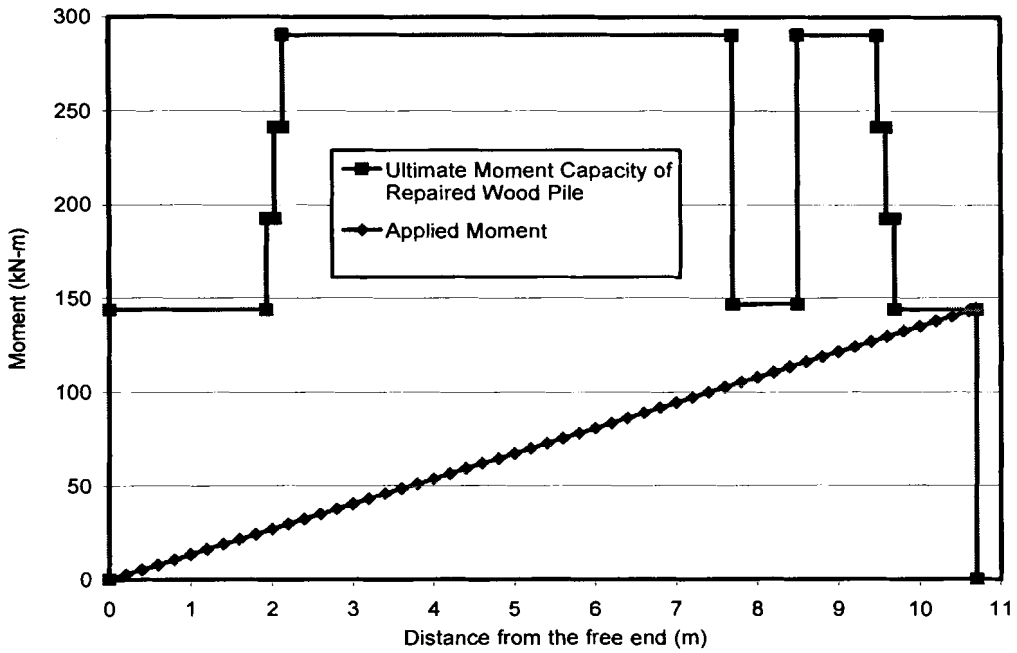

Figure 7.10 - Moment Capacity of Repaired Damaged Wood Pile and Applied Moment for Cantilever Beam Model (Repair System C)

7.5 Correlation with Experimental Results

The results from the beam model with the three-point configuration were correlated with the experimental results obtained from the bending tests (See Chapter 6). The correlation for peak load is shown in Table 7.6. The beam model peak load for the intact reference pile (IW) was approximately 20% lower than the experimental value. This was due to the fact that the reported bending strength for wood piles was 15% lower than the strength obtained from the bending test. The peak load for the pre-damaged control pile (DW) was well predicted with a difference of approximately 1%.

Table 7.6 – Peak Load Correlation between Beam Model and Experimental Results

System	Failure load (including self weight), kN		Difference, %
	Beam design model	Experimental results	
Intact reference wood pile (IW)	67.4	84.5	20.2
Pre-damaged control wood pile (DW)	12.3	12.4	0.8
Repair system B	99	126.0	21.4
Repair system C	64	58.5	9.4

For the wood piles repaired with both systems B (cement-based grout) and system C (shear connectors) the bending strength obtained from the intact reference pile was used. The peak load predicted by the beam design model for the pile repaired with system B (cement-based grout) was lower by approximately 21%. The predicted peak load for

the pile repaired with system C (shear connectors) was approximately 9% higher than the experimental.

It is assumed that the beam model predictions for peak load for the intact reference pile (IW) and the pile repaired with system B (shear connectors) were not well correlated with the experimental values because the predicted peak load was based on wood bending strength that has high variability.

The correlation for mid-span deflection at peak load is shown in Table 7.7. The beam model mid-span deflection for the intact reference pile (IW) was approximately 8% lower than the experimental value. The mid-span deflection for the pre-damaged control pile (DW) had a difference of approximately 1%.

Table 7.7 – Mid-Span Displacement Correlation between Beam Design Model and Experimental Results

System	Mid-span deflections, mm		Difference, %
	Beam design model	Experimental results	
Intact reference wood pile (IW)	188	204	7.8
Pre-damaged control wood pile (DW)	178	179	0.6
Repair system B	182	197	7.6
Repair system C	132	158	16.5

The mid-span deflection at peak load predicted by the beam model for the pile repaired with system B (cement-based grout) was lower by approximately 8%. The predicted mid-span deflection at peak load for the pile repaired with system C (shear connectors) was approximately 17% lower than the experimental. The deflection of the pile repaired with system C (shear connectors) was not well correlated. It is assumed that this difference is due to bending in the shear connectors (not accounted for in the design model), which allowed greater flexibility of the system.

The modes of failure for all tested piles predicted by the beam design model correlated well with the experimental response, as shown in Table 7.8.

Table 7.8 – Failure Mode Correlation between Beam Design Model and Experimental Results

System	Failure mode and location	
	Beam model	Experimental results
Intact reference wood pile (IW)	Tension failure in wood at mid-span	Tension failure in wood at mid-span
Pre-damaged control wood pile (DW)	Tension failure in wood at damaged location	Tension failure in wood at damaged location
Repair system B	Tension failure in wood at edge of FRP composite shield	Tension failure in wood edge of FRP composite shield
Repair system C	FRP composite shield longitudinal compressive failure at mid-span	FRP composite shield longitudinal compressive failure at mid-span

7.6 Conclusions and Recommendations

Based on the results presented in this chapter the following conclusions are drawn:

1. The proposed beam design model predicted, with reasonable accuracy, the peak load within 21% and the mid-span deflections at peak load within 17% for three-point bending tests (See Chapter 6). The failure modes were captured by the model.
2. The design example showed that an installed damaged wood pile repaired with both system B (cement-based grout) and system C (shear connectors) can be restored. The mode of failure remains the same as for an intact installed wood pile, which is wood failure at the fixed end.

The following commentary and proposed practical recommendations are offered:

1. The equations presented can be used to design the FRP composite shields for both repair systems B and C (see Chapter 5) and for various end supporting conditions.
2. Future work is needed to obtain the strength properties of the FRP composite shield.
3. The cement-based grout enclosed by the wood pile and the FRP composite shield develops limited confinement. The beam design model does not account for this confinement. The confinement of the cement-based grout if included in the beam model may result in better prediction of the bending moment capacity of the encased portion of the wood pile.

7.7 Notation

The following symbols are used in this chapter

a = Distance of FRP composite jacket edge from the support (simply supported beam)

a_1 = Distance of FRP composite jacket edge from the butt of the wood pile

a_2 = Distance of FRP composite jacket edge from the level of fixity of the wood pile

c = Distance of the extreme wood fiber from the neutral axis

c_f = Distance of the extreme FRP composite jacket fiber from the neutral axis

C_u = Empirical reduction coefficient

e = Distance the FRP composite shield is embedded into mud and distance it extends above high tide

D_1 = Tip diameter of a tapered wood pile

D_2 = Butt diameter of a tapered wood pile

L_{fix} = Depth below the mud line at which the wood pile is assumed to be fixed

D_{red} = Diameter of wood pile at damaged location

D_w = Design diameter of tapered wood pile

E_f = Modulus of elasticity of the fibers

$(EI)_{cs}$ = Stiffness of repaired wood composite section

E_c = Cement-based grout modulus of elasticity

E_m = Modulus of elasticity of the matrix

E_w = Wood pile modulus of elasticity

E_x = Longitudinal modulus of elasticity of FRP composite shield

E_y = Transverse modulus of elasticity of FRP composite shield

E_1 = Modulus of elasticity in the fiber direction

E_2 = Modulus of elasticity in the transverse direction of the fiber

F_b = Reference bending strength of wood pile

f'_c = Compressive strength of cement-based grout obtained from cylinder tests

F_{xc} = Longitudinal compressive strength of FRP composite shell

h_f = Thickness of FRP composite shell

I_f = Moment of inertia of FRP composite jacket

I_{red} = Moment of inertia of wood pile at damaged location

I_w = Moment of inertia of intact wood pile

L_{emb} = Length of wood pile embedded into mud

L_{dam} = Distance between the bottom of the damaged area and the mud line

l_{db} = Development length of FRP composite shield with shear connectors

l_{dc} = Development length of cement-based grout

l_{df} = Development length of FRP composite shield when using cement-based grout
L_f = Length of FRP composite shield
L_r = Length of damaged portion of the wood pile
M = Moment from applied load
M_{fu} = Moment capacity of FRP composite shield
M_{red} = Moment capacity of damaged portion of wood pile
M_w = Moment capacity of intact wood pile
n = Number of shear connectors
P = Applied load
P_p = Force transferred by each shear connector
r_c = Outer radius of cement based grout
r_f = Outer radius of FRP composite jacket
r_w = Outer radius of wood pile
s = Spacing of shear connectors
t_{csm} = Thickness of CSM layer
V = Shear force
V_f = Fiber volume fraction
ΔF = Force difference in the equilibrium section
Δ_{max} = Maximum deflection
ζ = Empirical parameter
η = Empirical parameter
θ = Angle formed by the radius of a point and the horizontal passing through the center of the section
v = Poisson's ratio of the FRP composite
τ^{c}_{xr} = Average shear stress of wood pile and cement-based grout interface
τ^{f}_{xr} = Average shear stress at FRP composite jacket and cement-based grout interface
τ_0 = Apparent slip-shear strength of the interface

Subscripts

cs = Composite section
f = Fiber
m = Matrix
w = Wood

BIBLIOGRAPHY

Abood, K. A., Ganas, M. J., and Matlin, A. (1995). "The Teredos Are Coming!" Ports '95 Conference on Port Engineering and Development for the 21st Century. Part 1, Tampa, FL, 677-690.

AF&PA. (1996). LRFD Timber Poles and Piles Supplement, American Forest and Paper Association & American Wood Council.

Aquascope. (2000). "http://www.vattenkikaren.gu.se/fakta/arter/crustace/isopoda/limnlign/limnlie.html." Tjärnö Marine Biological Laboratory, Strömstad, Sweden.

Arroyo, M. R., and Francois, J. J. (1996). "New Shear Stud Connector Proposal." 1996, Composite Construction in Steel and Concrete III, Proceedings of an Engineering Foundation Conference, Irsee, Germany, 298-311.

ASTM. (1990). ASTM D 3966-90 Standard Test Method for Piles Under Lateral Loads., American Society for Testing and Materials, West Conshohocken, PA.

ASTM. (1994). ASTM D 5573-94 Standard Practice for Classifying Failure Modes in Fiber-Reinforced-Plastic (FRP) Joints, American Society for Testing and Materials, West Conshohocken, PA.

ASTM. (1995). ASTM D 5868-95 Standard Test Method for Lap Shear Adhesion for Fiber Reinforced Plastic (FRP) Bonding, American Society for Testing and Materials, West Conshohocken, PA.

ASTM. (1999a). ASTM D 25-91 Standard Specification for Round Timber Piles, American Society for Testing and Materials, West Conshohocken, PA.

ASTM. (1999b). ASTM D 1036-99 Standard Test Methods of Static Tests of Wood Poles, American Society for Testing and Materials, West Conshohocken, PA.

AWPA. (1999a). AWPA Standard Appendix G: Marine (Salt water) Applications, American Wood Preservers' Association, Granbury, TX.

AWPA. (1999b). AWPA Standard C3-99: Piles - Preservative Treatment by Pressure Process, American Wood Preservers' Association, Granbury, TX.

Baileys, R. T. (1995). "Timber Structures and the Marine Environment." Ports '95, 703-710.

Brody, J., Richard, A., Sebesta, K., Wallace, K., Hong, Y., Lopez Anido, R., Davids, W., and Landis, E. (2000). "FRP-Wood-Concrete Composite Bridge Girders." Structures Congress 2000 - Advanced Technology in Structural Engineering, Philadelphia, PA.

Cartwright, K. S. G., and Findlay, W. P. K. (1958). Decay of Timber and its Prevention, Forest Products Research Laboratory, Her Majesty's Stationary Office, London, London, England.

Chellis, R. D. (1961). "Deterioration and Preservation of Piles." Pile Foundations, McGraw-Hill Book Company, Inc., 339-372.

Coburn, S. K. (2000). "Corrosion Factors to be Considered in the Use of Steel Piling in Marine Structures." Pile Buck, Palm City, FL, 10A-18C.

Denso North America, I. (2000). "Marine Systems." Denso North America Inc.

Douglas, J. (1986). "Groundline Repair for Wood poles." EPRI Journal, 29-31.

Dow. (1999). DERAKANE Epoxy Vinyl Ester Resins / Chemical Resistance and Engineering Guide, Dow Chemical Company, Midland, MI.

Doyle Publishing. (1996). "The Marketplace: Pile Encapsulation and Repair Products." UnderWater Magazine.

EDM. (1995). "Full-Scale Destructive Tests of TYFOTMS FibrwrapTM System for Wood Pole Restoration." Engineering Data Management, Inc, Fort Collins, CO.

Five Star. (2001). "Five Star Structural Concrete Underwater PG." Five Star Products, Inc., Fairfield, CT.

Fyfe. (1998). "Tyfo Systems for Wood." Fyfe Co. LLC, The Fiberwrap Company, San Diego, CA.

Gillis, R., and Haro, R. J. (2001). "http://bioweb.uwlax.edu/zoolab/Table_of_Contents/Lab-05/Shipworms_1/Shipworms_1a/shipworms_1a.htm." Department of Biology, University of Wisconsin - La Crosse.

Goodell, B. (2000). "Wood Products: Deterioration by Insects and Marine Organisms." Encyclopedia of Materials Science and Technology, Elsevier.

Haeberle, D. C., Starr, B. C., Lesko, J. J., and Riffle, J. S. (2002). "Effect of UV Aging on Vinyl Ester and Vinyl Ester Matrix Composites." Durability of Fibre Reinforced Polymer (FRP) Composites for Construction, Montreal, Canada, 273-284.

Hardcore Composites. (1999). "The City of Monterey Wharf No. II Hardshell Timber Pile Wrapping." Hardcore Composites and William P. Yong Construction, Inc., New Castle, DE.

Hardcore Composites. (2000). "Hardshell Composite Jackets." Hardcore Composites Inc.

Highley, T. L. (1999). "Chapter 13: Biodeterioration of Wood." Wood Handbook - Wood as an Engineering Material, USDA, Forest Products Laboratory, Madison, WI.

ICBO. (2001). Acceptance Criteria for Concrete and Reinforced and Unreinforced Masonry Strengthening Using Fiber-Reinforced Polymer (FRP), Composite Systems, ICBO Evaluation Service, Inc, Whittier, CA.

Instron. (1998). "Instron Fast Track 8802 Materials Test Control System." M21-10006-EN, Instron Corporation, Canton, MA.

Johnson, B. R. (2002). "Pest of the Quarter Of Shipworms and Gribbles, Pillbugs, and Pholads." AWPA Newsline, 4-6.

Karbhari, V. (2001). "HITEC Evaluation Plan for FRP Composite Bridge Decks." Civil Engineering Research Foundation, Washington, DC.

Kelly, S. W. (1999). Underwater Inspection Criteria, Naval Facilities Engineering Service Center, Port Hueneme, CA.

Klekowski, L., and Klekowski, E. (1997). "http://www.bio.umass.edu/biology/conn.river/shipworm.html." Biology Department, Morrill Science Center (South), University of Massachusetts Amherst.

Kshirsagar, S., Lopez-Anido, R., and R. K.Gupta, R. K. (2000). "Environmental Aging of Fiber-Reinforced Polymer-Wrapped Concrete Cylinders." ACI Materials Journal, 97(6), 703-712.

Lawson, M. R. (1996). "Shear Connection in Composite Beams-Influence of Steel Deck Shape." 1996, Composite Construction in Steel and Concrete III, Proceedings of an Engineering Foundation Conference, Irsee, Germany, 312-324.

Lebow, S. T., Foster, D. O., and Lebow, P. K. (1999). "Release of Copper, Chromium, and Arsenic from Treated Southern Pine Exposed in Seawater and Freshwater." Forest Products Journal, 49(7/8), 80-89.

Liddell, O. E. (1967). "Protection of Submerged Piling." United States Patent Office, USA.

Lopez-Anido, R., and Karbhari, V.M. (2000a). "Chapter 2: Fiber Reinforced Composites in Civil Infrastructure." Emerging Materials for Civil Engineering Infrastructure - State of the Art, R. Lopez-Anido, and Naik, T.R., ed., ASCE Press, Reston, VA., 41-78.

Lopez-Anido, R., and Xu, H. (2002). "Structural Characterization of Hybrid FRP-Glulam Panels for Bridge Decks." Journal of Composites for Construction, ASCE, 6(3), 194-203.

Lopez-Anido, R., Falker, E., Mittelstadt, B., and Troutman, D. (1999). "Shear Tests of FRP Pultruded Beam-to-Column Connection with Clip Angles." Materials and Construction: Exploring the Connection, Reston, VA, 92-99.

Lopez-Anido, R., Gardner, D.J. and Hensley, J.L. (2000b). "Adhesive Bonding of Eastern Hemlock Glulam Panels with E-Glass/Vinyl Ester Reinforcement." Forest Products Journal, 50(11/12), 43-47.

Maine DOT. (1986). Port Inventory and Evaluation, Maine Department of Transportation, Augusta, ME.

Master Builders. (2001). "Product Information: A-P-E Process." Master Builders Inc.

Measurements Group. (1997). "Strain Gage Applications With M-Bond AE-10 Adhesive System." Measurements Group, Inc, Raleigh, NC.

Menzies, J. B. (1971). "CP 117 and Shear Connectors in Steel-Concrete Composite Beams Made With Normal Density or Lightweight Concrete." The Structural Engineer, 49, 137-154.

National Instruments. (2000). "LabVIEW." National Instruments Corporation, Austin, TX.

NBEC, C. (2000). "NBEC Nonshrink Grout Nonmetallic." The NBEC Corporation, Greenfield Hill, CT.

NBEC, C. (2000). "NBEC Nonshrink Grout Nonmetallic." The NBEC Corporation, Greenfield Hill, CT.

Osmose. (2001). "Railroad/Marine Products and Services." Osmose Marine Inc.

Rockwater. (1999). "Integrated Systems and Innovative Solutions." Rockwater Manufacturing Corp.

Shepard, M. (1987). "Managing America's Wood Pole Inventory." EPRI Journal, 31-37.

Shim, C. S., Kim, J. H., Chang, S. P., and Chung, C. H. (2000). "Behaviour of Shear Connections in a Composite Beam With a Full-Depth Precast Slab." Institution of Civil Engineers, Structures and Buildings, London, England, 101-110.

Sika. (1998). "SikaFix HH Expanding, polyurethane, chemical grout." Sika Corporation, Lyndhurst, NJ.

Snow, R. K. (2000). "Polymer Pile Encapsulation: Factors Influencing Performance." Bridge Repair and Rehabilitation. ACI Compilation 29, 44-50.

SPSS. (1999). "SYSTAT." SPSS Inc., Chicago, IL.

Superior Polymer. (2000). "Technical Data Sheet: Hydrobond 500 Underwater Epoxy Adhesive."

Tapecoat. (2001). "Marine Products." Tapecoat Company.

TPI. (2001). "An Overview of the SCRIMP™ Technology." TPI Technology, Inc, Warren, RI.

TRANSPO. (2000). "Technical Data Sheet Multiple Coat Epoxy Overlay T-48." New Rochelle, NY.

U.S. Army. (1978). "Army TM 5-622: Chapter 2 - Timber Structures." United States Army.

U.S. Army. (1990). "Chapter 8 - Pile Wharves." PORT CONSTRUCTION AND REPAIR, US ARMY, Fort Leonard Wood, MO 65473, 1-31.

U.S. Navy. (1987). "Polyvinyl Chloride (PVC) Wraps Reduce the Cost of Maintaining Timber Piling." Naval Civil Engineering Laboratory, Port Hueneme, CA.

US Army Corps of Engineers, Naval Facilities Engineering Command, and Agency, A. F. C. E. S. (2001). "Unified Facilities Criteria (UFC) - Operation and Maintenance: Maintenance of Waterfront Facilities." UFC 4-150-07, Washington, DC.

Veldanda, M. R., and Hosain, M. U. (1992). "Behaviour of Perfobond Rib Shear Connectors: Push-Out Tests." Canadian Journal of Civil Engineering, 19, 1-10.

Wallour, D. B. (1959). "13th Progress Report on Marine Borer Activity in Test Boards Operated During 1959." 11466, William F. Clapp Laboratories, Inc., Duxbury, Massachusetts.

Wilson, M. A. (2001). "http://www.wooster.edu/geology/Bioerosion/Bankia.html." Department of Geology, The College of Wooster, Ohio.

Wood, K. S. (2000). "Characterization of Environmental Exposure of Fiber Reinforced Polymer Materials Used in Bridge Deck Systems," University of Maine, Orono, ME.

APPENDICES

APPENDIX A

Detailed procedure for the fabrication of Fiber Reinforced Composite shells using the SCRIMPTM fabrication process

Summary of Fabrication Method

Cylindrical Fiber Reinforced Polymer (FRP) composite shells with a longitudinal opening along their length were fabricated in the laboratory using the Seemann Composites Resin Infusion Molding Process (SCRIMP^{TM}). The fiber reinforcement was placed dry on the mold and then sealed with a tube vacuum bag. Vacuum pressure of –102 kPa was applied with a vacuum pump and resin was pulled through a resin pot. The reason for the selection of –102 kPa of vacuum pressure instead of –85 kPa that others use was the following: It is suggested that vacuum lines are spaced every 0.914-1.219 m but for the 4.878 m long shells we only had two and we thought –102 kPa would help keep the vacuum at the high twenties in between the two vacuum lines. Once the resin impregnated the fiber reinforcement the vacuum pressure was reduced to –51 kPa till the resin gelled. The vacuum pressure compacted the dry fiber reinforcement. The vacuum also removed all the air from the fiber lay-up before and during resin infusion. The pressure differential between the atmosphere and the applied vacuum allowed infusion of the resin into the fiber lay-up. After the resin gelled vacuum pressure was removed and the part was allowed to cure. The part was then removed by pulling open the longitudinal opening.

Apparatus

- Sixteen inch diameter PVC pipe used as a mold

- Two end supports for the PVC pipe
- Vacuum pumps and tubing
- Resin pot
- Coil and sisal rope

Materials

- E-Glass unidirectional woven fabric. It comes in rolls of 1.219 m width and has a weight of 880 g/m^2.
- Chopped Strand Mat. It has a width of 1.270 m and a weight of 305 g/m^2.
- Vinyl ester resin. It is an Epoxy based resin from DOW Chemicals known as Derakane 411-C-50 and it suitable for SCRIMP^{TM} because of its low viscosity (0.15 Pa.s).
- Sealant tape
- Plastic tubing, connectors and valves
- Coil and sisal rope
- Release film
- Peel ply
- Flow media
- Tube vacuum bag

Fabrication Procedure

Fabrication Set-Up

1. Cut fabrics and other materials to the appropriate dimensions.
2. Clean the mold thoroughly.

3. Apply mold release agent and release film. Use tape to hold release film in place.
4. Place a layer of peel ply. Use spray adhesive to hold it in place. Care should be taken to use minimal amount of adhesive because of potential void pockets in the part.
5. Place E-glass fabrics in the appropriate sequence to build your lamina on top of the peel ply. In the case of wood pile repair the fiber stacking sequence is [CSM, 0^0, 90^0, 0^0, 0^0, CSM]. Use spray adhesive to prevent the fabric layers from shifting. The Fiber Volume Fraction (FVF) that this process yields is about 45%.
6. Place a layer of peel ply on top of the fibers.
7. Place the sisal rope at the bottom where the longitudinal opening will be located. Use sealant tape to attach it to the mold. The sisal rope should be 150 mm shorter than the part and placed 75 mm from each edge of the shell.
8. At the two ends of the sisal rope attach the vacuum hoses using sealant tape and dug tape.
9. Bring together the peel ply in such way as to cover the rope in order to maintain uniform vacuum during fabrication. Stable the edges of the peel ply together to hold them in place.
10. Place the flow media on top of the peel ply. The flow media should be 75 mm from the edges of the part.
11. Place the resin tube 50 to 70 mm in the coil and then wrap the coil with the same material as the flow media. The coil should be the same length as the

flow media, which in this case is 150 mm shorter than the length of the part. Place the coil on the top and use pieces of sealant tape to hold it in place

12. Place the whole system into the tube vacuum bag and use sealant tape to seal the system. At the bottom and top where the rope and the coil are, create a fold to the vacuum bag to accommodate the extra space needed for those not to cause any distortion to the fabricated part.
13. Connect the vacuum tubing (vacuum lines) to the vacuum pump. Clamp the resin tubing (feed line) to prevent air from entering the system.

Vacuum of Dry Reinforcement Lay-Up

14. Turn on the vacuum pump and draw vacuum pressure. Check for any leaks and seal them. When no more leaks can be found make sure the indicator on the resin pot is reading –102 kPa.
15. Close the valve in order to isolate the system from the vacuum pump and then turn off the pump as well. Record the indication immediately after you turn off the valve.
16. Watch the indicator on the resin pot to see if how much vacuum is lost in 5 minutes. If less than –3.4 kPa is lost in that period the system is ready for impregnation. If not then look for more leaks and seal them. Then run the test for another 5 minutes to make sure you are not still loosing vacuum.

Resin Mix

17. Mix the appropriate amount of resin. For a 4.877 m long shell 16 kg of the resin are needed while for a 0.864 m long one 4.5 kg. Add 1% catalyst by

weight to the resin and mix thoroughly for 5 minutes. Mixing should be done under the ventilation hood. The resin has a pot life of 1.5 hours when mixed with 1% catalyst (at ambient temperature of 21 °C).

18. Let the resin sit for an hour under the hood. This is necessary since the time that the part is impregnated is 25 to 30 minutes. If the resin is used right away then resin will be pulled out of the part and possibly go into the vacuum tubing blocking it and vacuum pressure will drop.

Resin Infusion

19. When is time for impregnation turn the pump on and then place the resin tubing in the bucket the resin was mixed in.
20. Unclamp the resin tubing and allow resin to flow through and into the coil. The distribution media will allow it to be distributed around the part.
21. When the part is completely impregnated clamp the resin tubing and turn off the valve to isolate the system from the pump. This will maintain the pressure till another pump is connected to the system.
22. Connect a pump to the system that is able to yield –51 kPa or that has the ability to regulate the amount of vacuum with a valve.
23. Drop the pressure to –51 kPa of Hg and let it run till the resin in the part gels. Although the resin in the bucket gels really fast due to the high concentration of resin the resin in the part usually takes about 35 to 40 minutes to gel.
24. Turn off the pump after the resin gels and let the part cure on the mold.
25. Allow any excess resin that was left in the bucket to cure under the hood.

Removal of Part, Disposal of Materials and Cleaning of Set-Up

26. After curing of the resin, remove SCRIMP™ materials (plastic bag, peel ply, distribution media, coil and rope).
27. Remove the FRP shell from the PVC pipe my pulling open the longitudinal opening and sliding it off.
28. Dispose of all the SCRIMP™ materials and any cured resin in a trash bin since after curing the resin material becomes toxicologically and ecologically inert.
29. Clean the PVC pipe and get it ready for the next shell.

Specimen Size

FRP composite shells with a diameter of 406 mm and two different lengths ranging from 0.864 m to 4.877 m were fabricated. The thickness of the FRP composite shells is typically 3.3 mm.

APPENDIX B.

Detailed cost analysis for FRP shell manufacturing and bonding

Table B.1 - Calculation of Fiber Reinforcement Cost

Calculation of Fiber
UMain 8-May-
Fiber Reinforcement

Laminate lay- 1 (oz/ft2 CSM) + 4 (26 oz/yd2 uniweave) + 1
CSM 2
VEW260 4
Shell width 4
Shell length 16
Number of 4
Number of 1
Waste 1.1

Item	Reinforceme per Shell	Reinforceme total	Weight/are (lb)	Total (lb)	Weight/ro (lb)	# require	# adopte	$/roll	Cost
Mat	128	512	0.06	35.2	86	0.41	0.50	137.	68.8
VEW26	256	1024	0.18	203.3	232	0.88	0.90	371.	334.0
Total fiber reinforcement									**$402.8**

Cost per **$100.7**

Table B.2 - Material Fabrication Supplies and Labor Preparation and Application Cost

Material cost items
UMaine

	8-May-02		
Length of FRP shell (ft)	16		
Number of shells	4		
Fabrication supplies	Cost per ft	Total cost	
Release film	$1.47	$24.99	
Sisal rope	$0.35	$5.60	
Sealant tape	$0.42	$6.72	
Bagging film	$0.70	$11.90	
Distribution media	$0.30	$15.98	Note: The unit price is per sq. foot
Peel ply	$2.35	$39.95	
Total cost per shell		$105.14	
The following items can be used for all shells not just one			
Tubing	$0.95	$23.75	
Fittings		$10.00	
Total cost		$33.75	
Total cost per shell		$8.44	
Total fabrication supplies cost for shell		$113.58	

Labor cost items
UMaine

	# Laborers	# Hours	Cost ($/hr)	Total cost ($)
Labor Preparation	2	3.5	10	$70.00
Labor Application	1	1.5	10	$15.00

Table B.1 - Calculation of Fiber Reinforcement Cost

Table B.1 - Calculation of Fiber Reinforcement Cost

Table B.3 - Total FRP Shell Cost

Calculation of Total FRP Shell Cost
UMaine
8-May-02

Shell width (ft.)	4
Shell length (ft.)	16
Number of shells	4

Cost per shell		Cost Source
Fiber reinforcement	$100.72	UMaine - BTI
Resin Derakane C-50	$70.00	Umaine
Catalyst DHD-9	$8.00	Umaine
Fabrication supplies	$113.58	Umaine
Labor preparation	$70.00	Umaine
Total material Cost	$362.30	
Labor application	$15.00	Umaine
Total cost per shell	$377.30	
Cost per square foot of shell	**$5.90**	
Total cost for 4 FRP shells	$1,509.21	

		Total
Adhesive cost per ft of shell	$12.50	$200.00
# of hours	1.5	
Application cost per hour	$10	$15
Total cost for adhesive application		$215.00
Cost for 2 bonded shells	$969.60	

APPENDIX C.

Analysis of variance results for control and freeze-thaw specimens from SYSTAT

Table C.1 - Paired Samples t-Test Results

	CONTROL	FREEZETHAW
N of cases	9	9
Minimum	14.990	8.847
Maximum	17.393	9.547
Range	2.403	0.700
Sum	145.836	82.733
Median	16.226	9.231
Mean	16.204	9.193
95% CI Upper	16.815	9.361
95% CI Lower	15.593	9.024
Std. Error	0.265	0.073
Standard Dev	0.795	0.219
Variance	0.633	0.048
C.V.	0.049	0.024
Skewness(G1)	-0.343	-0.349
SE Skewness	0.717	0.717
Kurtosis(G2)	-0.637	0.093
SE Kurtosis	1.400	1.400

Paired samples t test on CONTROL vs FREEZETHAW with 9 cases

Mean CONTROL = 16.204
Mean FREEZETHAW = 9.193
Mean Difference = 7.011 95.00% CI = 6.337 to 7.686
SD Difference = 0.878 t = 23.957
df = 8 Prob = 0.000
Dunn-Sidak Adjusted Prob = 0.000
Bonferroni Adjusted Prob = 0.000

Table C.2 - Two Sample t-Test on Strengths Grouped by GROUPVAR

SYSTAT Rectangular file C:\Program Files\SYSTAT 9\Data\Research Data\Tony's stuff.SYD, created Thu May 09, 2002 at 14:13:06, contains variables:

CONTROL FREEZETHAW

Two-sample t test on STRENGTHS grouped by GROUPVAR

Group	N	Mean	SD
0	9	16.204	0.795
1	9	9.193	0.219

Separate Variance t = 25.497 df = 9.2 Prob = 0.000
Dunn-Sidak Adjusted Prob = 0.000
Bonferroni Adjusted Prob = 0.000
Difference in Means = 7.011 95.00% CI = 6.391 to 7.631

Pooled Variance t = 25.497 df = 16 Prob = 0.000
Dunn-Sidak Adjusted Prob = 0.000
Bonferroni Adjusted Prob = 0.000
Difference in Means = 7.011 95.00% CI = 6.428 to 7.594

Paired samples t test on CONTROL vs FREEZETHAW with 9 cases

Mean CONTROL = 16.204
Mean FREEZETHAW = 9.193
Mean Difference = 7.011 95.00% CI = 6.337 to 7.686
SD Difference = 0.878 t = 23.957
df = 8 Prob = 0.000
Dunn-Sidak Adjusted Prob = 0.000
Bonferroni Adjusted Prob = 0.000

BIOGRAPHY OF THE AUTHOR

Antonis Michael was born in Larnaca, Cyprus on March 22, 1975. He was raised in Avgorou, Cyprus and graduated from Pancyprian Lycium, Larnaca in 1993. He attended the Higher Technical Institute, in Nicosia, and graduated in 1996 with the diploma of Technician Engineer in Civil Engineering. He jointed the Army of Cyprus after graduation and served in the Army Corps of Engineers.

He came to the United States in the Fall of 1997 and attended Tennessee Technological University. He graduated in 1999 with a Bachelor of Science degree in Civil Engineering. He moved to Maine and entered the Civil Engineering graduate program at the University of Maine in the Spring of 2000.

After receiving his degree, Antonis will be joining the University of Florida, to begin his studies towards a Doctor of Philosophy degree in Civil Engineering. Antonis is a candidate for the Master of Science degree in Civil Engineering from the University of Maine in December, 2002.